AFCRL-62-954

SWITCHING PROPERTIES OF FERRITES AND GARNETS

by

Harvey Rubinstein

Division of Engineering and Applied Physics

Cruft Laboratory, Harvard University

Cambridge, Massachusetts

Contract AF19(604)-5487

Project 5633 - Task 56332

Scientific Report No. 6(Series 2)

November 30, 1962

Prepared for

Electronics Research Directorate

Air Force Cambridge Research Laboratories

Office of Aerospace Research

United States Air Force

Bedford, Massachusetts

ACKNOWLEDGMENTS

It is a pleasure to express my gratitude to the many people who have given me assistance during the course of this work.

The original suggestion for this research came from Dr. C. L. Hogan, to whom I am indeed grateful. The work was carried out under the counsel of Prof. R. V. Jones, and I am deeply indebted to him, not only for advice and guidance, but also for his assistance in the preparation of this report.

The pulse generator which was used to obtain the original data presented herewith resulted from a suggestion made by Dr. J. Narud. For this idea, the author offers his thanks.

I wish to express my appreciation for the help given me in the preparation of materials to Mrs. L. Lin, Mr. C. Quadros, and Mr. F. Molea; for the construction of apparatus to Mr. J. Meehan and the late Mr. C. Nyholm; and for the typing of this manuscript to the technical typing staff of the editorial group of the Laboratory for Electronics, Inc.; and for aid and encouragement during the course of this work to Shirley Rubinstein.

The helpful discussion with my many colleagues: Drs. C. Buffler, J. Green, B. Harris, I. Kaminow, J. Pippin, G. Rodrigue, and T. Strauss; and Messrs. C. Nowlin and R. Temple, are gratefully acknowledged.

TABLE OF CONTENTS

TABLE OF CONTENTS (Continued)

TABLE OF CONTENTS (Continued)

TABLE OF CONTENTS (Continued)

LIST OF FIGURES AND TABLES

LIST OF FIGURES AND TABLES (Continued)

LIST OF FIGURES AND TABLES (Continued)

LIST OF FIGURES AND TABLES (Continued)

Scientific Report No. 6 (Series 2)
Contract AF19(604)-5487
AFCRL-62-954
November 30, 1962

ERRATA

Page

1-53 Equation 1.75b should read $M \sin\theta \frac{d\phi}{dt} = -\gamma MH \sin\theta$

" 1.77 " " $= -\gamma MH \sin\theta - \alpha M \frac{d\theta}{dt}$

" 1.76b " " $= \gamma H$

" 1.78a " " $= -\frac{\gamma}{1+\alpha^2} H$

" 1.78b " " $= -\gamma H \frac{\gamma}{1+\alpha^3} H$

1-54 " 1.82 " " $\frac{dE}{dt} = -\left(\frac{\gamma}{M}\right) \cdot \frac{\alpha}{1+\alpha^2} (M \times H)^2$

1-67 " 1.86 " " $M_H = M \tanh\left[\frac{(t-t_o)+t_o}{T}\right]$

$t_o = T \tanh^{-1}(\cos\theta_o)$

$\cos\theta_o = \cos\theta\,(t = t_o)$ (initial condition)

SYNOPSIS

This work presents the results of an experimental and theoretical study of the switching properties of ferrimagnetic oxides. Much attention has recently been given to these properties, since these materials are used in ever increasing amounts in switching applications such as memory and logic circuits of digital computers. Two terms – the switching time, τ, the time required by the magnetization to reverse, and the switching parameter, S_w, the inverse slope of the curve of the variation of the reciprocal switching time with the applied field – which describe these properties are the prime considerations of this thesis.

The six chapters into which this work is divided are described below.

Chapter I is a review of switching and related fields and, thus, is an introduction to the work presented in later chapters.

In Chap. II, the experimental techniques and the associated specialized equipment required for the measurements which were performed during this work are described. These techniques were used to measure the switching characteristics (or the field dependence of the switching time), the field dependence of the flux switched, and the grain sizes of garnet and ferrite toroidal cores and to observe domain patterns on the surfaces of these cores.

The manner in which these single and polycrystal garnet and ferrite toroids were prepared and their magnetic properties are presented in Chap. III. Where the magnetic properties were not known from previous measurements, the required quantities were calculated by methods described in this chapter.

The switching characteristics and the flux switched measurements obtained during the course of this work are given in Chap. IV. From these data and microwave resonance data it would appear that the switching speed is limited by self imposed processes, since S_w is found to decrease

as the microwave resonance relaxation frequency, λ, decreases until λ reaches a critical value and then to remain constant when λ is further reduced.

In the remainder of this chapter these data are discussed only in so far as they relate to the variation of the switching characteristic with core fabrication parameters. The height of the toroid and reasonably large variations in the sintering time are shown to produce no effect on the switching. On the other hand, the quality of the dielectric body of these toroids is shown to influence the switching. Decreasing the quality of the dielectric results in increasing S_w. This seems to result partially, if not entirely, from the inhomogeneity introduced by a second phase, which appears as the dielectric becomes poorer, rather than from an increase in its conductivity.

Because of the difficulty encountered in the preparation of cores of varying diameters the effects of these changes were considered theoretically. This calculation showed that when the core's outer diameter is so large that the field which switches the core is insufficient to reverse its entire magnetization, the switching time will be longer than when the entire core is reversed. In other words, faster switching can be obtained in certain low field applications by the mere expedient of reducing the outside diameter of the toroid.

Examination of previous calculations of switching by domain wall motion shows that these are valid only when the loss of energy from the magnetic system is rapid. Since some of the materials which are dealt with here appeared, from microwave measurements, to have relatively long relaxation times, these calculations were extended in Chap. V to treat these materials. It was found that the reciprocal of the switching time is proportional to the square root of the applied field when the relaxation frequency is small and is proportional to the applied field when the relaxation frequency is large.

This calculation also showed that there exists a nonzero lower limit to the domain wall velocity and, consequently, to the switching time as the relaxation frequency is reduced and that this limit is reached when the relaxation frequency vanishes.

In the final section of Chap. V, some of the results found earlier in this chapter are rederived on the basis of a model in which the damping is interpreted in terms of wall collisions. From this treatment the reason for the switching time's dependence on the inverse square root of the applied field when the relaxation frequency vanishes (i.e., in the absence of wall collisions) is readily seen.

In Chap. VI, the experimental results are interpreted on a domain wall motion model, after several relationships are derived which permit results taken from the theory of domain walls in ferromagnetic materials to be used with ferrimagnetic materials. It was found that those garnets which do not contain rare earth ions and the gadolinium substituted yttrium iron garnets are all characterized by relatively low coercive forces and switching parameters and possess identical relaxation frequencies. The switching properties of a toroid cut from a single crystal of yttrium iron garnet were found to be in accord with these polycrystalline properties and to support the domain wall motion model, since the single crystal toroid switched much more slowly than its polycrystalline counterpart.

The rare earth garnets are then examined with a model which presupposes that, when rare earths are added to yttrium iron garnet, the existing loss mechanisms are augmented by independent ones. Good agreement is obtained between the S_w's measured at room temperature and 55°C and those expected on the basis of this model. From an entirely different point of view, which is independent of a particular dynamic model, the domain walls which reverse the magnetization are shown to move less than a grain size, and this conclusion is also verified by the above model.

The total anisotropy of nickel ferrite with increasing cobalt additions changes sign, and it was expected that switching experiments might show some indication of this behavior. However, only a continuous increase in the switching parameter was found as the cobalt concentration was increased. If the cobalt is considered to be an impurity atom in the nickel ferrite, these results can be interpreted with a domain wall model.

An explanation depending on nonlinear interactions is proposed for the switching properties of yttrium iron garnet. This explanation uses the high power effects occurring in ferromagnetic resonance as an analogy. A consequence of this explanation is that the model described above, where the relaxation frequencies of the iron and rare earth ions are treated as independent, should be modified to include their dependence.

Finally, high field behavior is considered, and it is shown that a linear relationship between these data and low field data is obtained when $\sqrt{1/\tau}$ is plotted as a function of the applied field. From this observation it follows that the relaxation frequency must be field dependent.

CHAPTER I: EXPERIMENTAL AND THEORETICAL BACKGROUND

1. INTRODUCTION

The mechanisms which bring about changes in the magnetization of a ferromagnetic material have been under study for a considerable time. The early examinations of these changes were predominantly concerned with the static relations between the change in magnetization and the force required to produce it. Later, through studies of the frequency dependence of the permeability and of the aging of magnetic properties, time dependent changes were studied.

Presently, as a result of the requirements of digital computers and of electronic pulse techniques and as a result of the introduction of ferrites into technology, an understanding of the irreversible changes in low coercive force magnetic materials has taken on an increased importance. Of particular interest is the study of the time required for the magnetization to change irreversibly after the sudden application of a magnetic field. This effect has become known as remagnetization, or switching, and the time required for it to occur is called reversal, remagnetization, or switching time. It is this effect which will be examined here.

The present work originated with the need to explain the results of a class of experiments in the switching of a ferromagnetic toroidal core. In these experiments the core is first brought to one of its remanent states by passing a current through a wire which links it. A reverse current is then applied, and it is found by observing the rate of change of flux in the core that a finite time is required for the magnetization to reach its reversed or switched state.

The objectives of this problem are twofold, as is common in many other studies of the properties of magnetic materials. On the one hand, through its solution an increased understanding of magnetism is acquired. On the other hand, through its solution improved materials may be obtained, or the

limitations imposed by materials on an application may become known. The technological significance of this problem exists because of the large number of applications of magnetic materials in digital computers and because of the need to increase the switching speeds in some of these applications.

In this chapter the background will be set for a study of the switching speed. The previous work in the field of magnetization reversals will be reviewed. In order to make this work somewhat self-contained, the various magnetic interactions required to understand ferromagnetic domain theory will first be discussed. The domain theory which is basic to an understanding of magnetization reversal processes will then be treated. Following this, static and dynamic magnetization reversals and processes will be discussed. In the latter discussion, relaxation mechanisms will be considered.

The discussion will be restricted in the following way. Dynamic processes will not be discussed in any conducting materials except thin films. Their switching properties will be reviewed since there exists a similarity in switching behavior between films and toroids, and it does not appear that the films' properties are effected by eddy currents.

The reader is assumed to be familiar with the origin of the magnetization of ferromagnetic and ferrimagnetic materials. There exist extensive discussions of these topics (1, 2).

Magnetic systems will be represented by a semiclassical model. The magnetization will be taken to be continuous, and, in dealing with ferrimagnetic systems, the properties of the individual sublattices will be so averaged as to make it possible to treat the material as consisting of a single magnetic lattice. The resulting model is identical to that used by Landau and Lifshitz (3). It is commonly used at the present time in ferromagnetic resonance problems (4, 5).

2. BASIC INTERACTIONS

In this section, the basic interactions which are required to understand magnetization processes in ferromagnetic materials will be discussed. It is

usual to treat these interactions phenomenologically (6), and it will be done so here. In part, this type of treatment is required since these basic interactions have not as yet been completely determined from fundamentals. The interactions which will be discussed arise from exchange, anisotropic, magnetoelastic, and magnetostatic effects.

a. Exchange interactions

In ferromagnetic materials strong short range interactions exist which order the spin magnetic moments in opposition to thermal randomizing effects and which are responsible for their ferromagnetism. The range of these interactions, which are known as exchange interactions, is generally limited to nearest neighbors and is written as a potential energy which has the form

$$-2JS_1 \cdot S_2, \tag{1-1}$$

when it is assumed that quantum mechanical spin operators can be replaced by classical vectors. Here S_1 and S_2 are spin angular momentums in units of $h/2\pi$ of two neighboring spins, and J is the exchange integral. The total exchange energy, F_{ex}, for a homogeneous system of spins is then

$$F_{ex} = -2J \sum_{i \neq j} S_i \cdot S_j, \tag{1-2}$$

where the sum is over nearest neighbors.

Equations (1-1) and (1-2), which apply to an atomic model, can be transformed to a continuous one. When this is done, the exchange energy density, E_{ex}, is found to be

$$E_{ex} = \frac{A}{M^2} [(\nabla M_x)^2 + (\nabla M_y)^2 + (\nabla M_z)^2] \tag{1-3}$$

for cubic materials. M is the magnetization, M_x, M_y and M_z are its rectangular components, and A is the exchange stiffness constant which is related to the exchange integral by

$$A = \frac{2JS^2}{a} \quad . \tag{1-4}$$

Here a is the lattice constant. The derivation of Eq. (1-3) from Eq. (1-2) is given by Kittel and Galt (7).

Examination of either Eqs. (1-1), (1-2), or (1-3) shows that an increase in the exchange energy can be expected if the magnetization takes on any orientation other than a parallel alignment. However, if the change in orientation is sufficiently gradual, the increase in energy may be small.

In ferrimagnetic materials, such as ferrites and garnets, where the net magnetization results from the vectorial addition of the magnetization on each sublattice, the exchange interactions take place through oxygen atoms. For the purpose of determining nearest neighbors only those ions which remain after the oxygen atoms are removed are considered. Two types of nearest neighbors are required; those which reside on the same sublattice and those which inhabit the other sublattices.

To account for the properties of ferrites Néel (8) and others have shown that two sublattices are sufficient. If these two sublattices are denoted by A and B, their spins by S_A and S_B (in units of $h/2\pi$), and the exchange interactions within A, within B, and between the two lattices as J_A, J_B and J_{AB} respectively, then the exchange stiffness parameter which reduces the normal ferrite problem to a single lattice continuous problem has been found by Kaplan (9) to be

$$A = \frac{2}{a}\left[\frac{11}{2} J_{AB} S_A \cdot S_B + J_{AA} S_A^2 + J_{BB} S_B^2\right], \tag{1-5}$$

where a is the side of the unit cell. All exchange integrals are usually negative and $|J_{AB}|$ is much larger than either $|J_{AA}|$ or $|J_{BB}|$. For inverted ferrites, i.e., those ferrites in which one of the sublattices has two species of ions, additional terms proportional to the difference in their spin are required, as shown by Kouvel (10).

In the iron garnets, the situation is similar. However, three sublattices are required in order to account for the magnetization. Two of the three sublattices contain ferric ions while the third sublattice contains either a nonmagnetic yttrium ion or a trivalent rare earth ion. The interaction of this third lattice with the other lattices is sufficiently weak so that its presence may be ignored in computing the effective exchange stiffness constant so that the value of A,

$$A = \frac{1}{4a}\left(32J_{BB}S_B^2 + 20J_{AB}S_AS_B + 12J_{AA}S_A^2\right), \tag{1-6}$$

which has been determined for yttrium iron garnet by Douglas (11) and Harris (12) is applicable to all the rare earth garnets. For the iron garnets

$$S_A = S_B = \frac{5}{2},$$

and (1-7)

$$A = \frac{25}{4a}\left(8J_{BB} + 5J_{AB} + 3J_{AA}\right).$$

The value of A for the garnets is discussed further in Chap. VI.

The value of A for almost all materials is of the order 10^{-6} erg/cm. Measurements of A have been few. Until recently A has been predominantly determined from specific heat data. It can also be determined from the decrease with temperature of the saturation magnetization, but the effects are extremely small in the low temperature region where the best determination is available. Specific heat measurements, which are proportional to the derivative of the magnetization with respect to temperature, improve the accuracy of the determinations.

More recently determinations of the exchange constant have utilized ferromagnetic resonance techniques. By exciting certain nonuniform modes, Tannenwald and Seavey have measured A in thin films of cobalt (13) and iron nickel (14) alloys. Using another ferromagnetic resonance technique, LeCraw and Walker (15) have determined the temperature dependence of A in yttrium

iron garnet. These workers have found that A decreases with increasing temperature and may be accounted for by substituting for S in Eq. (1-6) the appropriate values determined from the sublattice magnetizations. For a ferromagnetic material, this is equivalent to A varying as M^2.

Many authors have determined A from an approximate relation of the form,

$$A = CkT_c/a, \tag{1-8}$$

when other measurements were not available. Here T_c is the Curie temperature, k is Boltzman's constant, and C is a constant of order 1. From an elementary point of view, the proportionality between A and T_c can be understood by noting that the stiffer the exchange interaction, the less will be the randomizing influence of temperature and, hence, the higher Curie temperature.

b. Magnetostatic energy

The work done when a magnetic dipole of moment, μ, is immersed in a magnetic field, H, is known as the magnetostatic energy. The magnetostatic energy, F_m, is

$$F_m = -\mu \cdot H \tag{1-9}$$

and may be thought of as the work required to bring the dipole from infinity to the field H. From Eq. (1-9) stems the alternate interpretation that F_m is the work done in rotating μ against the field from a position normal to H.

If the magnetic moment is a part of the total magnetization, M, of a material, this type of energy may arise from the magnetic moment's interaction either with an external field, H, or with a field, H_D, produced by the remainder of the magnetization. In the former case, the magnetostatic energy density can be written as

$$E_H = -M \cdot H, \tag{1-10}$$

while in the latter case

$$E_D = -\frac{1}{2} M \cdot H_D. \tag{1-11}$$

The field, H_D, and the energy, E_D, are known as the demagnetizing field and energy. The one half arises, as in all self energy calculations, to avoid the counting of mutual interactions twice.

The field, H_D, is the solution of Maxwell's equations in the absence of currents. The appropriate equations for this case are

$$\nabla \cdot H_D = -4\pi(\nabla \cdot M) \tag{1-12}$$

$$\nabla \times H_D = 0 \tag{1-13}$$

with the boundary conditions

$$n \cdot (H_{D_1} - H_{D_2}) = -n \cdot 4\pi M_1 \tag{1-14}$$

and

$$n \times (H_{D_1} - H_{D_2}) = 0. \tag{1-15}$$

Here H_{D_1} and M_1 are the field and magnetization, respectively, inside the sample while H_{D_2} is the field outside the sample at the boundary.

Equations (1-12) and (1-14) show that the origins of the field can be taken as the volume pole distribution, ρ_v, given by

$$\rho_v = \nabla \cdot M, \tag{1-16}$$

and the surface pole distribution, ρ_s, determined from

$$\rho_s = n \cdot M. \tag{1-17}$$

Hence, the energy, E_D, may be thought of as arising equivalently from the work done in either the creation of the field, H_D, or the establishment of the pole distributions, ρ_s and ρ_v.

H_D is zero in a toroid when the magnetization has the distribution shown in Fig. 1-1.

H_D is uniform only in ellipsoids. For these shapes H_D is proportional to the magnetization. The proportionality factors which are also known as demagnetizing factors have been tabulated by Osborn (16). From this tabulation or by direct calculation, the demagnetizing factors are found to be 4π for the magnetization which lies normal to the surface of a thin slab, zero for the magnetization which lies parallel to the slab, $\frac{4\pi}{3}$ for a sphere, 2π for the transverse magnetization of an infinite cylinder and zero for the axial magnetization.

c. Anisotropy energy

The amount of work required to saturate a magnetic material has been found to be related to the direction which the applied field makes with the body. The additional energy required to magnetize the body in a particular direction over that energy which is required to magnetize the body in the lowest energy direction is known as the anisotropy energy. The directions requiring the largest and least energy are referred to as hard and easy directions, respectively.

Anisotropic magnetizing effects have their origin in a number of sources. The three sources which are of importance here are: the shape of the specimen, the interaction of the magnetization and the crystal lattice, and the interaction of the magnetization with the strains which exist in, or are applied to, the specimen.

The first of these is accounted for by demagnetizing fields, the strength of which depend not only on the shape of the body but also on the direction of the magnetization.

The second source, known as the magnetocrystalline anisotropy, results from the interaction of the magnetization and its environment in the crystal. Since the anisotropy is an interaction with the crystal lattice and the magnetization orientation, it must be expressible as an angular function which reflects

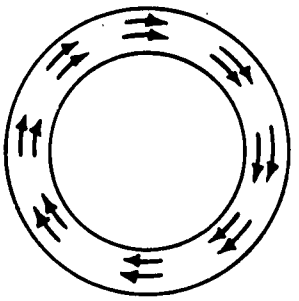

FIG. 1-1 MAGNETIZATION DISTRIBUTION WITHOUT DEMAGNETIZATION.

the over-all symmetry of the crystal. For cubic crystals the anisotropy energy, E_K, may be expanded as

$$E_K = K_1 (\alpha_1^2 \alpha_2^2 + \alpha_3^2 \alpha_1^2 + \alpha_3^2 \alpha_2^2) + K_2 \alpha_1^2 \alpha_2^2 \alpha_3^2 + \ldots + \ldots, \tag{1-18}$$

where α_1, α_2, and α_3 are the direction cosines describing the magnetization's orientation with the three mutually perpendicular principal axes of the crystal. When K_2 is zero or small compared to K_1 and $K_1 > 0$, the six $\{100\}$ directions are the axes of easiest magnetization; when $K_1 < 0$, the eight $\{111\}$ are the easy directions. With the exception of cobalt ferrite, all the ferrites of composition MFe_2O_4, where M is an appropriate divalent ion, and the garnets have a negative K_1.

The magnetocrystalline anisotropy is extremely temperature sensitive and strongly dependent on chemical composition. K_2 is small in most materials and will be neglected in what follows.

The measurement of the anisotropy constant is always made in single crystals and is frequently made either at microwave frequencies using the methods of ferromagnetic resonance or at d.c. by measuring the torque, which is the angular derivative of the energy, that is required to turn a specimen in a magnetic field through an angle θ. Comparison of the data taken by these methods shows generally good agreement. However, low temperature measurements of ytterbium iron garnet and ferrites which contain ferrous ions show deviations.

Typical values of K_1 for a number of cubic ferrites and garnets may be found in Chap. III. The anisotropy of ferrimagnets is further discussed in Chap. VI.

In hexagonal materials, the anisotropy energy has the form

$$E_K = K_1 \sin^2\theta + K_2 \sin^4\theta + \ldots, \tag{1-19}$$

where θ is the angle that the magnetization makes with the c-axis. When $K_2 < K_1$ and $K_1 > 0$, the c-axis will be preferred, and the crystal can be

referred to as uniaxial. When $K_1 < 0$, any direction within the basal plane is an easy direction.

The third cause of an anisotropic dependence, the magnetoelastic effect, is due to the coupling of the magnetization with the stresses that arise during the material's preparation, are externally applied, or are due to a magnetization process. In the phenomenological treatment of this effect, it is introduced as the strain dependence on the magnetocrystalline energy, and it is found that this energy depends on the direction which the magnetization makes with the stress and with the crystal lattice. However, for most purposes, it has been found sufficient to account for these properties by using a form for the magnetoelastic energy, E_λ, which neglects the crystal directions and considers only the angle, θ, between the strain, σ, and the magnetization.

$$E_\lambda = \frac{3}{2} \lambda \sigma \sin^2 \theta . \qquad (1\text{-}20)$$

λ is the so-called isotropic saturation magnetostriction constant, and, within a factor of the order of 1, it represents an average, over all directions, of the fractional change in length accompanying the saturation of the magnetization. Several cases should be distinguished; those materials which contract and those which expand along the direction of the applied field, and those which expand and contract transverse to the applied field. The sign for the two directions may, or may not, be the same. These latter effects are neglected when the isotropic constant is employed.

For yttrium iron garnet (17), the isotropic magnetostrictive constant is

$$\lambda = -2 \times 10^{-6},$$

while for nickel and cobalt ferrite (18), it is

$$\lambda(\text{Ni}) = -26 \times 10^{-6}$$
$$\lambda(\text{Co}) = -110 \times 10^{-6}.$$

In general, λ is negative for all the ferrites, except magnetite (18).

3. DOMAINS AND DOMAIN WALLS

Having introduced the elementary magnetic interactions, the magnetization processes which they enter into and produce will be examined. We begin with the effects that may be discerned in static or quasi-static observations of a specimen's magnetization distribution. In these cases, magnetostatic effects having their origin in surface poles will be seen to give rise to a systematic structure of uniformly magnetized regions – magnetic domains. The boundaries of these regions, domain walls, will be examined, and the role they play in determining domain structure will be indicated. The domains which are produced by other than surface magnetostatic effects will then be discussed.

a. Domain theory

Consider a circular disk which is uniformly magnetized transverse to its axis as shown in cross section in Fig. 1-2a. The poles which are formed on the edges of the disk by this distribution produce a demagnetizing field, H_D, inside the disk which can, to a first approximation, be taken as uniform. H_D can then be written as

$$H_D = 2\pi kM, \tag{1-21}$$

where M is the disk's magnetization and k is a constant which depends on the disk radius, R, and its thickness, T. Under these conditions, the magnetic energy is the magnetostatic energy, E_D, which from Eq. (1-11) is

$$E_D = \pi^2 kM^2 R^2 T. \tag{1-22}$$

If, however, we neglect, for the moment, the material's magnetocrystalline anisotropy, and its magnetization is distributed as shown in Fig. 1-2b, the magnetostatic energy can be eliminated at the expense of the exchange energy. To compute this increase in exchange energy, a cylindrical polar coordinate system is established such that the z-axis is normal to the disk, and the origin is at its center. Taking θ as the polar angle, the

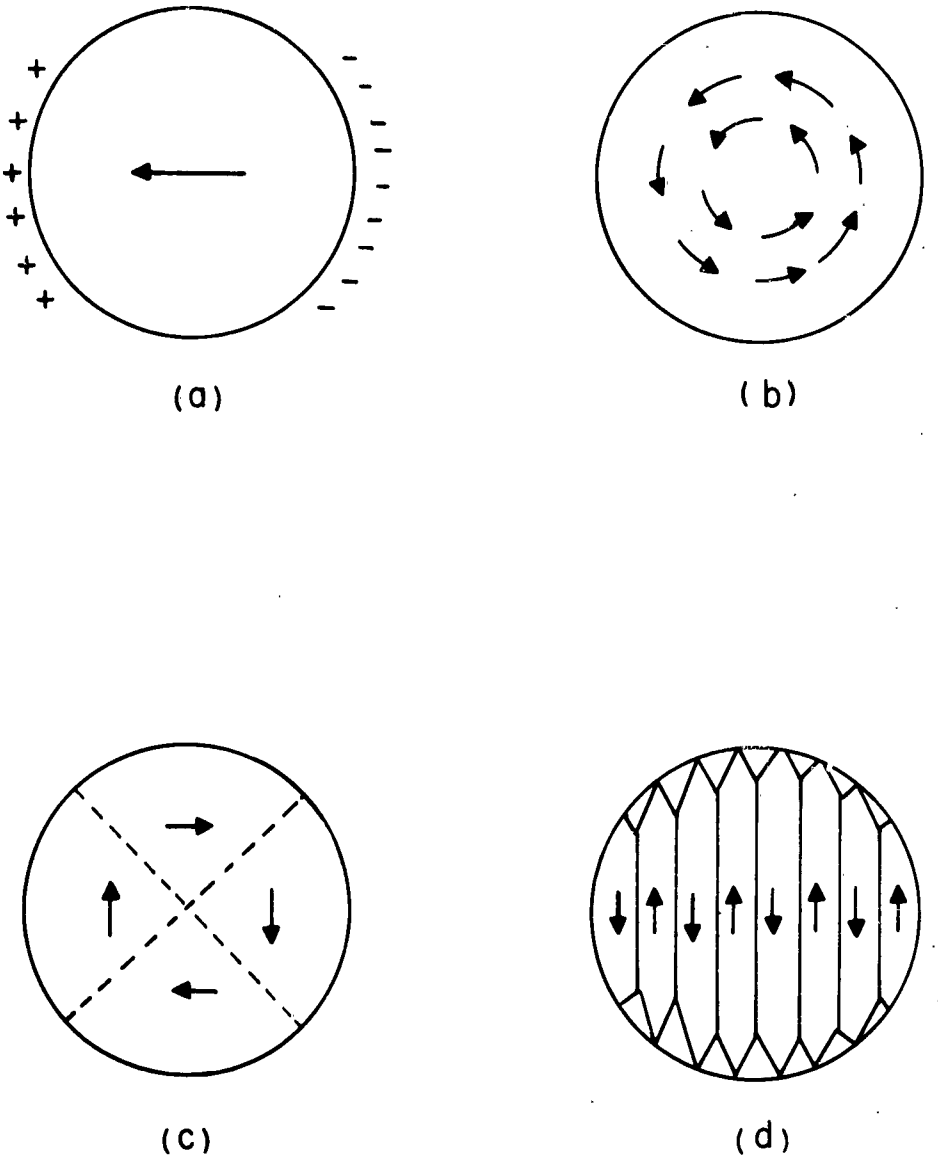

FIG. I-2 EVOLUTION OF DOMAIN STRUCTURE

direction cosines of the magnetization distribution shown in Fig. 1-2b are $\sin\theta$, $\cos\theta$ and 0. Then from Eq. (1-3), the increase in exchange energy is found to be

$$f_{ex} = A\left[\left(\frac{d\theta}{dx}\right)^2 + \left(\frac{d\theta}{dy}\right)^2\right].$$

Since $\tan\theta = \frac{y}{x}$, the above equation becomes

$$f_{ex} = \frac{A}{r^2}, \tag{1-23}$$

where r is the radius vector to the point in question. The total exchange energy is then

$$E_{ex} = AT\int_a^R \int_o^{2\pi} 1/r^2\, rdrd\theta = 2\pi AT \log R/a, \tag{1-24}$$

where a is the lattice constant. The integration proceeds from a in order to avoid a singularity which would otherwise appear at the origin. This difficulty is avoided by the discreteness of the actual lattice.

Comparison of Eqs. (1-22) and (1-24) then shows that, for a sufficiently large disk radius, the magnetization distribution of Fig. 1-2b has lower energy than that of Fig. 1-2a, and it is this distribution which is favorable when the anisotropy energy can be neglected.

If, however, the anisotropy is appreciable, the energy of the distribution of Fig. 1-2a would have to include a term in the anisotropy energy. If the crystal symmetry is cubic and if the disk is a single crystal whose surface is a (100) plane, then from Eq. (1-18) the anisotropy energy density, f_K, in this plane is found to be

$$f_K = K_1 \sin^2\theta \cos^2\theta = \frac{K_1}{4}\sin^2\theta.$$

The total anisotropy energy contribution, E_K, to the energy is then

$$E_K = \pi R^2 T K_1. \tag{1-25}$$

A comparison of this energy with the exchange energy, Eq. (1-24), shows that $E_K > E_{ex}$, and a new minimum energy distribution must be sought. The anisotropy energy can be considerably reduced if the arrangement shown in Fig. 1-2c is adopted by the magnetization. In this distribution, the magnetization only changes direction in the vicinity of the planes indicated by the dashed lines. Whether this distribution has a lower energy than that of Fig. 1-2b will depend on the energy of these transition regions.

b. Domain walls

The transition regions referred to above are also known as Bloch walls, domain walls, or domain boundaries. Here a number of properties of the walls will be discussed. In the example of the preceding section, the walls appeared between domains whose magnetizations differ in direction by 90°. However, under circumstances which will be discussed below, walls occur between domains whose magnetization directions differ by angles other than 90°.

It should immediately be recognized that a domain wall represents a higher energy state than a uniformly magnetized region, since it is in the wall that the magnetization rotates from one easy direction to another, bringing about an increase in the exchange energy. In addition, if the wall has any significant width, an increase in the anisotropy energy will also occur since the magnetization inside this region cannot be along an easy direction. Indeed, if the magnetization within a domain is not along an easy direction, this also will represent a high energy state. Hence it may be expected that generally the magnetization within a domain will lie along an easy direction, and this is found to be true. Under these circumstances the difference in the direction of the magnetization on each side of a wall will reflect the angular differences in easy direction.

It may be expected that a magnetostatic contribution should also exist. However, in the cases which we shall presently discuss $\nabla \cdot M$ will always vanish.

Although the problems in domain theory require the energies and shape of domain walls in a finite sample, and since these have not as yet been determined, the results for walls in infinite media which have been obtained must be used. The wall energy obtained in this way is probably a lower bound. Also, since our purpose here is to illustrate the principles of domain theory and not to give an exhaustive treatment of the subject, the energy calculation will be performed for a uniaxial material whose exchange energy has the form for cubic materials and whose anisotropy energy takes the form for a uniaxial material. For such a material the mathematical aspects of the problem are less complex than for a cubic material and yield almost identical results. Since the calculations for cubic materials proceed along the same lines, the work of others will be cited. The anisotropy energy density that will be used is

$$E_K = K \sin^2 \theta . \tag{1-26}$$

In uniaxial materials only two preferred directions, $\theta = 0$ and π, exist so that the walls always separate antiparallel domains. Choosing the positive z-axis of a rectangular coordinate system as the $\theta = 0$ direction, a 180° domain wall is formed between the two oppositely oriented domains on either side of the z-x plane.

If the rotation of the magnetization in the wall occurs with the y component of the magnetization vanishing and if the magnetization has a constant orientation in any plane parallel to the y-z plane, no magnetic poles will be formed, and the formation of a wall will not increase the magnetostatic energy. The total wall energy, σ, per unit wall area normal to the y-axis is determined by exchange and anisotropy energies and is

$$\sigma = \int E_{ex}\, dy + \int E_K\, dy. \tag{1-27}$$

The integrations are taken over all space and E_{ex} and E_K are given in Eqs. (1-3) and (1-26). If cylindrical polar coordinates are used to describe the magnetization with θ as the polar angle, then, since $M_y = 0$, the exchange energy reduces to

$$E_{ex} = A \left(\frac{\partial \theta}{\partial y}\right)^2. \tag{1-28}$$

Since this equation considers only variations in a single direction, it is permissible to use Eq. (1-3) which pertains to cubic crystals here. Substituting Eqs. (1-26) and (1-28) in Eq. (1-27) gives

$$\sigma = \int A \left(\frac{d\theta}{dy}\right)^2 + K \sin^2\theta \, dy \tag{1-29}$$

for the wall energy, and our problem reduces to finding $\theta = \theta(y)$ such that σ is a minimum and $\theta = 0$ at $y = -\infty$.

The Euler equation for Eq. (1-29) is

$$A \frac{d^2\theta}{dy^2} = K \sin\theta \cos\theta. \tag{1-30}$$

A first integral is obtained by multiplying by $\frac{d\theta}{dy}$ and integrating. This gives

$$A \left(\frac{d\theta}{dy}\right)^2 = K \sin^2\theta + c. \tag{1-31}$$

A consequence of the variational procedure which leads to the Euler equation, Eq. (1-30), is that

$$\frac{d\theta}{dy} = 0 \tag{1-32}$$

at the boundary where $\theta = 0$ so that c in Eq. (1-31) vanishes, and this equation becomes

$$A \left(\frac{d\theta}{dy}\right)^2 = K \sin^2\theta \tag{1-33}$$

which may be integrated to give

$$\ln \tan \theta/2 = \sqrt{\frac{K}{A}}\, x, \tag{1-33a}$$

where $\theta = \pi/2$ has been placed at $x = 0$, i.e., the middle of the wall. This equation gives the course of the magnetization through the wall. The energy of the wall is determined by using Eq. (1-33) to find

$$dy = \sqrt{\frac{A}{K}}\, \frac{d\theta}{\sin \theta} \tag{1-34}$$

which is substituted in Eq. (1-29) together with Eq. (1-33) giving

$$\sigma = 2 \int_0^{\pi} \sqrt{AK}\, \sin \theta\, d\theta = 4\sqrt{AK}. \tag{1-35}$$

A domain wall in a uniaxial material has a surface energy density of $4\sqrt{AK}$, and it is infinite in extent as seen from Eq. (1-33a). However, a graphical examination of Eq. (1-33a) (see Fig. 1-3) shows that the significant part of the rotation is in a distance of 6 or 7 $\sqrt{A/K}$ units.

From Eq. (1-33) the total domain wall energy is seen to be composed of equal contributions of the exchange and anisotropy energies. Equation (1-30) shows that within the wall the exchange torques are balanced by the anisotropy torques. These last two characteristics are generally true of all types of domain walls.

In cubic materials the specifications of domain walls entail additional information. When $K > 0$, 90° walls, as shown in Fig. 1-2c, can be found in addition to 180° walls. In the negative K case, 70.5°, 109.5° and 180° walls must be considered. The transitions from one domain to another may also occur along various directions. Lilley (19) has evaluated the energies for many of these cases. From his results a number of wall energies and widths are given in Table 1-1.

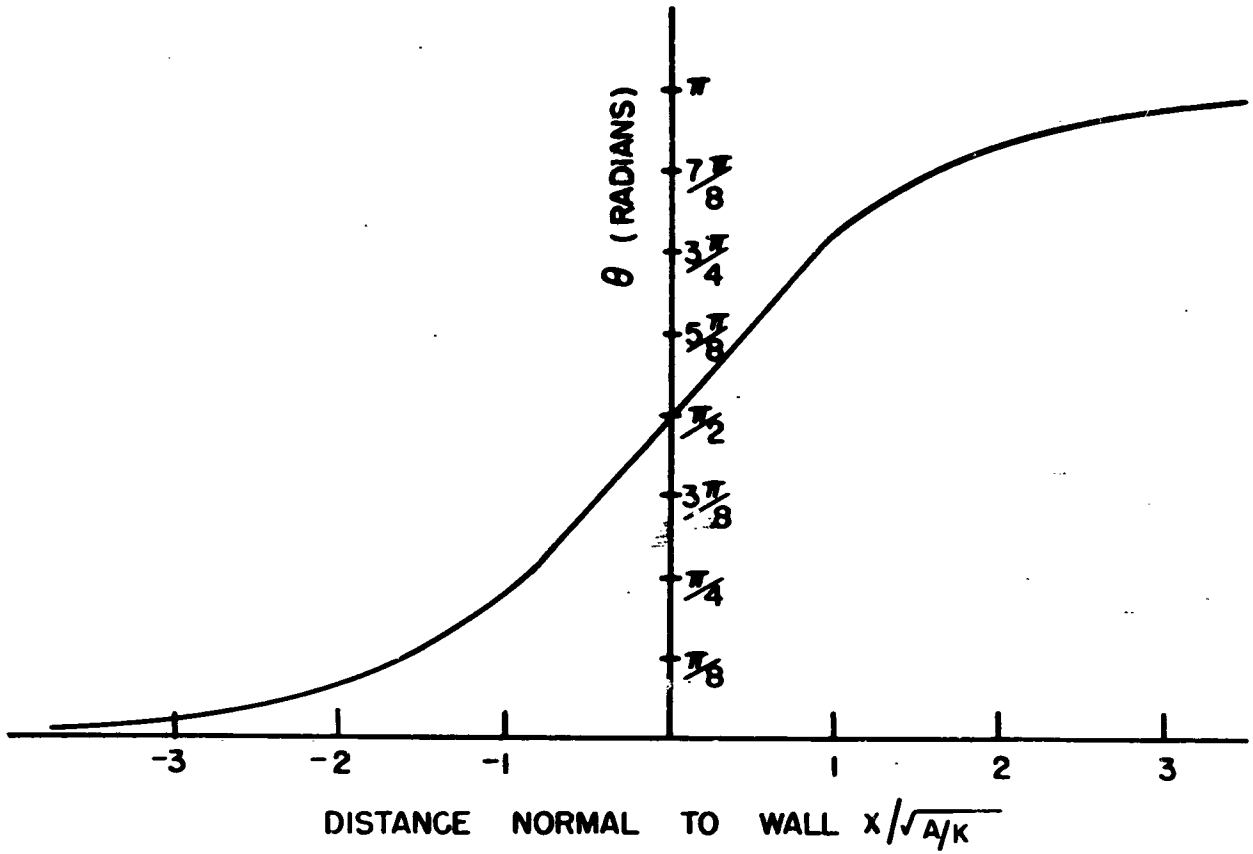

FIG. 1—3 THE ANGULAR ROTATION IN A 180° DOMAIN WALL IN A MATERIAL WITH UNIAXIAL ANISOTROPY.

TABLE 1—1

WALL WIDTHS AND ENERGIES (AFTER LILLEY[13])
ENERGY σ IN UNITS $\sqrt{AK}$; WIDTHS δ, UNITS $\sqrt{A/K}$
CUBIC ANISOTROPY

ANISOTROPY	WALL ANGLES	DIRECTION 001		OF WALL 110		NORMAL 111		$\bar{1}\bar{1}2$	
		σ	δ	σ	δ	σ	δ	σ	δ
$K<0$	70.53	0.54	3.8	0.46	4.3	—	—	—	—
	109.47	1.09	00	1.37	3.3	1.29	3.8		
	180			1.83	00	—	—	2.00	7.9
$K>0$	90	1.00	π	1.72	4.0	1.19	π	—	
	180	2.00	00	2.76	5.6			—	

c. Domain theory continued

Having obtained the properties of the domain walls which are required, the discussion of the domain structure of the disk is continued.

If the walls which occur in Fig. 1-2c have energy σ, then the energy of this arrangement, E_w, is

$$E_w = 4\sigma TR, \tag{1-36}$$

when the contributions to the magnetostatic energy are neglected. Since these walls have a normal along the [110] direction, their energy can be found from Table 1-1 to be

$$\sigma = 1.7\sqrt{KA} \tag{1-37}$$

which gives for the total energy

$$E_w = 6.8\ TR\sqrt{KA}. \tag{1-38}$$

When Eq. (1-38) is compared with Eq. (1-25), it is again seen that for sufficiently large R the arrangement of Fig. 1-2c is of lower energy. However, as a result of magnetoelastic effects, this configuration can have a large elastic energy. If this material has a positive magnetostriction, the quadrant domains are elongated and must be in a state of stress as long as the configuration is stable. This stress is greatly relieved, however, if there occurs a breakup of the domains into the slab-like construction shown in Fig. 1-2d. The strain energy is reduced at the expense of an increase in the number of domain walls. The magnetostatic energy, which again is neglected, has also been reduced below that of Fig. 1-2c. The dimensions of these slabs will now be determined using the symbols defined in Fig. 1-2d.

If an additional magnetostatic energy contribution is to be avoided by this structure, the walls must be placed so that the component of the magnetization normal to the wall is continuous. This requirement then fixes the angle between the 90° walls and the 180° walls in Fig. 1-2d as 135°.

Since the calculation can be managed more readily if the slab-like construction is uniform and if each slab has the shape and dimensions shown in Fig. 1-4, such an arrangement will be assumed.

The total energy then is in part the wall energy and in part the magnetoelastic energy stored in the wedges.

If the slabs are taken as rigid, the magnetoelastic energy stored in the wedges will be approximately

$$c\lambda^2 \frac{d_1^2}{4} T \quad ,$$

where c is the appropriate elastic modulus. Since the number of wedges is approximately $\frac{2R}{d_1}$, the total strain energy, E_λ, will be

$$E_\lambda = c\lambda^2 \frac{d_1 R}{2} T \quad . \tag{1-39}$$

The wall energy, E_w, is

$$E_w = \frac{2R}{d_1} d_2 T\sigma + \frac{4R}{d_1} \frac{d_1}{\sqrt{2}} T\sigma \quad , \tag{1-40}$$

so that the total energy is

$$E = c\lambda^2 \frac{d_1 R}{2} T + \frac{2R}{d_1} d_2 T\sigma + 2\sqrt{2}\, RT\sigma \quad , \tag{1-41}$$

and the d_1 which minimizes this E is

$$d_1 = \sqrt{\frac{4\sigma d_2}{c\lambda^2}} \quad . \tag{1-42}$$

From this specific discussion of domain structure several features which have a larger range of application may be noted. It is generally found that domain structure disappears in small particles since the driving force for the structure is magnetostatic energy, which is a volume effect, while the energy of the structure usually depends on surface effects. Since volume effects decrease faster than surface effects with a decrease in size, the disappearance

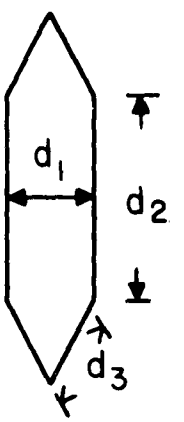

FIG. 1-4 A DOMAIN SHAPE

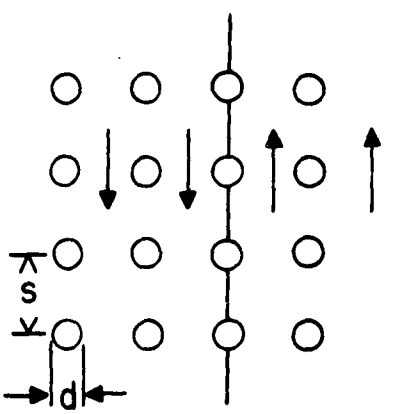

FIG. 1-6 DOMAIN WALL IN A POROUS MEDIUM IN ITS LOW ENERGY POSITION

of structure is to be expected. Further, the size of the domains is related to the size of the specimen. This may be seen in Eq. (1-42) by identifying d_2 with the specimen size. The point here is that the domain size is not a fundamental constant of the material.

The manner in which the domain discussion has proceeded should be noted, for it is a typical one. Instead of indicating the origin of the structure, domain theory assumes the structure and chooses the dimensions of the domains to minimize its energy. In each case the wall energy is determined from a separate calculation. The alternative, and more rigorous, procedure is to perform a calculation, much like the domain wall calculation, for a finite specimen and to include in it all the various energy contributions. As yet this variational problem has not proven tractable.

The experimental verification of domain theory has been made by a number of techniques. The two most useful have been the Kerr magneto-optic effect (20) and Bitter pattern (21).

The Kerr effect depends on the magneto-optic interaction which, in essence, rotates the plane of polarization of a polarized light beam when it is reflected from a magnetized surface. The direction and magnitude of the rotation are proportional to the orientation of the magnetization. 180° domains which are observed through a properly set analyzer give a black and white appearance.

The Bitter pattern technique employs a colloidal suspension of Fe_3O_4 in a soap solution. This suspension is deposited on a properly prepared surface of the specimen. The Fe_3O_4 collects wherever magnetic poles exist on the surface, and since this occurs most frequently when domain walls intersect the surface, the Bitter patterns usually show only the outlines of domains. It is in this manner that the technique has been most valuable. The surface preparation differs according to the structural form of the specimen which is to be examined. Thin films which have been vapor deposited in a vacuum and whiskers

require no surface preparation. However, the surfaces of bulk materials must first be polished and then treated to remove the resulting strain layer. In metals this layer is removed by an electrolytic polish, while in ferrites the surface is strain relieved by an anneal at the sintering temperature. This latter treatment preserves the polished surface and at the same time makes apparent the grain boundaries in polycrystalline specimens.

A number of the magnetic oxides are transparent when they have been made sufficiently thin, and for these oxides the magneto-optic Faraday effect (22) (polarized light in transmission as opposed to the Kerr effect in reflection) has been used to examine the domain structure. It appears, however, from the observations which have been made on yttrium iron garnet and other garnets that the mechanical operations which form the thin section leave large strains in the surface.

In preceding discussions, the relation of the external surface to the domain structure of a single crystal has been given. There do, however, exist other origins for the magnetostatic forces which bring about domains. A number of these will be considered here. In each of these cases it is again the reduction of magnetostatic energy which serves as the motivation.

Consider a nonmagnetic inclusion in a uniformly magnetized material as shown in Fig. 1-5a. Since poles form on the inclusion, the inclusion will cause an increase in the energy of the material. The size of this energy will, however, depend on the domain structure which surrounds the inclusion. If the inclusion's dimensions are large compared to the thickness of a domain wall, then, as Néel (23) has shown, the magnetostatic energy may be decreased by a domain wall which bisects the pore as shown in Fig. 1-5b. This will change the pole's configuration from dipole to quadrapole. The latter is a lower energy state. Other low energy states also occur. In cubic materials a typical state is shown in Fig. 1-5c. The magnetostatic energy is lowered in this state by a reduction in pole density.

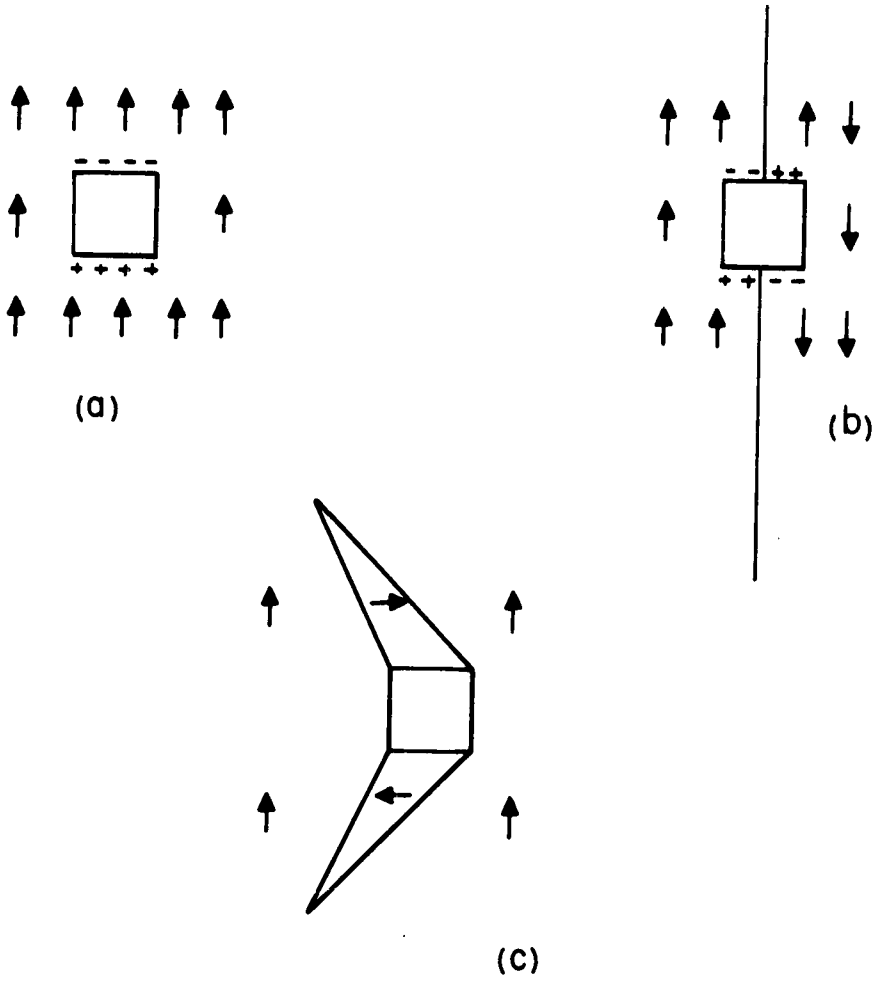

FIG. 1-5 MAGNETIZATION DISTRIBUTION AROUND A PORE

If a strain field which changes direction with position exists in a material, it can cause the magnetization to vary its orientation with position. Under these conditions pole concentrations can develop in various regions. If a domain wall bisects these pole concentrations, a reduction in domain wall energy again occurs by the transformation of the dipole-like distributions to quadrapole-like distributions. When these strain distributions make certain locations preferable for domain walls, the wall energy becomes a function of position through strain, and the total wall energy includes a magnetostatic contribution.

Polycrystalline materials have not yet been discussed, for, in principle, the same laws govern their domain distributions as govern the domain distribution in single crystals which are easier to study. A major difference between the two is that in the polycrystalline material magnetostatic energy depends not only on the specimen's surface but also on the relationship of the magnetization in a grain to the magnetization in surrounding grains. Large grains may contain many domains, and Goodenough (24) has proposed that the magnetization distribution in these grains consists of a periodic arrangement of domains.

From considerations identical to those which determined the minimum single crystal size required for domains, it might be concluded that domains should be absent from a fine grained dense material. However, direct observation of domains in fine grained thin magnetic films shows that this is not the case. Prahe (25) has suggested that in fine grained materials the domains will be aggregates of grains and that the domain boundaries will lie along grain boundaries.

4. MAGNETIZATION PROCESSES

The ways in which magnetization changes take place, without regard to the rate at which these changes occur, are considered here. The various processes by which the changes proceed, the forces required to initiate these

mechanisms, and the state in which they leave the material are examined. Since our interest lies in switching properties, coercive forces are restricted to about 10 oe and the range of applied fields to within an order of magnitude of the coercive force. Therefore, the maximum applied field always remains small compared to the field required to bring about absolute saturation.

a. Types of processes

From the discussion of domain structure it follows that the net magnetic moment along a particular direction in a ferromagnet is determined by the sum of the components of the magnetic moments of the individual domains in that direction. If there are N domains and if the magnetization of the i^{th} domain is M_i, its volume is v_i, and the angle it makes with the direction of measurement is ϕ_i, then the magnetic moment, I, of the material is

$$I = \sum_i M_i v_i \cos\phi_i . \qquad (1\text{-}43)$$

From this equation, one can see that the change in magnetic moment is given by

$$dI = \sum_i M_i \cos\phi_i dv_i - \sum_i M_i v_i \sin\phi_i \, d\phi_i + \sum_i v_i \cos\phi_i dM_i \qquad (1\text{-}44)$$

and that the changes occur by the one or more processes which change the volume of the domain, rotate the magnetization in a domain, and increase the intrinsic magnetization. Since this latter process only occurs at large fields, it will be ignored hereafter.

The change in domain volume can be brought about either by motion of the walls which surround it or by a rearrangement of the domain structure. This latter process, however, is a special case of a rotation process.

Rotation processes may be distinguished from domain wall motion processes by the sequence of rotations which transpires during a change. When, in regions of the size of domains, the change of every magnetic moment

occurs simultaneously, the process is rotational. On the other hand, if the change takes place through a sequential rotation of the magnetization, the process is domain wall motion. This type of motion may occur simultaneously in a number of places in the specimen.

Rotation processes may be further classified as pure or nonuniform. During a pure rotation, the aligned magnetization retains its relative spacial orientation. During a nonuniform rotation, all of the magnetization rotates simultaneously without retaining its initial relative spacial orientation. This may happen in a number of different ways.

Mixed processes in which a sequence of domain wall motions and rotation processes is needed to bring about the changes also transpire.

These various processes are distinguished in order that comparisons of their field dependent behavior in an applied field may be obtained; for, as in the domain structure problem, an analytical procedure from which the most favorable distribution can be obtained is lacking. Instead, the fields required to initiate and continue the magnetization change for each of the various processes are determined individually. The process which requires the smallest field for initiation can be expected to bring about the change. When the applied field is large, two processes may be activated. The process which requires the shorter time to complete is the important one.

Both rotation and domain wall motion may be thermodynamically reversible or irreversible. The irreversible processes are usually known as switching or flux reversal processes. When they are prevented from going to completion by fields either of insufficient strength or of too short duration, partial switching or partial reversal occurs.

When a magnetic field is applied to a specimen, its magnetic energy is augmented by a magnetostatic term, E_H. Writing E_ρ for the remaining contributions to the magnetic energy which are functions of the magnetization distribution, the total

energy, E, is

$$E = E_H + E_\rho. \tag{1-45}$$

If q is one of the variables describing the magnetization, a change in distribution will occur when the field is applied and when

$$\frac{\partial E}{\partial q} \neq 0 \tag{1-46}$$

or

$$\frac{\partial E}{\partial q} = 0 \tag{1-47}$$

and

$$\frac{\partial^2 E}{\partial q^2} < 0. \tag{1-48}$$

Equation (1-46) applies when the field places the magnetic system in a non-equilibrium state. Equations (1-47) and (1-48) cover the case of finding the system in an unstable equilibrium. All the derivatives in Eqs. (1-46), (1-47) and (1-48) are evaluated for the equilibrium distribution existing before H is applied. If, during the course of the change, H is increased and, at some q, $\frac{\partial^2 E}{\partial q^2}$ changes sign to become positive, then an irreversible change occurs.

b. Domain wall processes

Some of the concepts of the last paragraph above are applied here to domain wall processes. For simplicity, a 180° domain is considered, and the field is applied parallel to the wall.

The excess energy, E_H, due to the applied field is

$$E_H = 2MHV. \tag{1-49}$$

If this domain wall were in a perfect material with infinite dimensions, then there would exist no restoring or resisting forces, and the domain wall would move at the slightest urging. In any finite material, this wall exists only

because domains have formed to reduce the sample's total magnetic energy. Any attempt to move the wall is then resisted by an increase in this energy.

Ordinary materials, which abound with imperfections, can supply many resisting forces. Of these, those which are known to have the greatest effect on wall motion are stress, nonmagnetic inclusions, pores and impurities.

The potential energy of these imperfections has been considered in Sec. 3c where it was seen that walls can lower the energy of a concentration of poles by taking a position which bisects them. An attempt to change this distribution is met with opposition.

As an example of the resistance imposed on wall motion by porosity, consider a regular array of spherical pores whose separation is s and whose diameter, d, is large with respect to a wall width but small enough so that no domain structure forms about the pore, as shown in Fig. 1-6. A wall which finds itself amidst all these pores will take up the position shown by the dotted line. This is the lowest energy position since the domain wall area is minimum here and since the magnetostatic energy is a minimum. If the wall moves, these two contributions to the total energy are increased.

The total wall energy, E, is then

$$E = E_H + E_w + E_M$$

in which E_w is the energy of the wall and is the product of the specific wall energy and the total wall area, and E_M is the magnetostatic energy associated with the position of the wall. For a 180° wall E_H takes the form

$$E_H = 2MHV = 2MHSx. \qquad (1\text{-}50)$$

Here S is the area of the wall, and x is the domain width measured normal to the wall. The wall moves when

$$\frac{dE}{dx} = 0 \qquad (1\text{-}51)$$

or when

$$H = -\frac{1}{2MS}(E_w + E_M). \tag{1-52}$$

The calculations based on this model will not be carried further, for, as Néel (26) has shown, any model which assumes a uniform distribution of obstacles to wall motion is not in agreement with fact, and the results determined from such a model cannot be correct. Moreover, in determining H above, the domain wall has tacitly been assumed to be a rigid plane wall. Usually, one expects this, for if, as an example, a 180° domain wall were not parallel to the magnetization on either side of it, a magnetic field would arise which would restore the parallelism. However, Néel (26) has shown that under appropriate conditions the walls can deform and, hence, leave the imperfections one at a time, thereby giving a smaller value of the coercive force than in the rigid case. Neel also shows that E_M is far more important than E_w and determines the coercive force when the deviations which give rise to E_M have their origin in either magnetoelastic interactions or non-magnetic inclusions.

Although Neel has shown that the term in E_w may be neglected, earlier treatments (27) have used its variations with position to determine coercive forces. Since on numerous occasions these calculations have been in good agreement with experiment, their results will be presented. The factors which may produce variations in E_w can be obtained from the relation

$$E_w = \sigma_w S, \tag{1-53}$$

where σ_w and S are the wall energy and area respectively. An extension of the treatment for domain walls given above shows that the magnetoelastic effects also shape the wall and determine its energy. When account is taken of these effects through λ, the saturation magnetostriction, and σ, the stress, the wall energy becomes

$$\sigma_w = a\sqrt{(K + 3\lambda\sigma/2)A}.$$

α is a constant which depends on the type of wall. It can then be seen that changes in anisotropy, stress, and porosity affect E_w. In some cases variations in A may occur.

This treatment always leads to coercive force variations which are proportional to wall energy and, hence, to $\sqrt{K}$ in the absence of stress.

Néel's (26) treatment, in contrast, leads to the coercive force being proportional to K. The coercive force, H_c, for a material with a volume fraction, v, of nonmagnetic inclusions is

$$H_c = \frac{2Kv}{\pi M}\left[0.386 + \log\sqrt{\frac{2\pi M^2}{K}}\right]. \qquad (1\text{-}54)$$

This equation was evaluated for approximately 40 alloys of iron for which v was known, and the results were compared with experimental determinations. The agreement is indeed impressive.

If the material is in the form of a polycrystalline closed ring or has the shape of a picture frame each of whose sides is an easy direction, then the geometrical shape of the specimen plays no role in providing the domain walls which may be useful to change the magnetization. Under these circumstances, if a domain wall process changes the magnetization, the domain wall needs to be formed. The field required to form this wall, i.e., to form a domain of reverse magnetization, is the nucleating field. It may or may not be greater than the field required to move the wall. Unless extreme care is taken during the determination of the specimen's hysteresis loop, this field value will appear to be the minimum field which can change the magnetization.

Goodenough (24) has established a theory of hysteresis curve shapes in which the curve's shape is determined by the field required to nucleate a reverse domain. When, as in some materials, reverse domains are formed by the reduction of an applied field, a state of low retentivity is left in the

material. The hysteresis curve of this type of material is shown in Fig. 1-7. As the field is reduced and the portion of the curve which lies between A and C is traced out, reverse domains form. When the field is reversed and subsequently increased, these domains grow until the reversal is complete. At this time point D is reached, and when the field is decreased, identical nucleation processes occur from D to E as did in going from A to C. In square loop materials, according to this theory, no domains are nucleated during the AC portion of the loop. Domains only form when the field is reversed and increased. Then, according to this theory, when the reverse domains occur, they are accompanied by a large change in magnetization if the nucleating field, H_n, is larger than H_c, the field required to move the domain walls. Otherwise, further increases in the applied field are required to change the magnetization.

Goodenough has also determined the field required for the nucleation of reverse domains and the conditions for the existence of square loop materials. In this theory, the applied field is aided in bringing about the nucleation by the fields produced by the poles which reside on the boundaries between grains whose crystallographic directions do not coincide.

The coercive force is determined from the increase in magnetostatic energy arising from the displacement of the walls from their nucleated positions and the increase in wall area as a result of the growth of the nucleated domains. It is found to be

$$H_c = a_1 M + a_2 \frac{\sigma_w}{M} \tag{1-55}$$

$$= a_1 M + a_2 \frac{\sqrt{KA}}{M} . \tag{1-56}$$

a_1 is determined by the relative crystal orientations of the grains, and a_2 is the fractional rate of change of wall area with position.

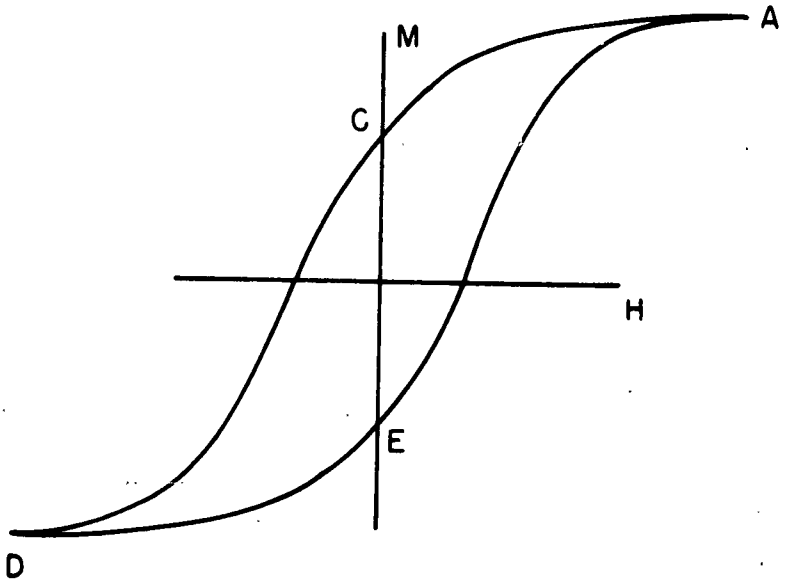

FIG. I-7 HYSTERESIS LOOP

c. Experimental observations

The presentation of a comparison of theoretical conclusions with experimental results has been postponed until now for two reasons. In the first place, we are now in a position to recognize that domain walls are affected by many influences beyond the reduction in external magnetostatic energy to which their existence was initially ascribed. In the second place, the experimental position appears in a better light when magnetization changes are considered together with the static distributions.

All of the essential predicated features of domains have been observed. Domain structure has been seen to exist about nonmagnetic inclusions which are sufficiently large (28). Predicted domain patterns on the surface of silicon iron specimens have been seen (29). Closure domains (29) and domain nucleation at grain boundaries have been observed. In many of these cases, the sizes of the domains have been calculated and have shown reasonable agreement with the observed values.

A number of difficulties beset the direct comparison of theoretical and experimental situations. Material parameters such as magnetization, stress, anisotropy constants, and exchange stiffness constants are not always known. As has been indicated, the walls also take up positions that are determined by internal defects (stress, inclusions) which are unknown to the theory. When the formation of domains cannot eliminate magnetostatic fields, these also determine the structure. However, these fields cannot be determined with great precision due to intractable geometries. A further difficulty which besets the study of domain structure is the production of specimens whose faces lie parallel to the planes in which the structure can be analytically determined. In silicon iron a secondary domain structure occurs when the specimen's surface deviates from a (100) plane by less than $0.5°$ (29).

Further evidence of the validity of the theory of domain structures comes from the interpretation of a number of observations in uniaxial materials.

Goodenough (30) has shown the origin of the rick-rack patterns on a manganese bismuth specimen, and Kooy and Enz (31) have interpreted the labyrinth patterns seen on the surface of transparent barium ferrite single crystals.

One of the fundamental successes achieved in experimental domain theory is the observation that displacement of domain walls is responsible for changes in magnetization. Elmore (32) noted that change in the position of walls was responsible for magnetization changes and concluded that previous observations of the erratic random nature of the change (Barkhausen jumps) were the result of the nonuniform motion of these walls.

Williams and Shockley (33), using a crystal in the shape of a frame, as described earlier, were able, as a result of the simple domain structure found in this shape, to measure both the position of the single mobile wall and the magnetization as functions of the applied field. This work showed in an unambiguous way that magnetization change can be attributed to domain wall motion. Here again the irregularities which imperfections imposed on the wall's motion were shown to be responsible for Barkhausen type changes.

Knowles (34) recently measured the position of walls in a grain of a polycrystalline ferrite as a function of the applied field from which he deduced the grain's hysteresis loop and then showed that it compared favorably with a hysteresis loop measured for the entire specimen.

Additional evidence for the existence of domain structure is provided by the calculation of magnetization curves. Néel and collaborators (35), as well as Lawton and Stewart (36), have shown that high field magnetization curves can be calculated if the domain structure is taken into account. The agreement between theory and experiment is excellent. In these calculations, however, the fine details of the domain structure are not required.

The application of domain structure to coercive force calculations has also been successful. As has been indicated, Néel's theory has been applied

successfully to iron. Wijn, Gorter, Esveldt, and Geldermans (37) have shown that this expression is also applicable to ferrites.

Due to the domain wall size, its experimental observation which could be correlated with theoretical deductions has been difficult. However, several attempts at correlation have had reasonable agreement. Measurements of domain wall energy by Bates and Davies (38) in an annealed perminvar toroid gave a value in good accord with theory. Craik (39) and others, examining under an electron microscope the Bitter patterns taken from a manganese zinc ferrite surface, found the wall width to be in accord with theory. Finally, Néel (40) has predicted that in extremely thin films the magnetization in the domain walls lies in a plane perpendicular to the walls. This is in contrast to bulk materials where the magnetization is always parallel to the plane of the walls. Néel's prediction has been observed (41). The Néel wall is a result of the magnetization within the wall seeking an orientation which will reduce demagnetizing energies.

d. Magnetization rotation

The description of magnetization rotation processes, which were defined in Sec. a, is continued here. The details of a number of nonuniform processes are given together with a discussion of the energy barriers which confront the rotation processes.

In any rotation process, as the magnetization changes its orientation, its anisotropy energy changes. If the process is irreversible, the magnetization must pass through an orientation for which this energy is a least a relative maximum. If the rotation occurs while the magnetization is part of a domain wall, the total energy of the system is not increased by this occurrence since the energy in the domain wall is transferred from magnetic moment to magnetic moment as the domain wall is translated. In a rotation process in which the entire magnetization is in motion simultaneously this transfer of energy is not possible, and the applied field must be of sufficient

strength to at least pull the magnetization over the anisotropy energy barrier. Whether other barriers of importance exist depends on the details of the magnetization's spacial distribution while the rotation is executed. The shape of the specimen, strain anisotropy, and porosity can provide these other barriers. Since the strain anisotropy is similar to the magnetocrystalline anisotropy, it will not be considered further.

The resistance to rotation offered by the magnetocrystalline anisotropy is evident from its definition. The field required to turn the magnetization irreversibly from one easy direction to another is readily found. We consider, again, a material with uniaxial anisotropy, for here this symmetry also introduces mathematical simplicity, and use the machinery introduced in Sec. a to find this field. Since, for the moment, only the effects of anisotropy are of interest, the specimen may be taken as an infinite and uniform body. Before the application of a field, θ, the angle which the magnetization makes with the easy direction, is zero. When a field is applied which is opposed to the magnetization, the total energy of the magnetization becomes

$$E = K \sin^2\theta + HM \cos\theta. \tag{1-57}$$

This energy will have an extremum when

$$\frac{dE}{d\theta} = K \sin 2\theta - HM \sin\theta = 0, \tag{1-58}$$

and the extremum will change from a minimum to a maximum when

$$\frac{d^2E}{d\theta^2} = 2K \cos 2\theta - HM \cos\theta = 0. \tag{1-59}$$

From these last two equations it follows that $\theta = 0$ defines the orientation of the magnetization until $H > \frac{2K}{M}$. Then the energy of this orientation becomes maximum and that of $\theta = \pi$ becomes minimum. Thus the height of the anisotropy barrier, which can also be called the rotational coercive force, H_c, for a field applied parallel to an easy axis, is

$$H_c = 2K/M. \tag{1-60}$$

The rotational coercive force also depends on the angle which the applied field makes with the easy axis, and this field is a minimum when the applied field is at an angle of 135° to the initial easy direction. The critical field then becomes K/M.

A similar analysis in cubic materials shows that the critical fields, H_c, are of the order of

$$H_c = K/M. \tag{1-61}$$

In the iron garnets, using the values given in Chap. III, H_c is found to be about 40 oersteds at room temperature.

When the shape of the sample is taken into account, similar considerations apply. As the magnetization rotates, poles are formed on the surfaces of the specimen and demagnetizing fields are created which oppose the rotation. Since the demagnetizing fields are sensitive to the specimen shape, a shape dependent parameter replaces the anisotropy constant in estimating the rotational coercive force. Since switching experiments are performed with toroids, the coercive force determined by this geometry will be estimated. For this purpose the toroid can be cut, unwrapped, and treated as an infinite cylinder. (This latter requirement is necessary to avoid the ends of a finite cylinder.) Since the demagnetizing field of a uniformly magnetized infinite cylinder vanishes when it is magnetized along its axis and is $2\pi M$ when it is magnetized transverse to its axis, its demagnetizing energy density, E_D, when it is transversely magnetized, is

$$E_D = \pi M^2. \tag{1-62}$$

It therefore has a shape anisotropy energy density, E_s, given by

$$E_s = \pi M^2 \sin^2 \theta. \tag{1-63}$$

Here θ is the angle between the magnetization and the axis of the cylinder. Hence fields of the order πM will be required to produce an irreversible change. Since in soft magnetic materials $\pi M > 2K/M$, the shape of the material is the deterrent to the occurrence of a reversal by a pure rotation. In yttrium iron garnet, for example, this shape barrier is some 300 oe high.

However, other rotational processes exist in toroids, or their equivalent cylinders, which avoid this shape barrier. In order to describe these processes it is convenient to replace the toroids by cylinders in which the cylindrical coordinates – ρ, θ, z – are used to specify the position of the magnetization.

One of these processes is the uniform rotation process (42). In this process the magnetization which is initially aligned with the axis of the cylinder reverses by rotating so as to remain approximately tangent to the cylindrical surface of constant ρ at which the magnetization is located. As long as the magnetization lies approximately in these surfaces, surface poles are not formed, and the demagnetizing barriers are unimportant. Neighboring surfaces interact through exchange forces so that they are almost aligned. These exchange forces act with the anisotropy forces to oppose the reversal.

In another rotation process (43), the spiral process, the magnetization in a plane of constant z rotates in unison. The components of the magnetization in the plane normal to the z-axis, M_x and M_y, depend on z and are

$$M_x(z) = M_{ox} \sin 2\pi kz, \tag{1-64}$$

and

$$M_y(z) = M_{oy} \cos 2\pi kz. \tag{1-65}$$

k is the wave vector. The shape barrier is avoided in this case by the distribution of positive and negative magnetic poles over the surface of the specimen. The proximity of these opposite surface poles reduces the strength

of their fields in the interior of the sample. Here again exchange effects augment the crystal anisotropy effects in increasing the barrier to rotation.

Various rotational reversal schemes which have been considered in the study of the coercive force of fine particles are applicable here. They will not be presented here for they give no additional physical principles. The reader may consult a review paper by Luborsky (44) for further details.

Attempts to find a low value for the rotational coercive force meet with difficulties as there does not appear to be any way for the internal interactions to aid in overcoming anisotropic barriers. However, a modified rotational reversal in a polycrystalline material might occur. In this case, the walls would move by jumps over the grains, or a portion of the grains, which would rotate as an entity. The additional fields required for this process come, perhaps, from the demagnetizing fields of poles on the grain boundaries. The nucleation process initiating domain wall motion serves as an example of a modified rotational scheme.

e. Comparison of domain wall motion with rotation – threshold effects

In this section the values of the coercive force found for pure rotational and domain wall motion models are compared. When the Néel model for wall coercive force is an adequate description, a comparison of Eqs. (1-54) and (1-60) shows directly that in high density materials the wall coercive force is less than the rotational one. However, when the porosity is low and if the strains are unimportant, it is reasonable to assume that Goodenough's result is a better description since it determines the coercive force in the absence of structural defects. This result is given in Eq. (1-56). The second term, which is the result of changes in wall area, is the product of the rate of change of wall area per unit area and the specific wall energy. Since wall energies are typically of the order of 1 erg/cm^2 and since the rate of change of wall area with distance is not greater than unity, this term is small in comparison to the rotational term. The term proportional to M is also small as its

coefficient is due to the difference in alignment of neighboring grains. Goodenough (24) shows that this coefficient is of the order of 10^{-3}, and again it appears that the coercive force on the wall model is smaller.

Experiments which show the difference between the rotational and wall coercive forces have been performed in single crystal iron whiskers (45). Crystals of this type possess large regions which are almost free of domain nuclei, while other regions possess a large number of structural defects which provide many domain nuclei. In the former regions, coercive forces were found to be about 500 oe, while in the latter, about 10 oe. The different magnitudes of these coercive forces are attributable to the absence and presence respectively of walls in the magnetization change process. The existence of domain walls in these materials is confirmed by Bitter pattern investigations.

It is interesting to note that the rotational coercive force for a perfect crystal was expected to have been of the same magnitude as the anisotropy barrier, i.e., some 560 oe. The lower value which was measured is probably brought about by the demagnetizing fields associated with the surface imperfections.

f. Remanent state

The magnetization distribution which remains in a polycrystalline toroid after the material has been saturated along its circumference and the field has been removed is, in the absence of intergrain interactions, expected to be such that the magnetization in each grain lies along the easy direction nearest the circumferential direction. Then, along this direction, the magnetization (37) has an average component, M_r, which depends only on the symmetry of the crystal, the sign of the anisotropy constant, and the grain orientation. The ratio of this component to the saturation magnetization for random grain orientation is:

Anisotropy	M_r/M
uniaxial $K > 0$	0.5
cubic $K > 0$	0.83
cubic $K < 0$	0.86

However, measurements on unoriented cubic materials show that such large remanent values rarely occur. These lower values can be attributed to either porosity, stress, or reverse domains, singly or in combination.

When a strain is present, it can either change the symmetry to uniaxial or make one of the easy axes more preferable than the others. If the degree to which this occurs is large, uniaxial symmetry is substituted for the crystallographic cubic symmetry with the resultant lowering of the remanence value.

In a material which has nonmagnetic inclusions, a reduction in the remanent magnetization results either from the domain structures which form about these inclusions, as has been indicated when the inclusions are large, or from deviations of the magnetization from easy directions resulting from the fields of the smaller pores. The manner in which these perturbations change the hysteresis loop and reduce the magnetization at remanence may be thought of in analogy to the demagnetizing effects introduced by deliberately forming an air gap in a toroid (18). The net result is to shear the loop as shown in Fig. 1-8 where the original loop is shown in part a and the sheared loop in part b.

It may readily be seen from the figure that the effect of these demagnetizing forces in producing reductions in the remanent flux is greatest in low coercive force materials.

The nucleation of reverse domains by grain boundaries has been considered in Sec. b.

In most discussions of the switching properties of ferrites, the remanent state is not considered. It is usually assumed that the ferrites are virtually

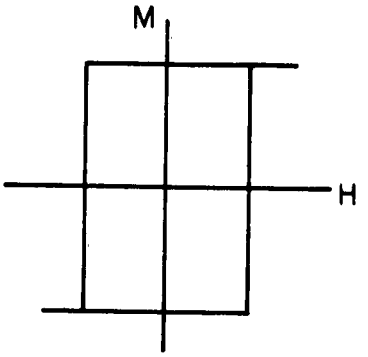

(a)

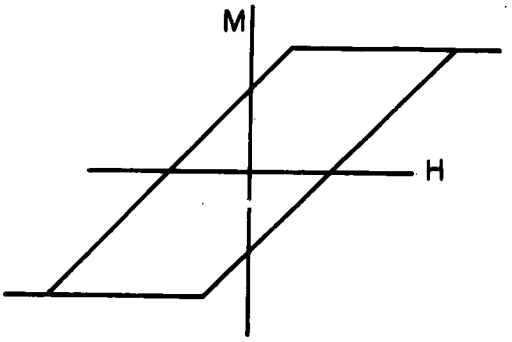

(b)

FIG. 1-8 (a) IDEAL HYSTERESIS LOOP

(b) SHEARING RESULTING IN (a) FROM POROSITY NOTE DECREASE IN REMENCE.

saturated since they possess a square hysteresis loop. This type of loop frequently is characterized by the ratio of its remanent flux density to the flux density obtained when a certain maximum size field, not more than 100 times the coercive field, is applied. The closer this ratio is to one, the greater is the resemblance of the material to the ideal. It is then assumed that, since the material has a low coercive force, the flux density at maximum field is the saturation flux density. The measurements on a manganese magnesium ferrite, having the composition frequently measured and discussed in respect to switching, which are given in the book by Wijn and Smit (18) show that, although the squareness ratio of this material is about 0.9, the ratio of the remanent flux to the saturation flux is only about 0.6.

In this connection, the recent observations by Knowles (34) on material of similar composition which also has a square hysteresis loop should be noted. Knowles found that domains already exist at remanence and that these domains are not nucleated. This is at variance with the Goodenough theory of nucleation and its relation to square hysteresis loops and is further discussed in Sec. 5e below.

5. TIME DEPENDENT EFFECTS

The time dependence of various magnetization processes will now be examined. The processes which will be considered are:

(1) Magnetization aging
(2) Time decrease of permeability
(3) Magnetic viscosity
(4) Switching
(5) Frequency dependence of the permeability
(6) Ferromagnetic resonance

Each of these has associated with it a characteristic time during which the magnetization changes and which ranges from nanoseconds to years. The slower processes head the list which is not complete but is representative.

a. Slow processes

The slow magnetization change processes are considered in order to show their relation to switching. A general characteristic of these processes is that they are brought about by changes in the materials' chemistry or crystal structure.

The room temperature aging (46) of certain magnetic materials is a particularly slow process which results in a change of their remanent flux. Such decreases of the magnetization appear over a period of years. They usually can be associated with either an unstable crystal structure or with the occurrence of chemical changes.

The time decrease of permeability and magnetic viscosity (47, 48), which are frequently referred to as after-effects, have time scales of the order of minutes to hours. The latter of these after-effects refers to a measurement of the flux changed after the application of an applied field and is similar to a switching experiment. Switching and magnetic viscosity are distinguished from each other by the magnitude of the field in which the change transpires. In a magnetic viscosity experiment the applied field is not large enough to bring about a magnetization change and requires a thermal fluctuation to augment its size in order to overcome the barriers to change. In a switching experiment the applied field is sufficiently large to carry the magnetization over the change barrier. However, in both experiments, the magnetization change is an irreversible process.

The time decrease of permeability is usually brought about by one of a number of diffusion processes. In each of these cases atoms find new positions in the lattice during the permeability experiment. These changes occur as a result of the preference of the atoms to be oriented in a definite manner

with respect to the magnetization. Magnetoelastic couplings are considered to provide the interaction between the diffusing atoms and the magnetization.

In the thermally activated model (49), the change in magnetization is the result of a thermal process which excites domain walls over the barriers preventing their motion. The application of fields reduces the height of these barriers and increases the rate of change of magnetization.

Similar considerations hold for the diffusion mechanism. In either case, when the field is large enough, i.e., greater than the coercive force, these processes are no longer important. In other words, the application of a field changes the potential energy contour from two wells separated by a barrier to a potential energy distribution in which the particles are on top of a constantly decreasing contour. When the field is larger than the coercive force, these mechanisms can be ignored. Since switching is an effect associated with fields greater than the coercive force, these processes are not considered further. In the following, only processes which occur when the magnetization is driven by an external field are treated.

b. Equation of motion

In order to study the dynamics of a magnetization system, a relationship giving the change of magnetization with time, as it is produced by the applied field, must be obtained. This will now be done. The equation of motion will first be obtained without consideration of dissipation, and then dissipation will be introduced in a number of different ways in a phenomenological manner. The consequence of each of the different dissipation terms will be examined.

When a field, H, is applied to a magnetic moment, μ, the magnetic moment experiences a torque, $\mu \times H$. Now, from mechanics, it is known that the rate of change of angular momentum is the torque. Then, if the angular momentum of our magnetic moment is L, its time variation is given by

$$\frac{dL}{dt} = \mu \times H. \qquad (1\text{-}66)$$

For an electron moving in a circular orbit of radius, r, the magnetic moment and the angular momentum are respectively

$$\mu = \frac{r \times ev}{2c}, \tag{1-67}$$

and

$$L = mr \times v. \tag{1-68}$$

From Eqs. (1-67) and (1-68), the gyromagnetic ratio, γ, the ratio of μ to L is

$$\gamma = \frac{\mu}{L} = \frac{e}{2mc}. \tag{1-69}$$

Substituting this value in Eq. (1-66), the equation of motion for a magnetic moment becomes

$$\frac{d\mu}{dt} = \gamma\mu \times H. \tag{1-70}$$

When the magnetic moments occur in a solid, it is more convenient to work with the magnetization, M, the density of magnetic moments. In terms of this variable, Eq. (1-70) becomes

$$\frac{dM}{dt} = \gamma M \times H. \tag{1-71}$$

Also, in a solid, the origin of the magnetic moment resides only partially in the orbital motions of the electrons; a large contribution comes from their spin. Then, it is no longer correct to take the gyromagnetic ratio as given in Eq. (1-69). For solids, the gyromagnetic ratio is written as

$$\gamma = \frac{ge}{2mc}. \tag{1-72}$$

The g-factor is unity for orbital magnetism and 2 for electron spin magnetism. When a combination of these contributes to the total magnetization, the g-factor can be greater than 2.

One further point concerning the torque $M \times H$ must be made. This torque, which was originally introduced as due only to the applied field, should include all the torques which can act on the magnetization. These torques may result from the magnetocrystalline anisotropy (including magnetoelastic effects), internal magnetostatic interactions, and exchange interactions and are derived from their respective energy densities in Chap. V.

When only an applied field is present, the solution of Eq. (1-71) shows that the magnetization precesses about this field as shown in Fig. 1-9. Note that in keeping the angle between M and H constant energy is conserved in this motion.

c. Equation of motion with damping

As a consequence of the conservation of energy, the solutions of the equation of motion found above should show no tendency for the magnetization to come into alignment with the total applied field. To account for the fact that the magnetization does obtain an equilibrium position, a term has to be added to the equation of motion which will cause the magnetization to move toward the total field. A number of different forms of this term have been used. Two of them, the Landau-Lifshitz (3) term and the Gilbert (50) modification, have been used in switching studies. We will discuss these equations here and then in Sec. 6 introduce Callen's (51) equation which is a generalization of these equations and has the advantage that its parameters can be identified with loss mechanisms. Another means of introducing the damping terms is the Bloch-Bloembergen (87) scheme which has proved useful in interpreting ferromagnetic resonance experiments. It has not as yet been applied to switching. Since it may be obtained as a special case of Callen's equation, we will not consider it any further.

Since a loss of energy accompanies the establishment of equilibrium, the term which must be added represents a dissipative mechanism, and it is

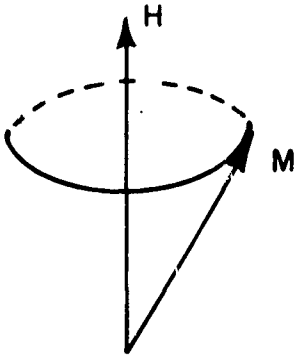

FIG. I-9 PRECESSION OF THE MAGNETIZATION ABOUT THE APPLIED FIELD.

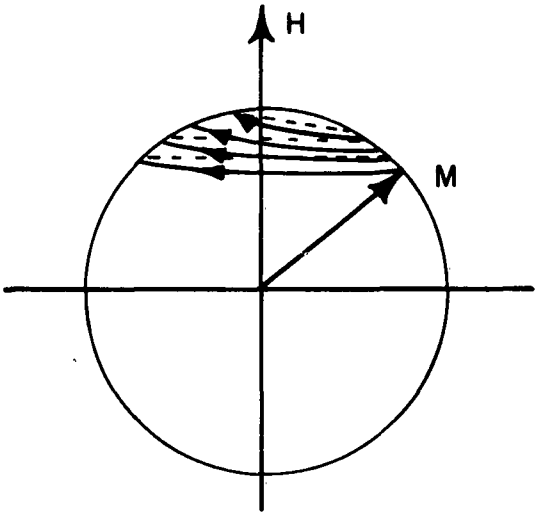

FIG. I-10 DECAY OF THE MAGNETIZATION WHEN THE EXCHANGE-LATTICE OR SPIN LATTICE INTERACTIONS DOMINATE. (AFTER CALLEN)

referred to as a damping term. This mechanism must act to decrease the angle between the total field and the magnetization. A change in M in the plane of M and H can cause this to occur. Landau and Lifshitz introduced this term as

$$-\frac{\lambda}{M^2}\,[\,M\times M\times H\,],$$

and Gilbert modified it to be

$$-\frac{\alpha}{M}\,(M\times\frac{dM}{dt})\quad .$$

The complete equations of motion with these terms are

$$\frac{dM}{dt} = +\,\gamma\,(M\times H) - \frac{\lambda}{M^2}\,(M\times M\times H) \tag{1-73}$$

for the Landau-Lifshitz equation and

$$\frac{dM}{dt} = +\,\gamma(M\times H) - \frac{\alpha}{M}\,(M\times\frac{dM}{dt}) \tag{1-74}$$

for the Gilbert equation.

The parameters α and λ may be functions of the applied field, the magnetization, the specimen shape, etc. to be determined by comparison with experiment. Their significance can be shown by taking H to be a d.c. applied field and the magnetization to be at a small angle θ_o with this field. If the orientation of M is described by the polar coordinate system θ and ϕ, where θ is the angle between M and H while ϕ is the angle in the plane normal to H measured from an axis normal to H, the Landau-Lifshitz equation becomes the set of equations

$$M\frac{d\theta}{dt} = -\lambda H\sin\theta \tag{1-75a}$$

and

$$M \sin\theta \frac{d\phi}{dt} = +\gamma MH \sin\theta, \tag{1-75b}$$

which for small θ become

$$\frac{d\theta}{dt} = -\lambda \frac{H}{M} \theta \tag{1-76a}$$

and

$$\frac{d\phi}{dt} \leftarrow \gamma H. \tag{1-76b}$$

Equations (1-76a) and (1-76b) show that as the magnetization precesses about the field with frequency γH, it is decaying into alignment, H, with the relaxation time, $\frac{M}{H} \frac{1}{\lambda}$. Hence, λ is a measure of the relaxation frequency. The relaxation time decreases with increasing relaxation frequency.

Using the same coordinate system, the Gilbert equation reduces to

$$M \sin\theta \frac{d\phi}{dt} = \gamma MH \sin\theta - \alpha M \frac{d\theta}{dt}, \tag{1-77a}$$

$$M \frac{d\theta}{dt} = \alpha M \sin\theta \frac{d\phi}{dt}. \tag{1-77b}$$

Substituting Eq. (1-77b) in Eq. (1-77a) and solving for $\frac{d\phi}{dt}$ gives

$$\frac{d\phi}{dt} = \frac{\gamma H}{1 + \alpha^2}. \tag{1-78a}$$

Using this result in Eq. (1-77b) together with the small angle approximation for $\sin\theta$ gives

$$\frac{d\theta}{dt} = \gamma H \frac{\alpha}{1 + \alpha^2} \theta. \tag{1-78b}$$

A comparison of Eqs. (1-78a) and (1-78b) with Eqs. (1-76a) and (1-76b) shows that the motion for the Gilbert modification is similar to that for the Landau-Lifshitz equation. Here, however, the relaxation time is related to α, and from Eq. (1-78b) it is seen that the relaxation time has a minimum.

One then expects a long relaxation time for either large or small damping parameters. The precession frequency in this case is also dependent on the damping. When α is identified with $\lambda/\gamma M$ and $\alpha \ll 1$, the results for the Gilbert equation are identical to those for the Landau-Lifshitz equation. A consequence of the existence of a minimum of the relaxation time for the Gilbert modification is the fact that the rate of loss of energy is a bounded quantity. Although only small angles were considered above, this result can be extended to include large angles. To this end the Gilbert equation can be transformed, using a method given by Harrington (52), to the form of the Landau-Lifshitz equation with the result that

$$\frac{dM}{dt} = \frac{\gamma}{1+\alpha^2}(M \times H) - \frac{\gamma}{M}\frac{\alpha}{1+\alpha^2}(M \times M \times H). \tag{1-79}$$

If again H is taken to consist solely of an applied field, then the rate at which energy is lost,

$$\frac{dE}{dt} = -\frac{d(M \cdot H)}{dt} = -\frac{H \cdot dM}{dt}, \tag{1-80}$$

can be shown for the Landau-Lifshitz equation to take the form

$$\frac{dE}{dt} = -\frac{\lambda}{M^2}(M \times H)^2 \tag{1-81}$$

and for the Gilbert modification the form

$$\frac{dE}{dt} = \frac{\gamma}{M}\frac{\alpha}{1+\alpha^2}(M \times H). \tag{1-82}$$

Again, from Eqs. (1-81) and (1-82), it is seen that the rate of loss of energy is limited in the Gilbert modification while it is limitless in the Landau-Lifshitz formulation.

In almost all applications of these equations where the damping constant is definitely known it is relatively small. When this is true the difference

between the descriptions vanishes. Consequently, it is impossible on the basis of experimental evidence to determine which of these phenomenological equations is a better description. The popularity of the Gilbert modification seems to stem from the fact that in certain magnetization reversal processes it predicts a lower limit on the reversal speed as the damping parameter is varied while all else remains constant. Since the existence of this limit also implies that there exists a limit on the rate of dissipation and as there is no reason to expect that the rate of dissipation should be bounded as the damping parameter is varied, it would appear that the Landau-Lifshitz formulation is closer to being the correct one.

d. Domain wall motion

In this section, the time effects associated with the motion of a domain wall after the establishment of a field in its presence will be discussed. The velocity of this domain wall will be given here, and it will be used to describe switching experiments.

In 1935, in a paper which is now classic, Landau and Lifshitz (3) used Eq. (1-73) to derive a relationship for the velocity of a domain wall. Since that time their work has been reinterpreted by other workers. Becker (53) and Doring (54) have shown the physical significance of these mathematical results, and Kittel (55) has used the physical models of Becker and Doring to extend the Landau-Lifshitz work to crystals with cubic anisotropy.

Landau and Lifshitz found that when a domain wall was displaced, its magnetization rotated about an axis normal to the wall. From the discussion of the precession of the magnetization in a field, it can be seen that a field normal to the wall is required to cause such a motion. The presence of this field, which does not exist in the static case, was interpreted by Doring to signify that the moving wall acted as if it had mass. That is, it acquired an energy while in motion which it did not have when it was static. Becker then noticed that, since the wall had mass and since it lost energy while it

was in motion, it is possible to represent the motion of this wall by a second order linear differential equation with damping. The restoring force was taken to arise from the same effects which lead to the coercive force of the material. This equation has proven useful in the study of initial permeabilities. The frequency dependence of the initial permeability can readily be derived from a representation of this type. Although some of the problems encountered in the initial permeability work are similar to those which exist in switching, this work will not be considered in the following since the points which are unclear in switching are equally unclear in the initial permeability studies.

In addition, since the measurement of initial permeability involves small excitations, the damping mechanisms are probably different. However, one point should be noted. Through initial permeability experiments, Pippin (56) was able to conclude that domain walls exist in nickel cobalt ferrites and garnet materials (these materials are identical, i.e., possess the same grain size, etc., to the materials which were used in the experiment to be described later) and that the motion of these walls contributed to the initial permeability. For recent work and a review of the initial permeability theory and experiment the thesis of Pippin (56) should be consulted.

When Galt (7) applied Becker's second order differential equation to switching, the inertial term was neglected, and the equation was reduced to a first order equation in which motion takes place in a system in which the applied force is opposed by friction and a restoring force. Through either this or the Kittel derivation, it is then found that the velocity of a domain wall is linearly related to the applied field, if the damping is not field dependent. The velocity of the domain wall is found to be

$$v = \frac{C(\gamma^2 M^2 + \lambda^2)(H - H_o)}{\lambda M} \sqrt{\frac{A}{K}} . \qquad (1\text{-}83)$$

In this equation, C is a constant which depends on the type of magneto-crystalline anisotropy, H is the applied field, and H_o is a threshold quantity which is similar to the coercive force. This equation holds only when the damping is large enough to substantially dissipate the energy acquired by the wall's magnetization from the applied field when the wall moves a distance equal to its own thickness. For small damping, the calculation of the wall velocity can be found in Chap. V.

The central theoretical problem in the study of switching is the computation of the time it takes for the magnetization to reverse. If the mechanism for reversal is domain wall motion, then, from a knowledge of the wall's velocity and the distance it moves during a magnetization reversal, the time elapsed during the reversal can be calculated. Taking d as the distance which the domain wall moves during the reversal, Goodenough (57) found that the inverse switching time, t^{-1}, is given by

$$\frac{1}{t} = \frac{1}{S_w}(H - H_o), \tag{1-84}$$

where S_w is found from Eq. (1-83) to be

$$S_w = \frac{\lambda M d}{C(\gamma^2 M^2 + \lambda^2)} \sqrt{\frac{K}{A}}. \tag{1-85}$$

If S_w is a constant, the 1/t vs. H curve of Eq. (1-84) is linear.

The two parameters, S_w and H_o, in Eq. (1-84), measure the performance of a core material in a switching experiment. Devices, which are discussed in some greater detail in Sec. 8, generally require that both S_w and H_o be small in order to keep the power dissipated as low as possible and to have simultaneously rapid switching.

Since the only attempts at theoretically understanding the relaxation process for wall motion have been made by Clogston (58), Galt (59) and

Néel (60) for the single case where the dissipation occurs by anisotropy relaxation due to the transfer of an electron between the ferric and ferrous ions which occur in y (dielectric) ferrites and since their calculations are only applicable in very small fields, the damping parameter, λ, cannot as yet be related to other material parameters. The relaxation of the anisotropy torques in this mechanism is a process similar to the after-effects discussed earlier. The relaxation is, however, much faster in this process since electrons, and not atoms, are the diffusing agent. The damping will be considered again below when damping processes in ferromagnetic resonance are reviewed.

The distance, d, as determined by Goodenough (24), would appear to be independent of the applied field. However, the Goodenough calculations which determined this distance were directed at determining the field required for nucleation. The computation found the barrier heights and did not treat the field dependence of d. Other domain processes have also been proposed. Although these have not yet been completely analyzed, they appear to explain a number of experimental results which are at variance with the Goodenough theory. In the next section, we return to these topics.

e. Experimental results in the study of domain wall motion

Single crystal as well as polycrystalline materials have been measured in order to determine the speed with which remagnetization takes place. In this section, these experiments will be discussed. It will be seen that in the single crystals the measurements have been predominantly directed towards studying domain wall mobilities while in the polycrystalline materials the measurements have been made to determine S_w and H_o. Also, in the polycrystalline materials a number of experiments have been made to decide whether domain wall motion contributes to the reversal process.

1. Single crystals

Galt (59) and Dillon (61) have cut single crystals of magnetite, nickel ferrite, and manganese ferrite to form frames (see Sec. 4b), each of whose

legs is parallel to an easy direction, in order to obtain a geometry which is convenient for the study of domain wall motions. Hagedorn and Gyorgy (62) have similarly formed frames of yttrium iron garnet. In these crystals a single domain wall moving from one side of a leg to the other may reverse the magnetization. Since these materials are cubic with an easy direction along the (111) axes, the frames were diamond shaped.

The principal result of the Galt and Dillon experiments is that, for small fields, the domain wall velocity is linearly related to the applied field in accord with the deduction from the Landau-Lifshitz equation. The qualification of small applied fields results from the observation that larger applied fields produce more than a single wall in the reversal.

This point is particularly clear in Dillon's work (61) with manganese ferrite. On two legs of this ferrite were wound small solenoids. In one of these solenoids a step function of current was produced to cause a wall to move from one face to the other in each of the legs in the frame. The other solenoid was used to obtain a signal which was proportional to the rate of flux change and which was displayed on an oscilloscope where it was noticed that, for exceedingly small fields, a time delay occurred between the application of the applied field and the initiation of the reversal. It appeared that a nucleation time was required before the initiation of the motion. This nucleation time disappeared as the applied field was increased. It was further observed that, for small fields, the output consisted of a constant amplitude pulse. When the applied field became larger, it was then seen that the amplitude of the output pulse was not constant, and so it was inferred that two walls were participating in the reversal.

The crystals used by Galt, unfortunately, contained a large number of ferrous ions, and it appears that the transfer of electrons from these ferrous ions to ferric ions dominated the magnetization damping.

As will be shown below, the damping parameter may be measured in a ferromagnetic resonance experiment. Although it is not as yet clear whether this quantity is the same quantity which occurs in domain wall processes, nevertheless, they may be compared. Since, for all these single crystals, data were also obtained by ferromagnetic resonance, a comparison of the relaxation frequencies obtained from domain wall motion and resonance could be made. It showed that, in the case of the presence of ferrous ions, the damping parameter, which was frequency sensitive in the resonance experiments, is larger than the parameters obtained from domain wall motion. On the other hand, in the case of the manganese ferrite, it was determined that the λ for domain wall motion is larger than that for the ferromagnetic resonance experiment. In the case of the ferrous ions this is in accord with Clogston's (58) theory which predicts the frequency dependence of the ferromagnetic resonance data and shows that the domain wall motion quantity is smaller. In the case of the manganese ferrite one could expect to find a situation similar to that of yttrium iron garnet since the magnetic ions in each of these materials is in an S state. With the aid of the experimental results which are given in Chap. IV it is seen that the relative sizes of the switching and resonance relaxation frequencies are about the same for both these materials. In the succeeding part of this section where polycrystalline measurements are considered the switching measurements made on single crystal and polycrystalline manganese ferrite will be seen to be in accord.

2. Polycrystalline materials

The experimental work on polycrystals has been directed at establishing a model for the domain wall motion and at obtaining relevant quantities which would describe the motion. The experimental situations have been similar to those described above for the single crystals. A means for applying a pulsed field to the core is provided as well as a means for observing the reversal on an oscilloscope. However, a number of variations of this experiment have been performed. In these, the applied field has been interrupted. Knowles

(34) has performed additional experiments in which the surface of the material is examined using the Bitter technique.

On the basis of the discussion in Sec. c above, it is seen that to describe the motion of domain walls in polycrystalline materials one requires a model showing where the walls are initiated and their path during the reversal. As has been indicated, Goodenough (24) has proposed that the stray fields, produced by the grain boundaries as a result of the difference in the orientation of the magnetization on each side of these boundaries, together with an applied field initiate the nucleation process. He concluded that, at these grain boundaries, a periodic structure of domains of reverse magnetization is formed. He further proposed that these domains grow in an applied field until they collide to reverse the core. In this model it is assumed that the magnetization in each grain lies in an easy direction nearest the last applied field. He then, as previously indicated, used this model to explain why certain materials have rectangular hysteresis loops. The explanation is that the fields at the grain boundaries are insufficient for a reversal and that they require the aid of an applied field, which is in the same direction as the reversed magnetization, to cause the nucleation. As a consequence, in this model it is assumed that, as the field is reduced from saturation to zero, no domain walls occur. It is, however, well known that not only is the major loop in these materials a square loop, but also the minor loops are square. In fact, the loop which possesses the maximum squareness is found to be a minor hysteresis loop. The Goodenough theory does not seem to account for this, for, in accord with this theory, minor loops should not exist. This theory predicts a unique field at which the reversal should occur. Further, it does not seem to take into account the fact that grains which have different relative orientations have different nucleating forces which could be responsible for a field dependence of d.

According to Goodenough's theory, the absence of walls at remanence implies that only rotational processes are responsible for the permeability measured at this point. However, measurements of permeability at remanence show that it is too large to be accounted for by only rotational processes. And so domain walls must exist at the remanent state.

Knowles, on the basis of his observations of Bitter patterns, has produced a model for the magnetization reversal based on the movement of a few boundaries which are always present within a grain. These boundaries move freely over most of the grain, but snag at either inclusions or stress centers. Using this model, Knowles accounts for the minor hysteresis loops in ferrites. The model is also useful for explaining results in experiments in which the fields for switching and resetting the magnetization are different.

Vogler (63), on the other hand, has taken some objection to Knowles' work in that he feels that the poles on the grain boundaries should be taken into account. In effect, he attempts to combine the Goodenough and Knowles theories. He also suggests that there are other places at which nucleation can occur. In particular, he believes that in small, fine grained materials domains are nucleated at grain boundaries whose adjacent magnetization does not lie along the easiest direction nearest the last applied field. These relative orientations produce much larger stray fields than can be obtained from Goodenough's arrangement. It appears clear that, if this model is accurate, it too could explain the results which are at variance with Goodenough's theory.

It is common to these various models that the distance the walls will move in the reversal process does not exceed one or two grain diameters. This places an upper bound on the size of d.

It should be noted that Goodenough's model without modification appears to have some validity in large grained materials such as commercial silicon

iron. Observations (64) here do seem to indicate some sort of regularity in the distribution of the nucleated domains, and they appear to occur on grain boundaries. Of course, the larger the size of the grain, the more energy is stored in the stray fields and, hence, the greater is the possibility that they can cause domain structure to appear.

Various interrupted pulse experiments (57, 65, 66) have been performed to show that domain wall motion is the cause of the magnetization reversal. It is believed that if domain walls are responsible for the magnetization reversal, they will move in a uniform manner from their initial to their final destination so that if the applied field is removed in the course of this experiment, the domain walls will stop, and when the field is reapplied, one will see a continuation of the process. For low fields, indeed, this is what is found. At higher fields, it has been reported that the ensuing motion is not the same as the motion which would have occurred if the applied field had not been removed. This has been used as an argument for looking for other than domain wall motion mechanisms as the cause of the magnetization reversal. However, these effects can be justified in a domain wall motion model. The basis for this interpretation is that the number of boundaries that participate in the reversal is a function of the applied field. More work has to be done in order to make any hypothesis concerning this effect convincing.

It has additionally been observed (67) in high field experiments that the curve of the reciprocal of the switching times as a function of the applied field changes slope. This also has motivated a search for alternative reversal mechanisms. Within the framework of wall motion, two possibilities exist for understanding these changes of slope. Either d or λ may be field dependent. The field dependence of d has already been discussed. In Chap. VI, the field dependence of λ is introduced.

It is difficult to make numerical comparisons of, or to reduce, the already published data taken for polycrystalline cores because the pertinent magnetic parameters for the materials under examination have not been measured, or the required structural information is unavailable. There are, however, a few cases for which we can compare the theoretical predictions with the experimentally determined values. In the first place, single and polycrystalline measurements of manganese ferrite can be compared. Matcovich and Kriessman (68) have measured polycrystalline manganese ferrite at room temperature for which they give 11μ as a value of d. Although Dillon's measurements on the single crystal material were made at temperatures of 200°K and lower, they can be extrapolated to room temperature if it is assumed that the empirically determined linear relationship between the wall mobility and the temperature which exists from 0° to 200°K is continued to room temperature. This extrapolation leads to a wall mobility of 3000 cm/sec oe, from which it follows that one can expect an S_w in the polycrystalline material of 0.37 oe μsec which agrees reasonably well with the measured value of 0.46 oe μsec. Not knowing the precise room temperature mobility makes commenting on the comparison difficult. If the estimated mobility value is correct, the uncertainty would be in the value of d. Matcovich and Kriessman have chosen d as an average value. A better method of estimation would account for the grain size distribution and employ this distribution to determine d. The fewer large d's would then influence the choice of d. Nevertheless, the closeness in the two values of S_w makes it appear that the same mechanism is in operation in both materials.

The effect of applying a circumferential compressive stress on a toroid which is being switched has been studied by a number of workers (69, 70) who found that the switching parameter, S_w, increases with increasing stress. They also found that the field, H_o, required to initiate the reversal increases with increasing stress. The increase in S_w is due in part to the increase in the anisotropy energy, as a result of magnetoelastic effects, and in part to

an increase in d. From Eq. (1-85), it may be seen that S_w increases with increasing anisotropy constant. In addition, the application of the stress tends to bring about a greater uniformity of the magnetization orientation in the remanent state. This is evident by noting that the squareness ratio also increases with applied stress. This increase in uniformity reduces the number of nucleating centers, and, hence, the domain walls must move over longer distances in order to bring about the magnetization reversal. Thus we see that S_w should also increase because of increases in d. The increase of H_o is attributable to the increase in anisotropy.

The range of values which has been experimentally found for S_w runs from several tenths of an oersted microsecond to one hundred oersted microseconds, as is evidenced by the values reported by van der Heide, Bruijning, and Wijn (70). It is interesting to note that the large values of S_w occur in materials which contain ferrous ions. These materials are also amenable to an anneal in a magnetic field which induces into the material a uniaxial anisotropy. The values of S_w given by these workers were for materials which had been annealed. As in the case of applying stress, the effect of the anneal is to align the easy axes in the various crystallites and thus reduce the number of available domain nucleating points. It is highly probable that one of the factors which is responsible for the large S_w's found for these ferrites is the lack of places from which the walls could nucleate. Earlier in this section it was indicated that relatively large damping could be anticipated in materials having ferrous ions. This damping is no doubt another factor leading to the large S_w's.

The temperature dependence of S_w has been noted by several workers (69, 70). In each case they have found that S_w increases with decreasing temperature. Undoubtedly the increase in anisotropy as the temperature decreases again plays some part in the increase of S_w. A complete discussion of the temperature dependence of S_w should, however, include the

temperature dependence of the relaxation frequency. Since such a dependence has as yet not been established, further discussion is impossible.

It is our strong belief, mainly as a result of coercive force considerations, that domain wall motion, or some mechanism closely resembling domain wall motion, is responsible for the important irreversible magnetization reversals in small fields. As yet, only domain wall motion has theoretically been shown to yield a low coercive force in materials which are commonly used in switching experiments.

f. Rotation mechanisms

Changes in the value of the switching parameter, S_w, as a function of applied field and the results of certain interrupted pulse experiments, as have been indicated, have been taken as the need to propose additional mechanisms for the magnetization reversal. Two such mechanisms which are rotational mechanisms have been described in Sec. 4d. Although, as has been discussed earlier, it appears that the threshold fields for these mechanisms are quite large due to the anisotropy energy, we will treat these mechanisms briefly since they have received a great deal of attention recently.

These two mechanisms have been proposed to take care of two different regions of switching characteristics, the uniform rotation being the faster. The theoretical treatment for these mechanisms (42, 43) has neglected the anisotropy contribution and has determined the switching time and the output waveform.

A detailed analysis of the nonuniform rotation (spiral) model shows that the effects of demagnetizing and exchange fields can be neglected in a first approximation thus simplifying the calculation for the waveform and the switching time. The problem then reduces to the one which we considered when we were looking for the physical significance of the damping parameter in which the only torque was that due to the applied field.

Integration of either Eq. (1-75a) or Eqs. (1-77a) and (1-77b) which were obtained prior to making the approximations in the solution of that problem gives for the component of the magnetization along H

$$M_H = M \tanh \frac{t - t_o}{T}, \tag{1-86}$$

with

$$t_o = T \tanh^{-1} \cos\theta_o. \tag{1-87}$$

θ_o is the angle which the magnetization initially made with the direction of the applied field.

$$T = \frac{M}{H} \frac{1}{\lambda} \tag{1-88}$$

for the Landau-Lifshitz equation, and

$$T = \frac{1 + \alpha^2}{\gamma\alpha} \frac{1}{H} \tag{1-89}$$

for the Gilbert equation.

The observed switching waveform is obtained by differentiating Eq. (1-86) to obtain $\dot{M}_H$:

$$\dot{M}_H = \frac{M}{T} \operatorname{sech}^2 \frac{t - t_o}{T}. \tag{1-90}$$

This aspect of the calculation has found excellent agreement with experiment.

The switching parameter can be shown to be approximately

$$S_w = 2HT, \tag{1-91}$$

which is

$$S_w = \frac{2M}{\lambda} \tag{1-92}$$

.he Landau-Lifshitz case and

$$S_w = 2\left[\frac{a^2 + 1}{a}\right]\frac{1}{\gamma} \tag{1-93}$$

for the Gilbert equation. In this latter case, S_w has a minimum which is

$$S_w = \frac{1}{\gamma} \approx 0.2 \text{ oe } \mu\text{sec.} \tag{1-94}$$

For details concerning the uniform rotation case, the original papers should be consulted.

Gyorgy (66), who proposed these mechanisms, has indicated that in small applied fields one should find domain wall motion as the important mechanism. He states that as the field is further increased, the nonuniform rotation mechanism becomes important, and in still larger fields, the uniform rotation mechanism applies.

Since the motion of a domain wall, as has been shown earler, consists of a sequence of rotations of the magnetizations and if the damping parameter is not an especially strong function of the mode of reversal, it would appear that a nonsequential process should be very much faster than a sequential process. It should be expected that the time required for the magnetization to reverse at any point in a domain wall would be approximately the complete reversal time of a rotation process. Therefore, if δ is the domain wall thickness parameter, the ratio of the reversal times should be approximately d/δ, which in most materials is of the order of 10. No observations have been reported which show this large a ratio.

6. RELAXATION MECHANISMS

The role which relaxation mechanisms play in controlling the speed of switching requires that the loss processes which produce them be determined. As has already been indicated, beyond the Clogston, Galt, and Néel calculations, which are applicable for only small applied fields and a special situation,

relaxation mechanisms for domain wall motion have not received any attention. Consequently, we must turn elsewhere to obtain such information.

A useful source is ferromagnetic resonance, where a great deal of work on loss processes has recently been done. Although the conditions under which the dynamic magnetization changes take place differ in switching and resonance, since the interactions are similar, one can, at least on an intuitive basis, expect that there exist similar loss processes. Since the extent of resonance relaxation studies is by now rather large, the subject can only be briefly treated here. Further details may be obtained from recent reviews by Buffler (71) and Rado (72).

In a typical ferromagnetic resonance experiment a small microwave and a large d.c. field are applied in a ferromagnetic material. These fields, which are at right angles to each other, are usually uniform over the extent of the material. The d.c. field aligns the magnetization, while the microwave field tilts the magnetization away from it. As the d.c. field is varied, a resonance absorption line is found. At the peak of the absorption, i.e., at resonance, the microwave field causes the magnetization to precess about the d.c. field with a maximum transverse component. The steady state value of this component is determined by the rate at which the absorbed microwave energy is dissipated. The microwave field raises the energy of the system by causing the magnetization to rotate away from the d.c. field, while the loss processes carry away this excess energy.

There exist two general ways in which this loss may come about. In the first, a spin-lattice interaction occurs in which energy is dissipated as the result of the interaction of the lattice with the magnetization. For example, this interaction may be caused by the modulation of the exchange or anisotropy interactions by the lattice vibrations. In the second, the dissipation process begins by a transfer of energy from the uniform mode brought about by internal stray fields. This transfer of energy increases the system's

exchange energy at the expense of decreasing the energy of the magnetization in the d.c. field (spin-exchange interaction). Finally, this exchange energy is transferred to the lattice where it is dissipated as heat (exchange-lattice interaction).

It can be shown (51) that the breadth of the resonance absorption line is proportional to the strength of these interactions and that the parameters describing these losses can be obtained from resonance measurements (73).

An equivalent method by which these relaxation mechanisms can be examined arises from considerations relating to the manner by which the magnetization which has been uniformly tipped away from the d.c. field by a small angle returns to equilibrium with this field. Callen (51) has shown that this may occur in several ways. The mode is dependent on the relative strength of the various mechanisms which can take energy from the applied field and transfer it to the lattice. Although the resulting relaxation parameters may be different in this case from those of resonance, the mechanisms are identical.

To describe these mechanisms, spin wave theory must be introduced. It is in this language that most of the recent work in resonance relaxation processes has been done. For our purposes, a spin wave may be considered as one of the modes obtained in a sinusoidal Fourier analysis of the spacial distribution of the magnetization with time dependent amplitudes. If the magnetization is predominantly aligned along the direction of the applied field, then the magnetization may be written as the Fourier series

$$M(t, x, y, z) = M_z(t) + \sum_k M_k(t) e^{ikr}. \qquad (1\text{-}95)$$

Here the applied field is taken in the z-direction. The M's are all vectors with M(t) the total magnetization, $M_z(t)$ the average magnetization along the applied field, and $M_k(t)$ the time varying vector magnitude of the spin

wave of wave vector k. Since these spin waves represent a nonuniform distribution of the magnetization, the creation of one of them produces an increase in the exchange and demagnetizing energies; the latter arising predominantly by virtue of internal demagnetizing fields. These internal fields provide a means for the coupling of energy between the spin waves. The spin waves of the wave vector, $k = 0$, also known as the uniform precession, represent the simple precession of the magnetization about the applied field.

The spin-exchange relaxation referred to above then represents the exchange of energy between the $k = 0$ mode and the $k \neq 0$ mode. This is equivalent to decreasing the energy of the magnetization in the applied field at the expense of increasing the exchange energy since the exchange energy is the dominant part of the spin wave energy. A number of perturbations are presently thought to bring about these interactions. In the inverted spinels, these perturbations (for example, spin-orbit interactions)(74) take on the randomness of the location of the ions. Structural defects (71), such as grain boundaries, pores, and surface pits, can also couple these modes.

The $k \neq 0$ mode then loses its energy directly to the lattice or other spin waves.

When a $k = 0$ spin wave is created, the total magnetic moment remains constant while its z component decreases. But when a $k \neq 0$ spin wave is created, the total magnetic moment and its z component are decreased.

Using these facts, we now can describe the modes, which were referred to earlier, by which the magnetization returns to alignment with the applied field when it has been uniformly rotated away from it. If no energy is lost, the magnetization precesses about the applied field. A $k = 0$ spin wave is formed. If this spin wave loses energy directly to the lattice or if it is

converted into a $k \neq 0$ spin wave which loses its energy rapidly, the decay will take the form shown in Fig. 1-10. On the other hand, if it loses its energy to a $k \neq 0$ spin wave which, in turn, does not lose its energy very rapidly, the relaxation will take the form shown in Fig. 1-11. Here the magnetization suffers a decrease in magnitude due to the long lifetime of the $k \neq 0$ spin wave.

These effects are summarized in a dynamical equation developed by Callen which is

$$\frac{dM}{dt} = a_1 M + a_2 M \times H + a_3 M \times M \times H. \tag{1-96}$$

Although this equation is similar to the Landau-Lifshitz equation, an immediate difference is that the change in magnitude of the magnetization for Eq. (1-96) is

$$\frac{d|M|^2}{dt} = 2a_1 M^2 \tag{1-97}$$

and does not vanish as in the case of the Landau-Lifshitz equation. Callen's equation allows for changes in the total magnetic moment. The coefficients, a_1, can be given definite physical meaning in quantum mechanical terms, i.e., in a scheme where the spin wave energies are quantized. The quantity a_2 is the gyromagnetic ratio.

There also has been found a nonlinear spin wave process (5, 75) which gives rise to energy absorption. In this process, which does not appear in Callen's formulation, again the uniform precession is excited, and it transfers its energy to a $k \neq 0$ spin wave. However, due to the nonlinear nature of the coupling when the $k = 0$ amplitude becomes sufficiently large (beyond a threshold), certain spin waves become unstable, grow rapidly, and absorb large amounts of energy from the uniform precession. In Chap. V, the time required to establish this instability is discussed.

In general, the results of these theories show that the relaxation times are inversely related to the linewidth and are dependent on the specimen size and shape, the d.c. field, and the perturbations.

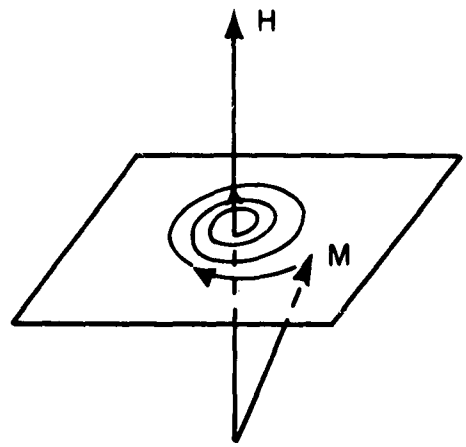

FIG. I – II DECAY OF THE MAGNETIZATION WHEN THE EXCHANGE LATTICE INTERACTION IS WEAKER THAN THE SPIN EXCHANGE INTERACTION

Although direct application of the results of these theories cannot be made to switching, these results enable one to make an intelligent guess at the type of effects, and their underlying origins, which can remove energy from the applied field. As an example, we consider a magnetization reversal process which is being carried out by domain wall motion. The motion of a wall is the result of the precession of the magnetization within the wall about an effective field normal to the wall. Roughly speaking, this is similar to a resonance experiment in a slab, with the d.c. field applied normal to the slab.

Clogston (76) has shown that the magnetic resonance linewidth, ΔH, that is broadened by an inhomogeneity which is not varying too rapidly, can be given by

$$\Delta H = \frac{H_p^2}{4\pi M} J(n_t, H/4\pi M).$$

Here, H_p^2 is the mean square value of the perturbation expressed in oersteds, and J is a function of the sample's shape through the transverse demagnetizing factor, n_t, and of the applied field, H. For a slab, $J > 1$ and increases with decreasing field and increasing magnetization. The relaxation parameter then also increases with decreasing field. In the nonsaturated state, which exists in materials which are switched, a large number of coarse grained inhomogeneities are possible. We have already seen how they effect the coercive force.

Other spin wave theories of loss, such as that of Clogston, Suhl, Walker, and Anderson (77), show that the linewidth vanishes when the transverse demagnetizing field vanishes.

It is not implied that spin waves should be, or would be, useful in switching, since the spin waves describe deviations from a uniform magnetization. A description of the deviation from the equilibrium which exists in small fields would be required. This equilibrium distribution would contain domain walls.

Wangsness (78) has shown that the decay of the magnetization must occur to the total field. If exchange, anisotropy, and demagnetizing fields are present in addition to the applied d.c. and microwave fields, the relaxation must take place to the resultant of these fields. From this one can conclude that if, in a resonance experiment, the relaxation occurs to an extremely large field, which also exists in a switching experiment, the relaxation parameters determined in the resonance will go over to switching. One such case occurs in certain rare earth garnets. It is an example of a spin-lattice relaxation process.

The magnetic garnets consist of three magnetic lattices. Two of the magnetic lattices consist only of iron ions. When the third lattice contains only diamagnetic ions, as in the case of yttrium iron garnet, the resulting material is seen to have a very narrow linewidth. However, when the third lattice contains a rare earth ion, the linewidths are broad. From the measurements of yttrium iron garnet, de Gennes et al (79) conclude that the iron lattices make a negligible contribution to the total linewidths of the rare earth garnets. And they have introduced a mechanism to account for these broad lines which postulates that the rare earth ions interact strongly with the lattice vibrations. The exchange field which couples the rare earth lattice to the iron lattices then acts as a random field on the iron lattices and brings about the relaxation of the total magnetic moment. Since this exchange field is larger than any of the other fields which are applied in the switching or resonance experiments, it fulfills the condition under which the relaxation mechanism can go over from resonance to switching. This is further discussed and applied in Chap. VI.

7. THIN FILM SWITCHING

Thin ferromagnetic films have recently received a great deal of attention. The interest is a result of the relative ease with which one can study their magnetization processes and of the possibility of their use as very rapid switching memory elements.

Wangsness (78) has shown that the decay of the magnetization must occur to the total field. If exchange, anisotropy, and demagnetizing fields are present in addition to the applied d.c. and microwave fields, the relaxation must take place to the resultant of these fields. From this one can conclude that if, in a resonance experiment, the relaxation occurs to an extremely large field, which also exists in a switching experiment, the relaxation parameters determined in the resonance will go over to switching. One such case occurs in certain rare earth garnets. It is an example of a spin-lattice relaxation process.

The magnetic garnets consist of three magnetic lattices. Two of the magnetic lattices consist only of iron ions. When the third lattice contains only diamagnetic ions, as in the case of yttrium iron garnet, the resulting material is seen to have a very narrow linewidth. However, when the third lattice contains a rare earth ion, the linewidths are broad. From the measurements of yttrium iron garnet, de Gennes et al (79) conclude that the iron lattices make a negligible contribution to the total linewidths of the rare earth garnets. And they have introduced a mechanism to account for these broad lines which postulates that the rare earth ions interact strongly with the lattice vibrations. The exchange field which couples the rare earth lattice to the iron lattices then acts as a random field on the iron lattices and brings about the relaxation of the total magnetic moment. Since this exchange field is larger than any of the other fields which are applied in the switching or resonance experiments, it fulfills the condition under which the relaxation mechanism can go over from resonance to switching. This is further discussed and applied in Chap. VI.

7. THIN FILM SWITCHING

Thin ferromagnetic films have recently received a great deal of attention. The interest is a result of the relative ease with which one can study their magnetization processes and of the possibility of their use as very rapid switching memory elements.

In the following, the switching properties of thin films will be discussed.

Since the loss mechanisms involved in the switching process have not as yet been resolved, little in a fundamental way can be learned from their switching. However, here, as compared with toroids, the experimental situation is clearer insofar as the experimental identification of the reversal mechanisms is possible, and there have been some verifications of the predictions of the Landau-Lifshitz equation which are worthwhile noting.

The ferromagnetic films whose switching properties have been studied are between 500 and 1500 angstroms thick and are usually made either by vapor deposition in a vacuum or by electroplating from an alloy consisting of 83% nickel and 17% iron. They have a coercive force between 1 and 2 oe. Unlike the bulk materials from which they are made, a uniaxial anisotropy can be induced in them through a magnetic anneal. This induced anisotropy provides a preferred axis for the magnetization within the plane of the film, and the induced anisotropy constant usually lies between 3000 and 5000 ergs/cc.

The films, as a result of thicknesses which are neglibible relative to their other dimensions, are free from demagnetization and can exist as a single domain whose magnetization lies entirely within the plane of the film. Multidomain states also exist.

It might appear that the prime motivation for the use of thin films as switching elements stems from the desire to eliminate eddy currents which are induced during the switching. In thicker materials these eddy currents serve as a brake on the magnetization reversal by preventing the applied field from rapidly penetrating the medium. However, it is known that eddy current losses are no longer the only factor which controls the speed of reversals in ferromagnetic tapes of less than 1 mil thickness such as are used in switching memory elements. Rather the incentive lies in another use of the films' geometry.

The effect of the films' shape (80) may be seen by considering a rotational magnetization reversal which is brought about by a field which is oriented along the easy axis in a direction opposite to the magnetization of a single domain film. If the applied field and the magnetization are not precisely antiparallel, a torque is applied to the magnetization. This torque will cause the magnetization to precess about the applied field. The magnetization will tend to turn out of the plane of the film, and when this occurs, a demagnetizing field will arise which is normal to the surface of the film. This field causes the magnetization to precess about it, and so the magnetization reverses.

The time for this reversal can be readily estimated. The frequency, ω, with which the magnetization precesses about the demagnetizing field, H_D, is

$$\omega = \gamma H_D. \tag{1-98}$$

Since the magnetization makes half of a revolution in reversing, the reversal time, T, is

$$T = \frac{\pi}{\gamma H_D} \tag{1-99}$$

H_D can be found from energy considerations. Since the demagnetizing field changes as the magnetization rotates, H_D is an average value. An approximate value for H_D would be its value after the magnetization has rotated and completed 50% of its reversal. At this time the magnetization has decreased its energy in the field, H, by an amount H_M, which, in the absence of losses, is converted entirely to demagnetizing energy. If the magnetization at this time makes an angle θ with the plane of the film, the demagnetizing field will be $4\pi M\theta$, and the demagnetizing energy will be $2\pi M^2\theta^2$. Equating the loss of energy in the applied field to the gain in demagnetizing energy, θ is found to be

$$\theta = \sqrt{\frac{H}{2\pi M}} \tag{1-100}$$

from which H_D is given as

$$H_D = \sqrt{8\pi MH}. \qquad (1-101)$$

Typically, M is approximately 700 emu, and H is 1 oe. With these values the demagnetizing field is about 100 oe. Using this value in Eq. (1-99) gives a reversal time of about 10^{-9} seconds. This has not been observed for reasons given below. However, in larger applied fields, the magnetization reversal of thin films has been brought about in times of this order of magnitude.

There are a number of reasons why the rapid reversal in small fields does not occur. In the first place, in small applied fields it is found that the magnetization reversal proceeds by domain wall motion and not by rotation. The induced uniaxial anisotropy provides the barrier which prevents a coherent rotation from taking place. Hence, fields of about 4 to 6 oe are required for rotational processes. Yet when fields of this size are applied, rapid switching does not occur. The details of what does occur at this time have been described differently by various authors.

Hanzel and Conger (81) argue that when an applied field is increased beyond the coercive force of the material, the number of walls contributing to the reversal process increases until the applied field is the size of the anisotropy field. The increase in the number of walls is the result of a nucleation process in which the nucleating field strengths have a statistical distribution. One would then expect that as the applied field increased, the distance a domain wall would move would decrease and this would be portrayed by a continual change in S_w. However, such a change in S_w has not been observed. Gyorgy has pointed out that the energy required for the number of nucleated walls needed in this mechanism is larger than the available energy. Smith (82) has recently, with the aid of a Bitter pattern examination of the domain structures which he believes take part in these reversals, clarified the situation. The magnetization distribution of these domains is

of a complex nature. From Smith's photographs it would appear that the magnetization change takes place by rotations and a discontinuous growth of these domains. This growth does not occur by domain wall motion, but rather the domain boundaries are extended by a continuation of the nucleation process.

That domain wall motion and magnetization rotation processes take place in this region between the coercive force and the anisotropy field is easily verified directly by experiment since both the magnetization change along and orthogonal to the applied field can be observed. When domain wall motion is the important process, there is no output from the transverse pick-up as a result of the domain walls always moving parallel to the easy direction. However, when rotational processes take place, the transverse component is seen, if there is any degree of coherence. Such observations have been made in which it has been seen that the rotational contributions increase with increasing field.

For fields larger than the anisotropy field there seems to be general agreement that the reversal mechanism is a uniform rotation. However, again, reversal times as low as those which we indicated above are not obtained in small fields. One of the reasons for this is that, in the above estimate, damping was neglected. Harte (83) has also pointed out that if the rotation is not perfectly uniform this would lead to longer than anticipated switching times, since some of the energy that would have brought about the rapid rotation goes into maintaining the nonuniform distribution.

In the description of rotational switching given above, no indication is given of why the magnetization finally comes into equilibrium with the applied field. It would appear, in the absence of damping, that the magnetization would rotate on past its equilibrium. A more careful examination of this situation, using the Landau-Lifshitz equation, shows that oscillations will occur when the damping parameter is sufficiently small. Dietrich and

Proebster (84) have observed such oscillations. These workers have also observed switching times of the order of millimicroseconds in a film whose coercive force is 1.7 oe. In a field of 6 oe applied at an angle of about 10 degrees to the easy axis, Wolf (85) has also observed free oscillations of the magnetization which has been displaced slightly from an easy axis.

8. DEVICES

As indicated earlier, devices used in conjunction with electronic equipment have brought about an interest in and have made important the study of the switching properties of magnetic materials. Although many applications for switching ferromagnets exist in radar and low frequency magnetic amplifiers, the predominant applications are in digital computers where ferromagnets are used for memory and logic devices. In this field, a large number of circuits have evolved which employ magnetic cores for these functions. Since a number of extensive reviews (86) exist on the subject of their operation, only the role played by the magnetic material will be treated here. For this purpose it will be assumed that the magnetic material has a square hysteresis loop, is toroidal in shape, and is wound with a single coil of N turns. In certain applications of importance the coil consists of a single turn.

We first note that during the switching of such a core its impedance is almost entirely resistive. This is most readily seen through consideration of the voltage induced in the winding by the switching of the core after the application of a current pulse of constant amplitude and the voltage which appears after its removal. When the current is applied, it is found that the core switches and produces a large output voltage. However, when the current is removed by opening the circuit which connects the current source with the core, only a relatively small reverse voltage appears. If the equivalent impedance had been reactive, energy would have been stored during the current pulse, and the subsequent removal of the current

would have been accompanied by a large voltage pulse. Hence, it must be concluded that the core acts as a dissipative element during the switching.

An average value for this resistance can be computed as follows. If the core reverses an amount of flux, $\Delta\phi$, in a time, t, then the average voltage, <V>, produced during the switching is

$$<V> = \frac{N\Delta\phi}{t} . \tag{1-102}$$

Since this voltage is the response to an applied current of amplitude, I, the average resistance, <R>, seen during the switching is

$$<R> = N \frac{\Delta\phi}{It} . \tag{1-103}$$

In order to proceed further a relationship between the applied field and switching time is required. In most applications it has been found that Eq. (1-84) holds. Using this equation and noting that in a toroidal core H = 4NI/d, the current which switches the core in a time, t, is found to be

$$I = (\frac{S_w}{t} + H_o) \frac{d}{4N} , \tag{1-104}$$

where d is an appropriate average diameter of the core.

Since $\Delta\phi = A\Delta B$, where A is the cross sectional area of the toroid and ΔB is the change in flux density, and using Eqs. (1-103) and (1-104), the average resistance can be written as

$$<R> = \frac{4N^2 A\Delta B}{(S_w + H_o t)\, d} . \tag{1-105}$$

In many high speed switching applications $S_w >> H_o t$. Under this condition the average resistance becomes

$$<R> = \frac{4N^2 A\Delta B}{S_w d} . \tag{1-106}$$

From these equations it is seen that the core's resistance is determined by its shape, the material, and the number of turns in the winding. When the core's dimensions are fixed, the resistance per turn squared is determined only by the material through the parameters, ΔB and S_w. With all other characteristics the same, the faster switching material, i.e., the material with the smaller S_w, will have the higher resistance.

The average power dissipated by the core is approximately

$$\langle P \rangle = 2I \frac{\Delta\phi}{t} = \frac{Ad\Delta B}{2t^2} (S_w + H_o t). \tag{1-107}$$

Since πAd is the volume of material in the toroid, the power dissipated by the switching is proportional to its volume and increases as the inverse square of the reversal time. For a given core size and switching time, a material with low S_w, low threshold fields, and small flux densities is required in order to reduce the driving power. Since other factors, such as signal-to-noise ratios and leakage inductance of wound cores, determine the flux density, and since for many applications $S_w >> H_o t$, the reduction of S_w is all that remains to decrease power consumption.

Since the energy required to switch a toroid is small as a result of the typically small volume which these cores possess, it would appear the further power reduction is not required. Whatever power dissipation does occur does serve to heat the toroid and, as a result, changes the material's properties. This is particularly deleterious in materials which have a low Curie temperature. In addition, when rapid switching is desired, expensive circuitry is required and the cost of this circuitry increases rapidly with increasing power. Since in many applications this cost exceeds that of the magnetic material and in practically all applications it represents a large fraction of the price of the magnetic device, improved magnetic materials can lead to substantial economies in circuitry.

CHAPTER I - BIBLIOGRAPHY

1. E. W. Gorter, Proc. I.R.E. 43, 1945 (1955).
2. L. F. Bates, "Modern Magnetism" (Cambridge U. Press, 1950).
3. L. Landau and E. Lifshitz, Physik. Z. Sowjetunion 8, 153–169 (1935).
4. C. Kittel, Phys. Rev. 73, 155 (1948).
5. H. Suhl, Proc. I.R.E. 44, 1270 (1956); J. Phys. Chem. Solids 1, 209 (1957).
6. C. Herring and C. Kittel, Phys. Rev. 81, 869 (1951).
7. C. Kittel and J. K. Galt, "Solid State Physics", Vol. 3 (Academic Press, New York, 1956).
8. L. Néel, Ann. phys. 3, 137 (1948).
9. H. Kaplan, Phys. Rev. 86, 121 (1952).
10. J. S. Kouvel, Cruft Lab. Tech. Rpt. #10, Harvard Univ. (1955).
11. R. L. Douglas, Phys. Rev. 120, 1612 (1960).
12. H. Meyer and A. B. Harris, J. Appl. Phys. 31, 49S (1960).
13. P. Tannenwald and R. Weber, Phys. Rev. 121, 715 (1961).
14. M. H. Seavey, Jr. and P. E. Tannenwald, J. Appl. Phys. 30, 227S (1959).
15. R. C. LeCraw and L. R. Walker, J. Appl. Phys. 32, 167S (1961).
16. J. A. Osborn, Phys. Rev. 67, 351 (1945).
17. I. P. Kaminow and R. V. Jones, Gordon McKay Lab. Sci. Rpt. #5 (Series 2), Harvard Univ. (1960).
18. J. Smit and H. P. J. Wijn, "Ferrites" (John Wiley and Sons, New York, 1959), p. 169.

19. B. A. Lilley, Phil. Mag., Ser. 7, 41, 792 (1950).

20. C. A. Fowler, Jr. and E. M. Fryer, Phys. Rev. 86, 426 (1952).

21. See ref. #7, p. 491.

22. J. F. Dillon, Jr., J. Appl. Phys. 29, 539 (1958).

23. L. Néel, Cahiers Phys. 25, 21 (1944).

24. J. B. Goodenough, Phys. Rev. 95, 917 (1954).

25. D. M. Prahe, Cables and Transmission 11, 32 (1957) and 11, 128 (1957).

26. L. Néel, Ann. univ. Grénoble Sect. Sci. Math. et Phys. 22, 299 (1946).

27. M. Kersten as reported in ref. #7, p. 521.

28. See ref. #7, Fig. 39.

29. H. J. Williams, R. M. Bozorth and W. Shockley, Phys. Rev. 75, 155 (1949).

30. J. B. Goodenough, Phys. Rev. 102, 356 (1956).

31. C. Kooy and U. Enz, Philips Rsch. Rpts. 15, 7 (1960).

32. W. C. Elmore, Phys. Rev. 54, 309 (1938).

33. H. J. Williams and W. Shockley, Phys. Rev. 75, 178 (1949).

34. J. E. Knowles, Proc. Phys. Soc. 75, 885 (1960).

35. L. Néel, J. Phys. Radium 5, 241 (1944) and L. Néel et al., J. Appl. Phys. 31, 27S (1960).

36. H. Lawton and K. H. Stewart, Proc. Roy. Soc. A 193, 72 (1948).

37. H. P. J. Wijn, E. W. Gorter, C. J. Esveldt, and P. Geldermans, Philips Tech. Rev. 16, 49 (1954).

38. L. F. Bates and P. F. Davies, Proc. Phys. Soc. 74, 170 (1959).

39. D. J. Craik et al., Proc. Phys. Soc. 72, 224 (1958).

40. L. Néel, Compt. rend. 241, 533 (1955).

41. H. Rubinstein, H. W. Fuller, and M. E. Hale, J. Appl. Phys. 31, 437 (1960).

42. E. M. Gyorgy and F. B. Hagedorn, J. Appl. Phys. 30, 1368 (1959).

43. E. M. Gyorgy, J. Appl. Phys. 29, 1709 (1958).

44. F. E. Luborsky, J. Appl. Phys. 32, 171S (1961).

45. R. W. DeBlois and C. P. Bean, J. Appl. Phys. 30, 225S (1959).

46. R. M. Bozorth, "Ferromagnetism" (D. Van Nostrand Company, New York, 1951), p. 797.

47. L. Néel, J. Appl. Phys. 30, 3S (1959).

48. G. W. Rathenau, J. Appl. Phys. 29, 239 (1958).

49. R. Street and J. C. Wolley, Proc. Phys. Soc. A 62, 562 (1949).

50. T. L. Gilbert and J. M. Kelley, Proc. of the Pittsburgh Conf. on Magnetism and Magnetic Materials (A.I.E.E., New York 1955), p. 253.

51. H. B. Callen, J. Phys. Chem. Solids 4, 256 (1958).

52. J. V. Harrington, Lincoln Lab. Tech. Rpt. #166, Mass. Inst. Tech. (1958).

53. R. Becker, J. phys. radium 12, 332 (1951).

54. W. Döring, Z. Naturforsch. 3a, 373 (1948).

55. C. Kittel, Phys. Rev. 80, 918 (1950).

56. J. E. Pippin, Thesis, Harvard Univ. (1959) and J. E. Pippin and C. L. Hogan, Gordon McKay Lab. Sci. Rpt #1, Harvard Univ. (Apr. 1959).

57. N. Menyuk and J. B. Goodenough, J. Appl. Phys 26, 8 (1955).

58. A. M. Clogston, Bell Syst. Tech. J. 34, 739 (1955).

59. J. K. Galt, Bell Syst. Tech. J. 33, 1023 (1954).

60. L. Néel quoted in Bell Syst. Tech. J. 34, 439 (1955).

61. J. F. Dillon, Jr. and H. E. Earl Jr., J. Appl. Phys. 30, 202 (1959).

62. F. B. Hagedorn and E. M. Gyorgy. J. Appl. Phys. 32, 282S (1961).

63. G. Vogler, Z. angew. Phys. 13, 185 (1961).

64. L. J. Dijkstra and U. M. Martius, Rev. Mod. Phys. 25, 146 (1953).

65. M. K. Haynes, J. Appl. Phys. 29, 472 (1958).

66. E. M. Gyorgy, J. Appl. Phys. 31, 110S (1960).

67. W. L. Shevel, Jr., J. Appl. Phys. 30, 47S (1959).

68. T. J. Matcovich and C. J. Kriessman, J. Appl. Phys. 30, 26S (1959).

69. J. B. Goodenough, Proc. I.E.E. 104, Part B. Suppl. (1957).

70. H. van der Heide, H. G. Bruijning and H. P. J. Wijn, Philips Tech. Rev. 18, 336 (1956/1957).

71. C. R. Buffler, Gordon McKay Lab. Sci. Rpt. #3 (Series 2), Harvard Univ. (1960).

72. G. T. Rado, J. Appl. Phys. 32, 129S (1961).

73. R. C. Fletcher, R. C. LeCraw and E. G. Spencer, Phys. Rev. 117, 955 (1960).

74. H. B. Callen and E. Pittelli, Phys. Rev. 119, 1523 (1960).

75. J. J. Green, Gordon McKay Lab. Sci. Rpt. #2 (Series 2), Harvard Univ. (1959).

76. S. Geschwind and A. M. Clogston, Phys. Rev. 108, 49 (1957).

77. Clogston, Suhl, Walker and Anderson, J. Phys. Chem. Solids 1, 129 (1956).

78. R. K. Wangsness, Phys. Rev. 111, 813 (1958).

79. P. G. de Gennes, C. Kittel, and A. M. Portis, Phys. Rev. 116, 323 (1959).

80. H. B. Callen, Proc. of Switching Conf., Harvard Univ. Press (1960).

81. A. L. Hanzel and R. L. Conger, J. Appl. Phys. 30, 1932 (1959).

82. D. O. Smith, J. Appl. Phys. 32, 70S (1961).

83. K. J. Harte, J. Appl. Phys. 31, 283S (1960).

84. W. Dietrich and W. E. Proebster, J. Appl. Phys. 31, 281S (1960).

85. P. Wolf, J. Appl. Phys. 32, 95S (1961).

86. R. K. Richards, "Digital Computer Components and Circuits" (D. Van Nostrand Company, New York, 1957), p. 187 and p. 354.

A. S. Meyerhoff, "Digital Applications of Magnetic Devices" (John Wiley and Sons, New York, 1960).

87. N. Bloembergen and S. Wang, Phys. Rev. 93, 72 (1954).

CHAPTER II: EXPERIMENTAL TECHNIQUES

1. INTRODUCTION

In this chapter a description will be given of the instrumentation and measurement procedures used in taking the data to be presented in later chapters.

The system used for measuring switching times is treated generally, and then it is followed by a fuller discussion of its various component parts. How this system may be used to determine the switched flux is shown. And the techniques used for grain boundary and domain wall observations are given.

2. EQUIPMENT FOR SWITCHING MEASUREMENTS

a. General discussion

The equipment which was employed to measure the switching properties of ferrite and garnet toroids consisted of a mercury relay pulse generator, a coaxial line, voltage sensing and cancelling coils, and an oscilloscope. Figure 2-1 is a block diagram showing the arrangement of this apparatus.

The toroids, whose inner and outer diameters were 70 and 100 mils respectively, were placed in the coaxial line for measurement.

The pulse generator supplied a series of positive and negative current pulses to switch and reset the cores. It is convenient in describing the experiments to use the term "switch" to denote that portion of the cycle during which the toroid is removed from its initial magnetic state and its switching time is measured and the term "reset" to denote the remaining portion of the cycle in which the initial state of the toroid is restored. As a rule the reset field was held constant, while the switching field was varied (see Chap. IV).

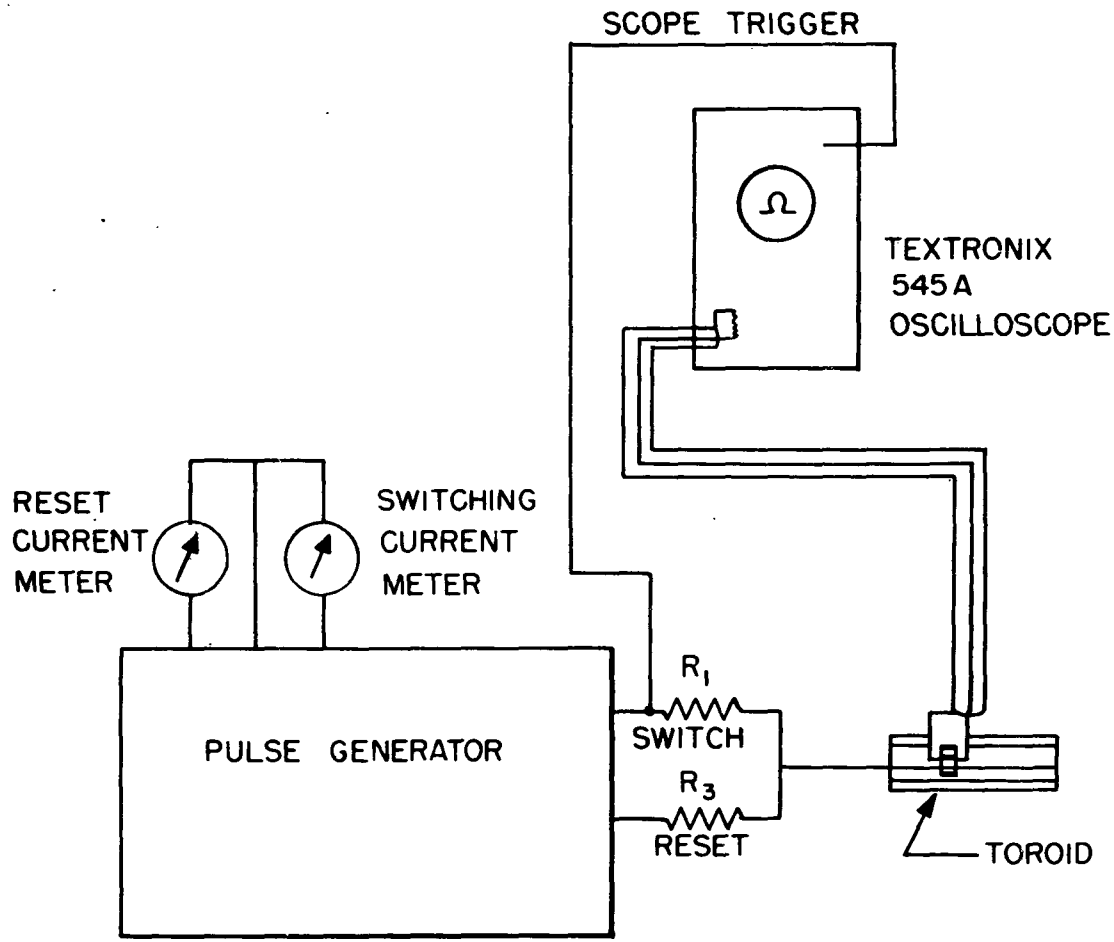

FIG. 2-1 BLOCK DIAGRAM SWITCHING TIME MEASURING EQUIPMENT

In order to observe on the oscilloscope the switching waveform from which the switching time was measured, a single turn voltage sensing coil was coupled to the toroid. Since this coil was also coupled to the applied field, an adjustable single turn cancelling coil, which coupled only to the applied field, was connected in series with it so as to subtract that part of the signal due to the changing applied field. When the cancelling coil was properly positioned, the voltage at the output terminals of the series connected coils consisted only of the voltage induced by the changing magnetization within the toroid.

The amplitudes of the current pulses were independently variable so that the switching time could be measured as a function of the applied field.

The mercury pulse generator could supply switching and reset current pulses up to 30 amps with a rise time better than 7 nsec (i.e., 7×10^{-9} sec) at a 60 cycle rate. Magnetic fields of 45 oe could be obtained at the outside diameters of the toroids which were used here.

b. Coaxial line and voltage sensing coils

The coaxial line which was used is shown in Fig. 2-2. It was made entirely of brass except for a polystyrene insulator which held the inner conductor in position at the non-short-circuited end. The plug on the other end shorted the line, and it was removable in order to admit the sensing and cancelling coils and the toroid which was to be measured. These coils are shown in Fig. 2-3a. The lower portion of the sensing coil was a brass tube which enabled it to fit and slide over the inner conductor from which it was insulated by a coating of varnish. One arm of the sensing coil was movable. When it was raised, the toroid could be placed over the tube. When it was lowered, it fit into a hole in the tube. This arm was made of phosphor bronze so that it held itself in position and made good contact because of its ability to act as a spring. A picture of the assembly is given in Fig. 2-3b.

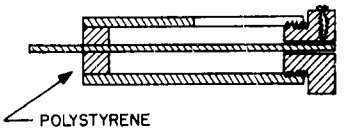

FIG. 2-2 THE COAXIAL LINE IN WHICH THE MEASURMENTS WERE MADE. IT IS MADE OF BRASS EXCEPT AS LABELED.

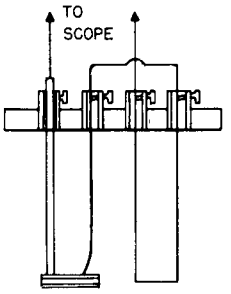

FIG. 2-3a THE VOLTAGE SENSING (LEFT) AND CANCELLING (RIGHT)(SINGLE TURN) COILS. THE TOROID WHICH IS MEASURED IS PLACED ON THE TUBE LOCATED AT THE BOTTOM LEFT.

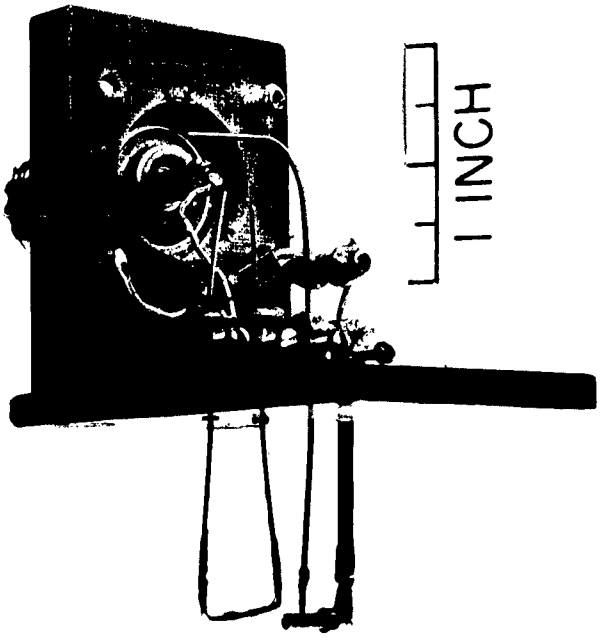

FIG. 2-3b PHOTOGRAPH OF THE VOLTAGE SENSING AND CANCELLING COILS ILLUSTRATED IN FIG. 2-3a.

The position of the toroid was fixed when it was placed inside the coaxial line, since the phenolic board (see Fig. 2-3b) to which the coils were connected slid in a pair of grooves which had stops to limit its travel and locate its position during measurement.

The toroid was measured in the coaxial line for two reasons. First, it was necessary to have a low inductance transmission line (see Sec. d below). Second, the coaxial line provided a geometry in which the applied fields had the required cylindrical symmetry and could easily be determined.

c. Operation of the mercury relay

The mercury relay was chosen as the switch to form pulses, since it can close its contacts in a time less than 1 nsec and can conveniently handle heavy currents. The relay consists of a mechanical switch enclosed in a glass tube in a high pressure hydrogen atmosphere. The switch has two back and two front contacts, as well as a swinging armature which is in a cantilever reed structure. The transfer of the swinger from the front to back contacts makes those circuits attached to the back contacts and breaks those connected to the front contacts. The reverse occurs when the swinging armature is returned to the front contacts. A pool of mercury at the bottom of the tube wets the contacts through a capillary formed by the swinger. The combination of the mercury wetting and the high pressure atmosphere results in an instantaneous make and break of contact. The initial circuit closure made by the swinger with a set of contacts is formed by a drop of mercury which acts as a flexible bridge.

The glass tube is placed inside a solenoid. Since the swinger is made of a magnetic material, it can be transferred from one set of contacts to the other by the magnetic field which results from a current in the solenoid.

d. The current pulse generator

The mercury relay pulse generator which was designed for the switching experiments was patterned after a pulse generator described by Narud (1).

In order to supply the required large currents with a minimum of power, the mercury relay discharged a charged capacitor into the coaxial line. The circuit used for this is shown in Fig. 2-4. Capacitor C_2 which was discharged into the coaxial line was charged when relay K-1 was closed and relay K-2 was open. It discharged when relay K-1 was open and relay K-2 was closed. The duration of the discharge was controlled by the time constant, R_1C_1. Since R_1 determined the current in the line, its value was determined by the d.c. voltage that could be applied to the relay. C_1 was determined by the available input power. (The energy stored in C_1 was proportional to its size and was dissipated each cycle.) These considerations led to a choice of R_1 as 10 ohms and C_1 as 0.6μf. With this time constant the current remained sufficiently constant so that switching times under 0.4μsec were measured and found to be within 1% of the times measured when C_1 was increased eight-fold. R_2 was chosen so that C_1 could fully charge during that part of the cycle in which K-1 was closed. Measurement of the power supply voltage, V, with the meter, M, in Fig. 2-4 gave the peak current, I, in the coaxial line,

$$I = \frac{V}{R} \quad , \tag{2-1}$$

which produced the switching field. The voltage measurement was made with a meter whose accuracy was ±1% of full scale. The errors in the field due to measurement were then ±0.4 oe between 15 and 40 oe, ±0.15 oe between 1.5 and 15 oe, and ±0.015 oe for fields below 1.5 oe.

When switching fields of a longer duration were required than could be furnished by C_1 and R_1, external capacity was added. The power requirements here were small, since the long switching times occurred at low values of the switching field.

The capacitor, C_1, consisted of six 0.1μf ceramic capacitors wired in parallel, while the added capacitors were either 2 or 4μf oil filled paper capacitors. The large external capacitors, due to the size of R_1, did not

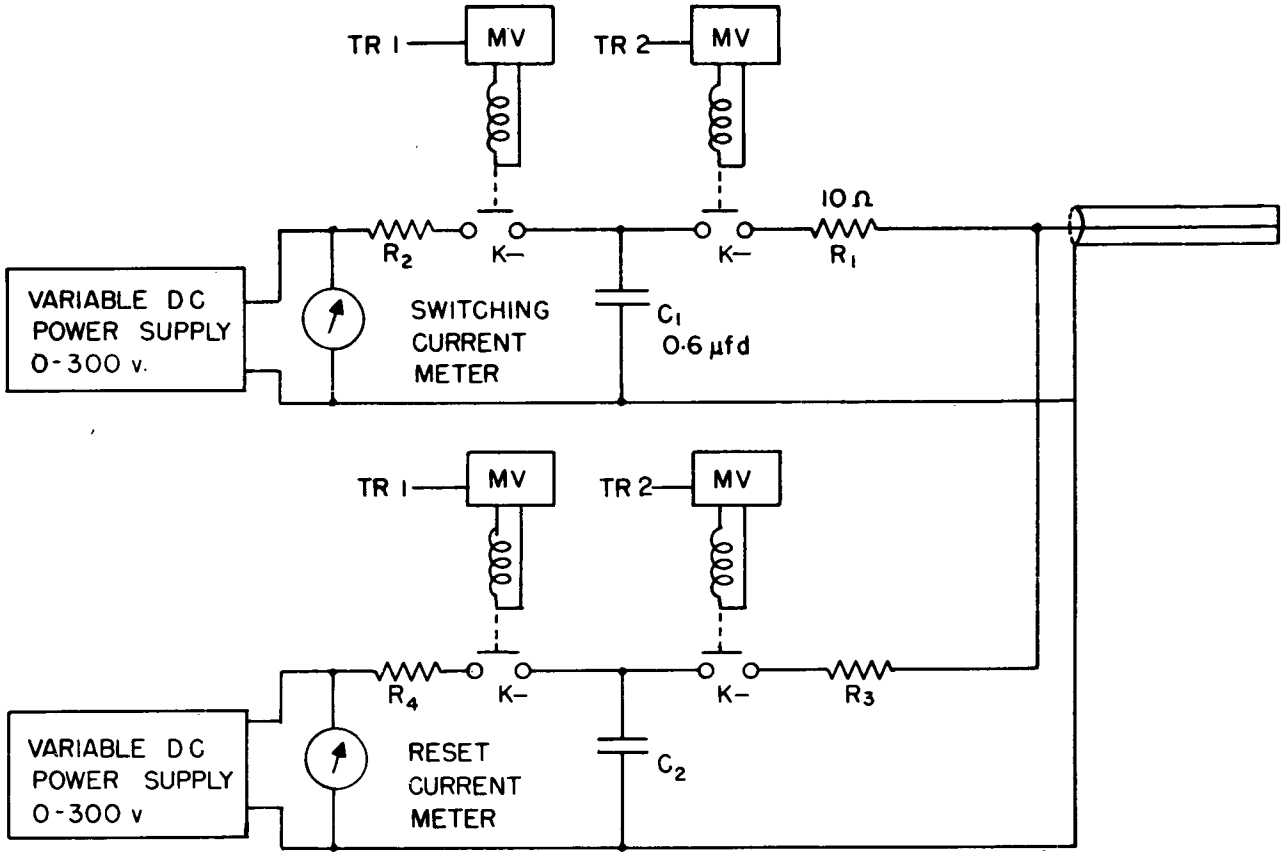

FIG. 2-4 PULSE GENERATOR: CIRCUT FOR CAPACITOR CHARGE AND DISCHARGE. MV ARE MULTIVIBRATORS WHICH ARE SYNCHRONIZED BY THE SIGNALS TR 1 AND TR 2 WHICH OCCUR AT A 60 CYCLE RATE.

always charge in the available time. When this occurred, the voltages were measured with an oscilloscope and had an accuracy of 3%.

In order to decrease the inductance of the contact circuit of the relay K-2, it was removed from its protective metal case, and connections were made directly to the mechanical elements. The rise time of the current in the circuit was determined by the inductance of the coaxial line (about 2 mμh) in conjunction with resistor R_1.

The multivibrators which operated relays K-1 and K-2 were adjusted to operate at a 60 cycle rate. They were triggered by the 60 cycle line to energize the relays out of phase.

The circuits which provided the reset current were similar to these and will not be discussed. The mercury relay was used wherever relays were required. Only in position K-2 did it serve as a fast switch. In the other positions it was used because of its noise free contact transfers. The particular relay used here was the Western Electric 276d.

e. Switching voltage display

The voltage produced at the output terminals of the sensing and cancelling coils was brought to the oscilloscope (Tektronix 545A), where it was displayed, by a coaxial cable terminated in its characteristic impedance. Typical output pulses are shown in Fig. 2-5. These particular curves were obtained from the switching of an yttrium iron garnet.

The switching time was defined as the time difference between the two points in the switching waveform whose amplitude is 10% of the maximum. If two maximums occurred, the second maximum was used with this definition. If two or three mechanisms are present in the switching process and if each occurs in substantial fractions of the material, this definition of the switching time produces a measure of the slowest mechanism since it encompasses almost the entire flux reversal. The flux which switches after the second 10% point is sufficiently small so that it cannot represent a significant mechanism.

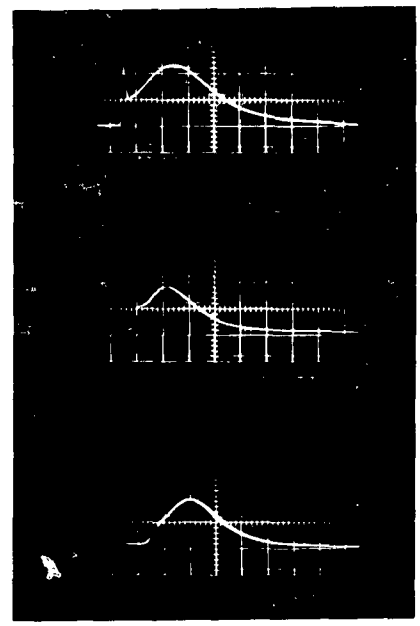

FIG. 2-5 TYPICAL SWITCHING WAVE FORMS OF YTTRIUM IRON GARNET. a) APPLIED FIELD 4 oe., HORIZONTAL DEFLECTION 0.1 μsec/div; (b) APPLIED FIELD 8 oe., HORIZONTAL DEFLECTION 0.04 μsec/cm. (c) APPLIED FIELD 11 oe. HORIZONTAL DEFLECTION 0.02 μsec/cm.

The calibrated time bases of the oscilloscope were found to be accurate to better than 1%. This was determined by measuring appropriate sine waves whose frequency was known to within 0.03%. However, a limitation was imposed on time measurements by the reading resolution. This amounted to 1% of the full scale value.

A far more serious error occurred in the time measurement if account was not taken of the finite bandwidth of the oscilloscope. The effect of this bandwidth was to broaden the pulses. Since the bandwidth of the oscilloscope and the plug-in unit combination which was used was 30 mc, these effects became important when the switching time was less than 30 μsec. However, these effects could be accounted for and the introduced error eliminated in the manner which follows.

Since the oscilloscope had a distributed amplifier, its transfer function could be approximated by a gaussian function. In Fig. 2-5 it can be seen that the faster switching pulses have a gaussian appearance. Then, from the solution of the transient circuit problem of a gaussian pulse in a gaussian filter the width, t_i, of a pulse at the input of the amplifier may be determined when the width, t_o, at the output of the amplifier is known. The result of this calculation is that

$$t_i^2 = t_o^2 - 374 \quad , \tag{2-2}$$

where t_i and t_o are measured in nanoseconds.

From Eq. (2-2) it was seen that, for pulses greater than 100 nsec, the response time of the instrument affected the measurement to less than 2%, so that the entire error in measuring the switching time was in the ability to read the scale. Since the available time bases were in the ratio of 1 to 2 to 5, the largest reading error occurred for a midscale reading on the 5 scale where the error was 2.5%.

For the switching times where Eq. (2-2) was important, the error became somewhat larger. At the limit of the scope's resolution, t_o was about 20 nsec. Since the reading was made on a 200 nsec time base, there was a possible 10% error from reading of the scale. Here the error introduced by the assumption that the switching pulse and the scope amplifier were gaussian must also be considered.

A check on the scope's resolution did indeed show that the limit of resolution was about 19 nsec when the fastest available core switching pulse was measured by the oscilloscope. However, it was found that the response possessed a 20% overshoot which was probably due to imperfect adjustment of the scope's vertical amplifier. (This was not a core characteristic, for the same signal appeared when the fast rising current pulse was differentiated and displayed.) The overshoot was barely discernible when the pulse was broadened to 40 nsec.

To avoid these errors, the measurements were limited to 40 nsec. In this region, the precise response of the amplifier was not important, and the reading error was only 5%.

f. High temperature measurements

The switching measurements which were made at temperatures above room temperature were obtained by placing the entire switching equipment in a Cenco drying oven. The temperature of this oven is thermostatically controlled. Since the field which is applied to the core is determined by the resistor in series with the coaxial line and since this resistor's value could change with temperature, its value was measured during the elevated temperature run and then used in the field computation.

g. Extension of the present system

In order to increase the usefulness of the arrangement for measuring switching times, it is necessary that the coaxial line be separated from the pulse equipment. This makes switching measurements over a wide

range of temperatures possible, for now the sample can be placed in either a refrigerator or an oven without endangering the mercury relay which can only operate over a restricted range of temperatures. In the present arrangement, this separation was prohibited by the manufacturer's maximum voltage rating of the relay. The impedance which could be used in series with the relay was determined by this rating in conjunction with the desired maximum current and rise time. This in turn set an upper limit on the length of the coaxial line.

However, it has recently come to the author's attention that this rating can be considerably increased if the voltage on and current through the relay is reduced to zero when the contacts are broken. As a result, it is possible to obtain the required currents at an impedance level such that the coaxial line can be terminated in its characteristic impedance, and then its length is not critical. This has the additional benefit of removing the limitation on the rise time of the current imposed by the cable inductance and should be useful for obtaining faster switching. For this to be meaningful, a sampling oscilloscope should be used for measurements, and the voltage sensing coil should be shielded from electrostatic switching transients. These transients were not seen in the present system, since they were attenuated by the oscilloscope's finite bandwidth.

3. FLUX SWITCHED MEASUREMENTS

When the data measured during a switching experiment is plotted, a relationship between the reciprocal switching time and applied field is obtained which exhibits a significant change in slope at a value of applied field several times the field at which switching was initiated. From a general consideration of hysteresis loops a variation of the flux change can be expected at values of the field up to that value at which this change in slope occurs. In order to determine if this change is related to the

quantity of switched flux, its measurement was undertaken under conditions which were identical to those of the switching experiment.

These measurements yielded information similar to that obtained from hysteresis loops since a flux field relationship was determined. However, when these loops are determined, switching and reset fields are equal, unlike those of a switching experiment.

The method employed to make these measurements also has the advantage, as will be seen below, that it is readily applied to the small toroids used here. The measurement of hysteresis loops of such small toroids presents a difficult problem since these toroids contain a small amount of flux. The considerations which led to the method of measurement and the manner in which measurements were made follow.

The most apparent way to make these measurements would be the integration of the voltage waveform resulting from application of the switching field. Since this waveform represents the rate of change of flux, its integration gives the flux. However, for small switching fields the voltage waveform has a long duration, and when an electrical integrator is used to measure the area of the signal, i.e., the flux switched, its time constant must be much longer than the duration of the signal. For a fixed flux output, it can be shown that the integrated voltage decreases as the time constant increases. Hence, to measure the flux switched at small driving fields, a large time constant would be required, and small voltages would result. A numerical example given below will illustrate that these voltages would be of insufficient magnitude to be detected.

This difficulty may be overcome by noting that almost the same flux change occurs when the reset field is applied. Since this field is large, the reset switching voltage is of short duration, and, consequently, the integrator time constant can be shorter than in the previous case. Hence,

to examine the flux change, an integrator was used to determine the area of the reset voltage as the switching field was changed.

The simple RC circuit shown in Fig. 2-6 served as the integrator. It had a 10 μsec time constant. The output voltage, e_o, of this type of integrator is

$$e_o = \frac{1}{RC} \int e_s dt \qquad (2\text{-}3)$$

in terms of the switching voltage, e_s, and the time, t. Since the switching signal, e_s, is given by

$$e_s = \frac{d\phi(t)}{dt} \quad , \qquad (2\text{-}4)$$

where $\phi(t)$ is the flux, and the total flux changed is $\Delta\phi$, Eq. (2-3) becomes

$$e_o = \frac{\Delta\phi}{RC} \quad . \qquad (2\text{-}5)$$

For yttrium iron garnet, whose maximum flux density change at room temperature is about 3600 gauss (twice the saturation magnetization), and for a toroid whose cross sectional area is 0.5 mm^2, $\Delta\phi$ is 18 lines. Then, the output voltage of the integrator described above, e_o, is about 18 millivolts. The minimum signal detected was one millivolt.

This measurement was made with a switching signal of about 50 nsec duration. If this measurement had been made using the other cycle's switching signal, which had a duration of about 1 μsec, the integrator time constant would have had to have been at least twenty times longer, and so the resulting signal would have been below the detectable level.

4. GRAIN SIZE MEASUREMENTS

The grains of oxides can be observed either by a polishing and etching technique followed by microscopic examination or by a direct microscopic observation of a smooth surface of the sample following its sintering. The

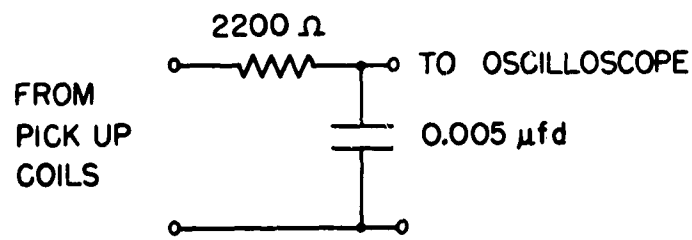

FIG. 2-6 THE FLUX SWITCH INTEGRATOR

former procedure gives a better indication of porosity and second phases than the latter.

When the samples were polished, a face of the sample was made flat with increasingly finer emery papers. This face was then polished at 200 rpm with 6 micron diamond dust, and then again with 1 micron diamond dust.

The samples were etched either with boiling HCl or thermally to make the grain boundaries visible. In the latter procedure, the sample was brought to sintering temperature in an oxygen atmosphere with full power applied to the furnace and held at this temperature for fifteen minutes. The power was then shut off and the sample and oven were cooled to room temperature.

Figure 2-7 shows a typical observation of grains in a garnet.

5. DOMAIN OBSERVATIONS

One of the advantages of using a thermal etch is that the surfaces are freed of the strains introduced during the polishing operations. Hence, surfaces so prepared are suitable for domain observations (2). These observations were made using the Bitter technique (3).

A typical observation is shown in Fig. 2-8.

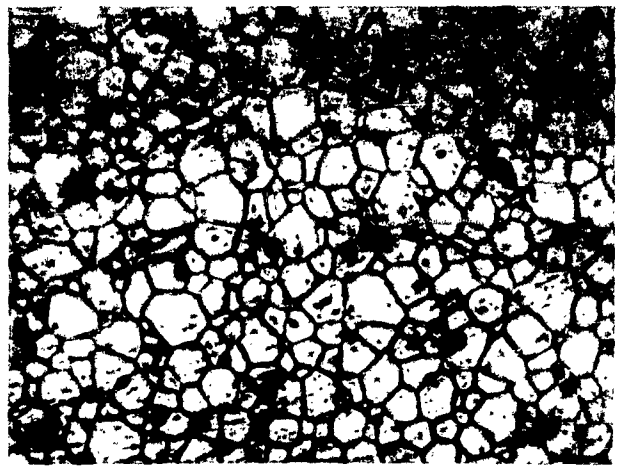

FIG. 2-7 CRYSTAL GRAIN STRUCTURE IN YTTRIUM IRON GARNET

10 MICRONS

FIG. 2-8 DOMAIN STRUCTURE IN YTTRIUM IRON GARNET. THE LIGHTER LINES (WITHIN THE GRAIN BOUNDRIES) ARE THE DOMAIN BOUNDRIES. THE OBSERVATIONS WERE MADE USING THE BITTER TECHNIQUE WITH A LIGHT FIELD OIL IMMERSION OBJECTIVE.

CHAPTER II – BIBLIOGRAPHY

1. J. A. Narud, High Energy Physics Lab, HEPL-34, Stanford Univ. (1955).

2. Sheffield Magnetism Conference Report, Brit. J. Appl. Phys. 11, 307 (1960).

3. C. Kittel and J. K. Galt, "Solid State Physics," 3 (Academic Press, New York, 1956) p. 491.

CHAPTER III: MATERIALS AND MATERIAL PREPARATION

1. INTRODUCTION

In this chapter the materials used in the switching study will be discussed. First, the preparation of the materials will be discussed. Later, their magnetic parameters will be considered.

Three types of materials were used in this study: single crystal garnets and polycrystalline garnets and ferrites. The garnets were chosen for these studies because of their unique crystal structure and chemical composition, while the ferrites were used as a system in which it is possible to vary the total magnetocrystalline anisotropy. These variations are not yet possible in the garnet system.

2. MATERIALS – PREPARATION

a. Polycrystalline garnets

The garnets which were prepared for this work are ferromagnetic oxides having the formula $5 \cdot Fe_2O_3 3 \cdot M_2O_3$, with M either yttrium, samarium, erbium, ytterbium, gadolinium, holmium, or a combination of two of them (mixed garnets). A few garnets having the general formula $(5 - x)Fe_2O_3 x \cdot M_2O_3 \cdot 3Y_2O_3$, with M either indium or gallium, were also prepared. Since Rodrigue and Wolf (1) have described in great detail the method by which the polycrystalline garnets discussed here were made, this topic will be treated briefly.

In the initial step in making the ceramic garnets, measured quantities of iron and rare earth oxides (or yttrium oxide) were dissolved in nitric acid to form nitrates. The resulting nitrates were then mixed and coprecipitated in ammonia water. The brown precipitate, which resembled a breakfast cereal, was then placed in a blendor and mixed in water. Following this, the water was removed, and the finely divided precipitate was fired in air at a temperature of 900°C to cause the garnet forming

reaction. The resulting material, which was green, was then placed in the blendor again and blended in water in order to reduce its particle size. It was then removed from the blendor and mixed with a binder (Elvacet) which was required for the next step in which the fired garnet was pressed into a desired shape. The binder was mixed in by a mechanical stirrer in the ratio of 50 parts garnet to 1 part binder. Following the pressing, the garnet was set on a platinum sheet in a ceramic boat and fired in a tube furnace at 1400° C, for about 15 hours. The fired piece was black with grains which varied from 2 to 20 microns. Unless otherwise noted, all the polycrystalline garnets were prepared as described above.

b. Single crystal garnet

The single crystal was prepared by the lead fluoride method (2). This method produces crystals from which small toroids may be removed.

The small toroid was made (3) by grinding the crystal flat and then mounting it on a piece of glass and drilling it with a rod whose tip had been impregnated with diamond. The hole was then enlarged and brought to the required size (70 mils) by lapping with silicon carbide. The piece was then mounted on a rod and placed in an index head which was turned while a rotating grinding wheel formed the outside diameter (100 mils).

c. Ferrites

The ferrites prepared for this work were nickel ferrite ($NiMn_{0.02}Fe_{1.9}O_{4\pm}$) and nickel ferrite doped with cobalt ($Ni_{1-a}Co_aMn_{0.02}Fe_{1.9}O_{4\pm}$). The procedure used in their preparation is identical to that described by Hogan and Pippin (4). The oxides of nickel, iron, and cobalt were balled, milled, and presintered at 1000° C. The material was then crushed, a binder added, pressed, and fired at 1250°C. In this case the resulting material had a grain size of about 2 microns.

3. MAGNETIC PROPERTIES

a. Magnetization and Curie temperature

The temperature dependence of the magnetization of the ferrites and garnets may, to a good approximation, be accounted for by Néel's theory of magnetization (5). According to this theory, a crystal's net magnetization is the sum of the magnetizations of a number of sublattices. Each magnetic moment within a sublattice is assumed to have an exchange interaction with members of its own sublattice, as well as with members of the other sublattices.

In the case of nickel ferrite (6, 7), two sublattices are required to explain the magnetization. One of the sublattices contains the iron and nickel located on the octahedral sites, while the other contains the iron which is found on the tetrahedral sites. These two sublattices are coupled in an antiferromagnetic manner.

In garnets, Pauthenet (8) found that three sublattices participate in the magnetization. Two of these sublattices contain iron, and the third contains the diamagnetic yttrium or rare earth ion. The strongest interaction amongst the sublattices is between the two iron sublattices. This may be seen from the fact that the Curie temperature of the garnets is substantially constant as the ion in the third sublattice is varied. Pauthenet has also found that the net magnetization results from the strong interaction of the iron lattices and the weaker interaction of the third lattice with the net magnetization of the two iron lattices. This third lattice is not magnetically saturated, while the two iron lattices are.

The room temperature magnetization and Curie temperature data for the ferrites are in Table 3-1. The magnetization data is taken from Pippin (9). In Table 3-2 this information is given for the garnets. It will be noted that the Curie temperature for all but the indium and gallium substituted garnets are the same. These substituted garnets have a lower Curie

temperature than the nonsubstituted materials, since the substitutions have replaced some of the iron. This reduces the number of ions which

TABLE 3-1

Magnetization, M, anisotropy, K, Curie temperature, T_c, g value, linewidth, ΔH, and damping parameter, λ, for $Ni_{1-x}Co_xMn_{0.02}Fe_{1.9}O_4$, at room temperature.

x	M(cgs)[9]	T_c(°K)[25]	$K \times 10^{-4}$(erg/cc)	g	ΔH(oe)[4]	$\lambda \times 10^{-7}$(rad/sec)
0	257	858	-5.1	2.34	420	28.8
0.02	264	858	-1.4	2.25	220	15.4
0.025	266	858	-0.5	2.27	210	15.7
0.03	268	858	+0.4	2.29	210	15.1
0.04	272	858	+2.2	2.28	280	20.6
0.05	275	858	+4.1	2.27	390	39.0

TABLE 3-2

Room temperature magnetization, M, anisotropy constant, K, g value, linewidth, ΔH, and damping parameter, λ, for various iron garnets. The Curie temperature, T_c, unless otherwise noted is 545°K. The data is from reference (11) except as indicated.

Yttrium, Yttrium Indium, Yttrium Gallium, Erbium, Ytterbium

Garnet	M(cgs)	T_c(°K)	$K \times 10^{-3}$(erg/cc)	g	ΔH(oe)	$\lambda \times 10^{-6}$(rad/sec)
Yttrium	137	545	5.8	2.01	0.2[28]	0.07
Y-In 5%	152[10]	500[10]	4.1[26]	2.01[27]	71[27]	27.4
Y-In 10%	142[10]	444[10]	2.9[26]	2.01[27]	85[27]	30.9
Y-Ga 5%	110[10]	519[10]	5.3[26]	2.01	–	–
Erbium	97	545	6.7	1.42	1070	132
Ytterbium	131	545	4.1	1.93	240	73.5

TABLE 3-2 (Cont.)

$3(1-x)\ Y_2O_3 \cdot 3xGd_2O_3 \cdot 5Fe_2O_3$

x	M(cgs)	$K \times 10^{-3}$(erg/cc)[26]	g	ΔH(oe)	$\lambda \times 10^{-6}$(rad/sec)
5	131	5.8	2.00	44	14.5
10	124	5.8	2.00	44	13.7
15	118	5.8	2.00	44	13.1
20	112	5.8	2.00	44	12.4
28	102	5.8	2.00	60	15.4

$3(1-x)\ Y_2O_3 \cdot 3xSm_2O_3 \cdot 5Fe_2O_3$

x	M(cgs)	$K \times 10^{-3}$(erg/cc)	g	ΔH(oe)[12]	$\lambda \times 10^{-6}$(rad/sec)
25	137	7.9	1.99	500	171
35	137	8.8	1.98	700	236
60	136	10.9	1.96	1200	396
80	135	12.6	1.95	1600	517
100	135	14.3	1.93	2000	635

$3(1-x)\ Y_2O_3 \cdot 3xHo_2O_3 \cdot 5Fe_2O_3$

x	M(cgs)	$K \times 10^{-3}$(erg/cc)[26]	g	ΔH(oe)[29]	$\lambda \times 10^{-6}$(rad/sec)
8	132	5.9	1.93	420	131
17	127	6.0	1.85	830	227
40	113	6.3	1.60	1350	246
50	107	6.4	1.50	1820	276
60	101	6.5	1.40	2310	288
75	92	6.7	1.25	3240	293
85	86	6.9	1.15	3980	285
100	77	7.1[16]	1.00	5400	262

partake in the exchange interaction between the iron sublattices and weakens this interaction, consequently lowering the Curie temperature. The magnetization of these materials has been studied by Gilleo and Geller (10).

The magnetization of the mixed garnets is obtained by averaging the magnetization of the individual components in proportion to their fractional presence in the garnet. The experimental work of Rodrigue (11), Sirvetz and Zneimer (12), and others shows this behavior for mixed garnet systems.

b. Anisotropy

The magnetocrystalline anisotropy of garnets has been reviewed recently in two publications (13, 14). It is shown in these reviews that the anisotropies of the garnets are the sum of the anisotropies of each of the sublattices. The anisotropy of each of these sublattices may be calculated by a method due to Wolf (15), if the ion has no angular orbital momentum. The trivalent iron and gadolinium ions which partake in the magnetization of the garnets fit this restriction, and calculations made of the anisotropy of these materials agree well (13) with measurements.

The room temperature anisotropy constants of the garnets which were used in this work appear in Table 3-2. These values for the simple garnets are taken from microwave measurements (13) on single crystals, except in the case of holmium garnet. This garnet's anisotropy (16) was measured by torque methods (17). The mixed garnets' anisotropy was obtained by averaging the anisotropy of the components in proportion to their presence in the crystal. In the case of the gallium and indium doped garnets, the anisotropy was obtained by calculation from that of yttrium iron garnet. The method is given in Sec. c below.

The anisotropy of all these crystals is cubic with the (111) axis, the preferred axis. The anisotropy energy, E_K, may be presented by

$$E_K = K_1(\alpha_1^2\alpha_2^2 + \alpha_2^2\alpha_3^2 + \alpha_3^2\alpha_1^2) + K_2\alpha_1^2\alpha_2^2\alpha_3^2, \qquad (3\text{-}1)$$

with K_1 negative. K_2 has been found to be small enough to be neglected for our purposes.

For the ferrites, the anisotropy data is taken from Healey (18) and Shenker (19) respectively. Since the nickel and cobalt ferrites have anisotropies of opposite sign, it is conceivable that a combination of these, in the correct proportions, would have a vanishing macroscopic anisotropy. Some evidence of this occurring is offered by the microwave measurements of Pippin (20) and Sirvetz (21). From their results, it appears that the resultant anisotropy may be found by again proportioning the anisotropy of the constituents by the amount each contributes to the total ferrite (see Table 3-1).

c. Anisotropy of indium and gallium substituted garnets

The indium and gallium substituted garnets are yttrium iron garnets in which some of the iron has been replaced by either indium or gallium garnet. To understand the effect of these substitutions, a more complete description of the garnet is required. It was indicated earlier that the magnetization of the garnet is the sum of the magnetizations in the three of its interacting sublattices. When the rare earth ion is absent (i.e., yttrium iron garnet), one of the three lattices may be neglected, for it contains only diamagnetic ions. The remaining two lattices contain the Fe^{+++} ions. These lattices are commonly known as the a and d lattices (22) and contain, respectively, the ions which are situated at sites which

are octahedrally and tetrahedrally coordinated with the oxygen atoms. In a unit cell there are 16 ions on the a sites and 24 ions on the d sites. The magnetization, M, per unit volume is given by

$$M = M_d - M_a . \tag{3-2}$$

M_a and M_d are the magnetizations per unit volume of the a and d sites. When indium and gallium are substituted into yttrium iron garnet, Gilleo and Geller (10) have shown through magnetization measurements that indium predominantly enters the a sites, while gallium enters the d sites. Since these ions are diamagnetic, the indium substitution results in increasing the sample's absolute saturation magnetization, while the gallium decreases it.

Wolf has shown that if the sublattice magnetization is known together with certain crystalline field and crystal parameters, the sample's magnetic anisotropy may be calculated. Jones (14) has shown that for yttrium iron garnet Wolf's procedure yields

$$K_1 = -4.0 \times 10^{-4} N_a r(y_a) + 4.22 \times 10^{-3} N_d r(y_d) \tag{3-3}$$

where N_a and N_d are the number of ions per unit volume of the a and d sublattices. $r(y_a)$ and $r(y_d)$ are functions of the sublattice magnetization which have been tabulated and graphed by Wolf.

From Eq. (3-3) we can find the anisotropy for substituted garnets by appropriate changes in the concentration factors, if the sublattice magnetizations are known. These sublattice magnetizations may be determined since it is known from the work of Pauthenet that the temperature dependence of the magnetization is governed by the simultaneous solution of

$$\begin{aligned} M_a &= M_{ao} B(g\beta S h_a/kT) \\ M_b &= M_{bo} B(g\beta S h_b/kT) . \end{aligned} \tag{3-4}$$

M_a and M_{ao} are the magnetization per mole at the temperatures T and 0°K respectively. B is the Brillouin function (23) which becomes

$$B(y) = \frac{5}{6} \coth \frac{5}{6} y - \frac{1}{5} \coth \frac{y}{5}$$

for the trivalent iron ion. g is the spectroscopic splitting factor, and S is the spin of the ion under concern. β is the Bohr magneton, and k is Boltzmann's constant. h_a and h_b are the Weiss molecular fields. These fields arise as a result of interactions within a sublattice and between the sublattices. Following Pauthenet these fields may be written as

$$\begin{aligned} h_a &= n_{ad}\mu M_d + n_{aa}\lambda M_a \\ h_d &= n_{ad}\lambda M_a + n_{dd}\mu M_d . \end{aligned} \tag{3-5}$$

Here n_{ad} and n_{aa} are interaction constants determined by Pauthenet. μ and λ are constants giving the fraction of the molar magnetization for which the d and a sublattices are respectively responsible.

If a substitution is made such that the fraction of x and z ions on the a and d sites respectively is replaced by diamagnetic ions, then the molecular field given in Eq. (3-5) becomes

$$\begin{aligned} h_d &= n_{ad}\lambda(1-x)M_a + n_{dd}\mu(1-z)M_d \\ h_a &= n_{ad}\mu(1-z)M_d + n_{aa}\lambda(1-x)M_a , \end{aligned} \tag{3-6}$$

assuming that the lattice constants do not change significantly. Gilleo and Geller (10 show that these changes are less than 0.5% for the compositions considered here.

The sublattice magnetizations are then determined from a solution of Eq. (3-5) using for the n's, λ, μ, etc. the values obtained by Pauthenet. These, together with Wolf's curves and Eq. (3-3), give the anisotropy.

However, the computation may be shortened by noting that in Eq. (3-3) the numerical part of the first term is a factor of ten smaller than that of the second term, that

$$\frac{N_d}{N_a} = 1.5, \tag{3-7}$$

and that for yttrium iron garnet

$$r(y_a) \approx r(y_d). \tag{3-8}$$

Thus the anisotropy is predominantly due to the d sites, and

$$K_1 \approx +4.22 \times 10^{-3} N(d)\, r(y_d). \tag{3-9}$$

The calculation may also be shortened, if x and z are small, by determining M_a and M_d from

$$\begin{aligned} M_a(x,z) &= M_a(o,o) + x\frac{dM_a}{dx} + z\frac{dM_a}{dz} \\ M_d(x,z) &= M_d(o,o) + x\frac{dM_d}{dx} + z\frac{dM_d}{dz} \ . \end{aligned} \tag{3-10}$$

If, as indicated by Gilleo and Geller, all the indium goes into the a sites, and the gallium goes into the d sites, then for garnets

$$3Y_2O_3 \cdot 1/4In_2O_3 \cdot 4\text{-}3/4Fe_2O_3,$$

$$3Y_2O_3 \cdot 1/2In_2O_3 \cdot 4\text{-}1/2Fe_2O_3,$$

$$3Y_2O_3 \cdot 1/4Ga_2O_3 \cdot 4\text{-}3/4Fe_2O_3,$$

x and z are respectively 0.125 and 0, 0.25 and 0, and 0 and 0.083.

Taking from Pauthenet (8) the values required for the various constants in the molecular field and the sublattice magnetizations, and computing the derivatives, the ratio of d lattice magnetization at room temperature to the d lattice magnetization at 0°K is found as shown in Table 3-3.

TABLE 3-3

Quantities required in the evaluation of the anisotropy constants of gallium and indium substituted garnets.

Garnet	M_d/M_{do}	r(y)	K/K_{yig}
1/4 In	0.8	0.412	0.71
1/2 In	0.76	0.312	0.502
1/4 Ga	1	0.6	0.92

Using these values, r(y) is obtained. The ratio of the anisotropy constants is then computed. In the case of the gallium substitution, this ratio is primarily due to the change in N_d. From the last column of Table 3-3, where the ratio of the substituted garnets' anisotropy to that of yttrium iron garnet, K/K_{yig}, is given, the estimates of the anisotropy constants given in Table 3-1 were determined.

d. g values, linewidths and damping parameters

The room temperature g values and linewidths which have been determined in magnetic resonance experiments for the ferrites and garnets used here are also given in Tables 3-1 and 3-2. Where single crystal values were available, they were used. The values quoted here are averages of the linewidths found in the 100, 110 and 111 directions. The values for holmium garnet have been extrapolated from high temperature linewidths for a polycrystalline specimen. Where available the mixed garnets' linewidths have been entered into the table. These, as well as the ferrites, have been polycrystalline specimens.

The Landau-Lifshitz damping parameter, which has been defined in Chap. I, Sec. 5c, has been determined using the relation (24)

$$\lambda = \frac{\Delta H}{H} \frac{\gamma M}{2} \qquad (3\text{-}11)$$

between the damping parameter and the linewidth and can be found in Tables 3-1 and 3-2.

e. 53°C magnetic parameters

The parameters required to discuss experiments performed at 53°C are given in Table 3-4. It can be seen that, for all cases, the anisotropy energy decreased from that at room temperature by about 30%. The linewidth decreased 25-30% and the magnetization about 10%. The g factors remained constant.

TABLE 3-4

Magnetization, M, anisotropy constant, K, g value, and linewidth, ΔH, at a temperature of 53°C for various iron garnets. All data from reference (11).

Garnet	M(cgs)	$K \times 10^{-3}$ (ergs/cc)	g	ΔH(oe)
Yttrium	125	4.1	2.01	—
Ytterbium	114	2.8	1.93	190
Erbium	83.5	4.5	1.45	750
Samarium	117	9.5	1.93	1560

CHAPTER III – BIBLIOGRAPHY

1. W.P. Wolf and G.P. Rodrigue, J. Appl. Phys. 29, 105 (1958).
2. J.W. Nielsen, J. Appl. Phys. 31, 51S (1960).
3. This toroid was made by C. Quadros.
4. J.E. Pippin and C. L. Hogan, Sci. Rpt. No. 8, Gordon McKay Lab., Harvard Univ. (1958).
5. L. Néel, Ann. Phys. 3, 137 (1948).
6. E.W. Gorter, Proc. I.R.E. 43, 1945 (1955).
7. J. Smit and H.P.J. Wijn, Ferrites (J. Wiley and Sons, New York, 1959) Chap. 8.
8. R. Pauthenet, Ann. Phys. 13, 424 (1958).
9. J.E. Pippin, Thesis, Harvard Univ. (1958).
10. M.A. Gilleo and S. Geller, Phys. Rev. 110, 73 (1958).
11. G.P. Rodrigue, Thesis, Harvard Univ. (1958).
12. M. H. Sirvetz and J.E. Zneimer, J. Appl. Phys. 27, 431 (1958).
13. G.P. Rodrigue, J.H. Meyer, W.P. Wolf, R.V. Jones, Tech. Rept. 322, Cruft Lab., Harvard Univ. (1960).
14. G.P. Rodrigue, J.H. Meyer, R.V. Jones, J. Appl. Phys. 31, 376S (1960).
15. W.P. Wolf, Sci. Rep. No. 12, Gordon McKay Lab., Harvard Univ. (1957).
16. R.F. Pearson, personal communication.
17. R.F. Pearson, J. Appl. Phys. 31, 160S (1960).
18. D.W. Healey, Phys. Rev. 80, 1009 (1952).
19. H. Shenker, Phys. Rev. 107, 1246 (1957).
20. J.E. Pippin, Sci. Rpt. 10, Harvard Univ. (1957).
21. M.H. Sirvetz and J.H. Saunders, Phys. Rev. 102, 366 (1956).
22. R. Pauthenet, J. Appl. Phys. 30, 290S (1959).
23. J.H. Van Vleck, Theory of Electric and Magnetic Susceptibilities (Oxford Univ. Press, London, 1952) p. 257.

CHAPTER III – BIBLIOGRAPHY (Cont.)

24. C.L. Hogan, Proc. I.R.E., 44, 1345 (1956).

25. J.E. Pippin and C.L. Hogan, Sci. Rpt. 1, Gordon McKay Lab., Harvard Univ. (1959).

26. Estimated values. See text for estimating procedure.

27. J.J. Green, personal communication.

28. R.C. LeCraw and E.G. Spencer, J. Appl. Phys. 30, 184S (1959).

29. Estimated values. See Chap VI for procedure.

CHAPTER IV: EXPERIMENTAL RESULTS

1. INTRODUCTION

The data obtained in the measurement of the switching characteristics of various garnets and ferrites are presented in this chapter. The features of these data which do not bear directly on a switching mechanism are discussed. The shape of the switching curves, the effect of dielectric loss on switching, and the flux or magnetization switched as a function of the applied field are among the topics discussed. All of the measurements, unless otherwise specified, were made at room temperature. Those which were not made at room temperature were made near 55°C.

2. FIELD DEPENDENCE OF THE SWITCHED MAGNETIZATION

The measurements using the technique and procedure given in Chap. II are discussed here. Figures 4-1 and 4-2 show respectively the flux or magnetization switched for a number of iron garnets and nicket cobalt ferrites as a function of the applied switching field. The ordinate has been normalized to the maximum flux switched in the experiment. The iron garnets whose data is shown here are yttrium, holmium, erbium, samarium, ytterbium, and one which had 10% of its iron replaced by indium.

The shape of these curves is similar to that of a hysteresis curve, as explained in Chap. II. The flux switched, which is measured without the application of the switching field, results from these materials not having flat topped hysteresis loops and the lack of perfect cancellation by the bucking loop.

It can be seen from these figures that all of the materials have a transition from "no switching" to complete switching during which the amount of reversed magnetization increases with increasing applied field. From the discussion of the coercive force in Chap. I, one might expect that the entire

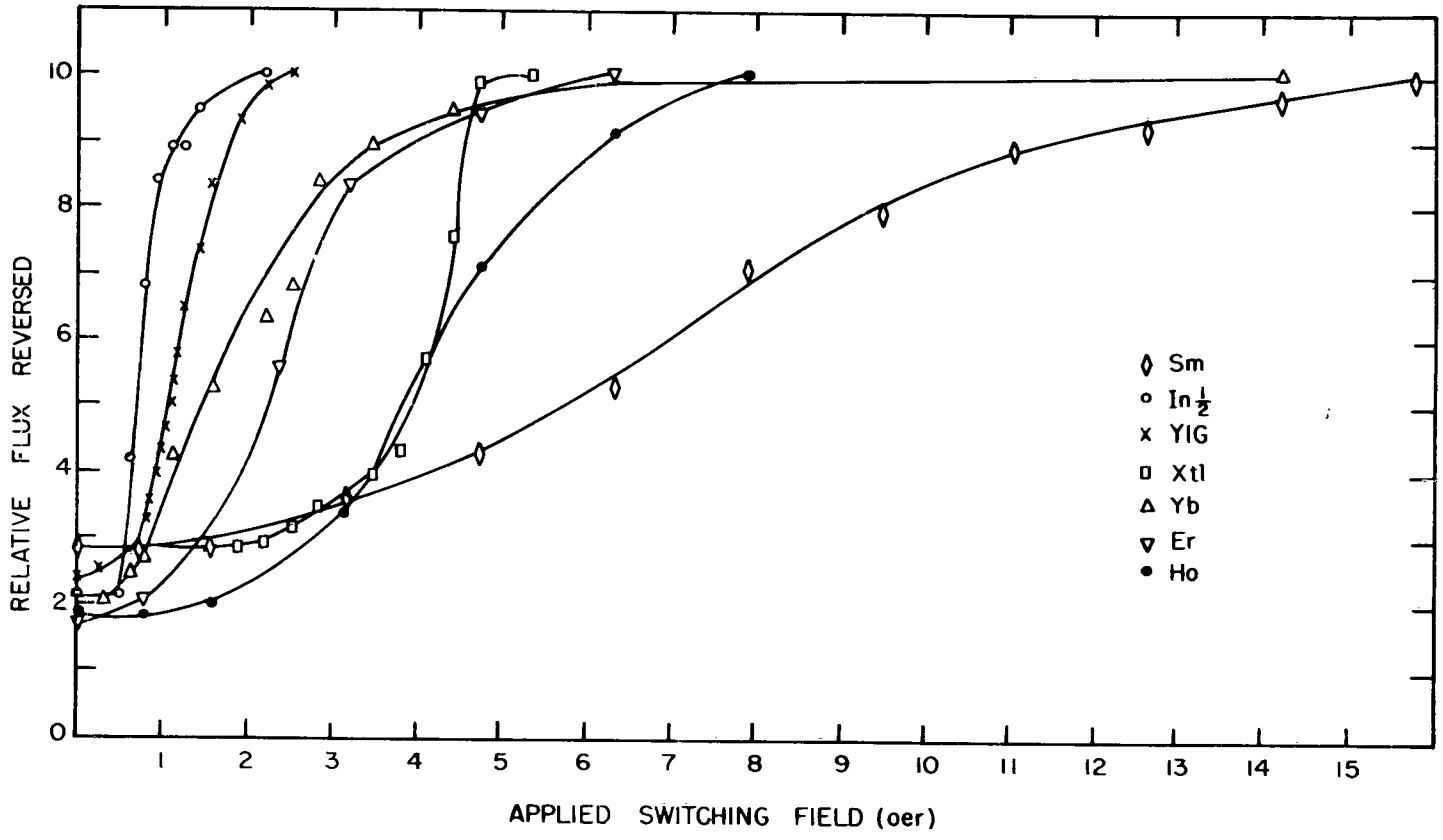

FIG. 4-1 FLUX SWITCHED AS A FUNCTION OF APPLIED FIELD FOR A NUMBER OF IRON GARNETS

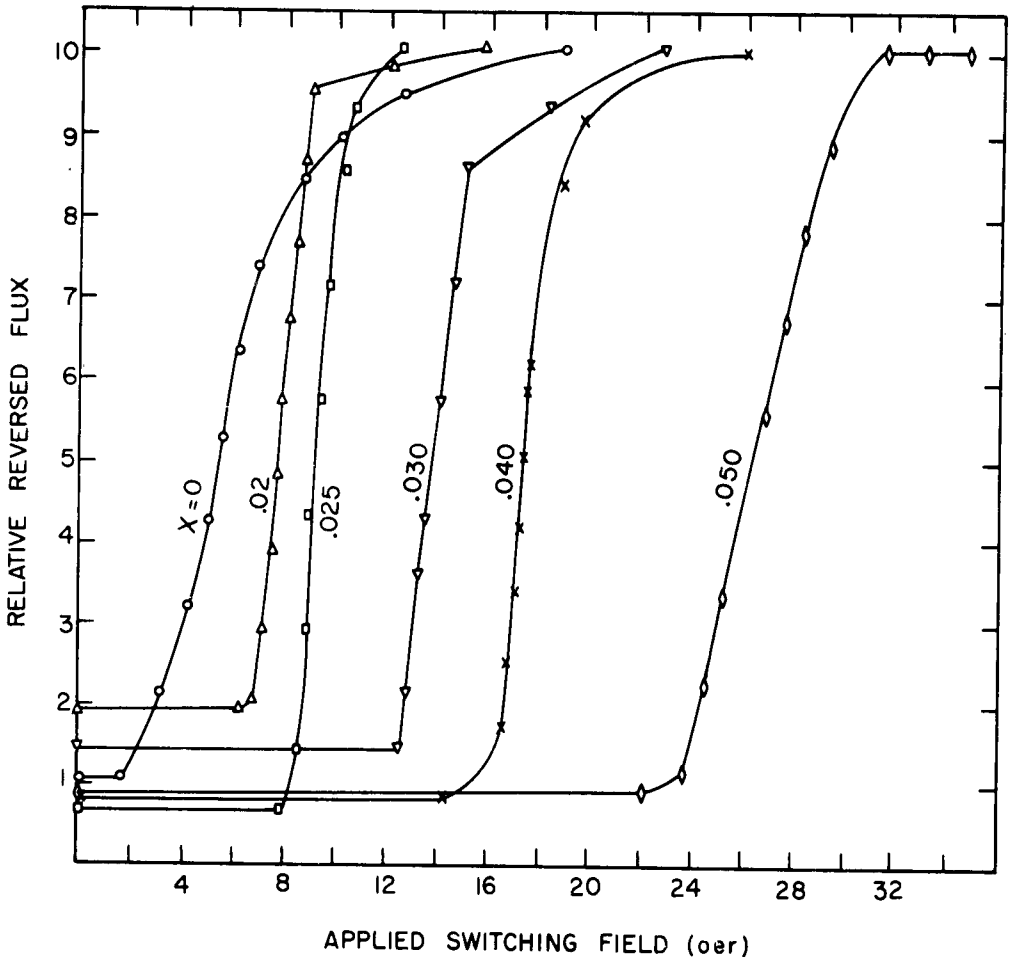

FIG. 4-2 RELATIVE REVERSED FLUX AS A FUNCTION OF APPLIED FIELD FOR $Ni_{1-x}Co_xMn_{.02}Fe_{1.9}O_4$

material reverses when the applied field exceeds the coercive force. However, this model idealizes the behavior by tacitly assuming that the specimen and applied field are uniform. In the coaxial line used here the magnetic field, H, decreases in passing from the inner to the outer conductor. As a result, the region near the inner diameter of the toroid may switch at a lower value field than a region near the outer diameter. (The curves of Figs. 4-1 and 4-2 were plotted using the fields calculated at the outside edge of the toroid. This convention is followed in the remainder of this report and is explained in Sec. 4b.) Secondly, the material may consist of regions of different characteristics, each requiring a reversing field of a different magnitude. And thirdly, on a domain wall motion model, the possibility exists that the distance a wall moves may be a function of the applied field. The barriers to wall motion may be arranged so that a continually increasing field is required to move the wall from its initial position to its remanent one.

From the data of Figs. 4-1 and 4-2, the variation in coercive force with composition may be obtained. For the nicket cobalts, Fig. 4-3 gives the coercive force obtained in this manner as a function of the fraction, x, of cobalt ferrite substituted in the nickel ferrite. The coercive force of the garnets was plotted in Fig. 4-4 as a function of K/M and $\sqrt{K}/M$, since, as discussed in Chap. I, these quantities are responsible for the coercive force. Here K and M have the same meanings as in Chap. I.

3. FIELD DEPENDENCE OF THE SWITCHING TIME

The variation of the reciprocal of the switching time, 1/t, as a function of the applied field, H, is shown in Fig. 4-5 through Fig. 4-9 for the polycrystalline materials discussed in Chap. III. The data was taken with the apparatus described in Chap. II in the manner to be described below. An

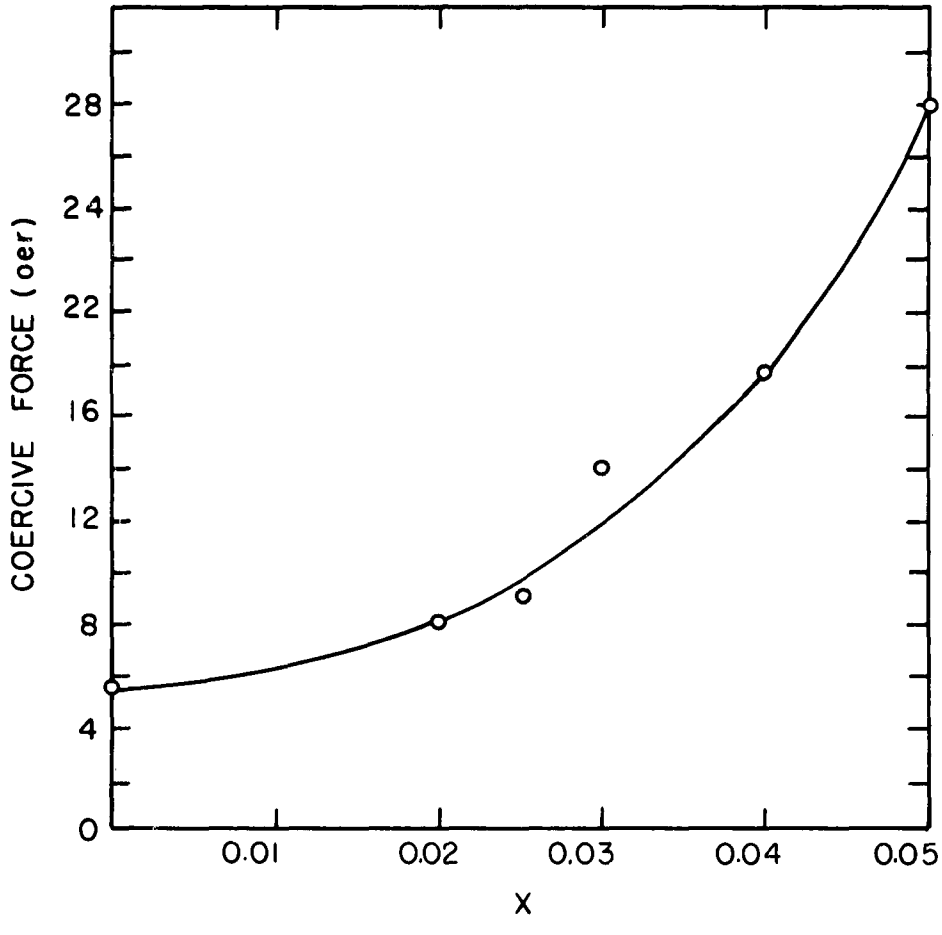

FIG. 4-3 COERCIVE FORCE AS A FUNCTION OF X IN Ni_{1-x} Co_x $Mn_{.02}$ $Fe_{1.9}$ O_2

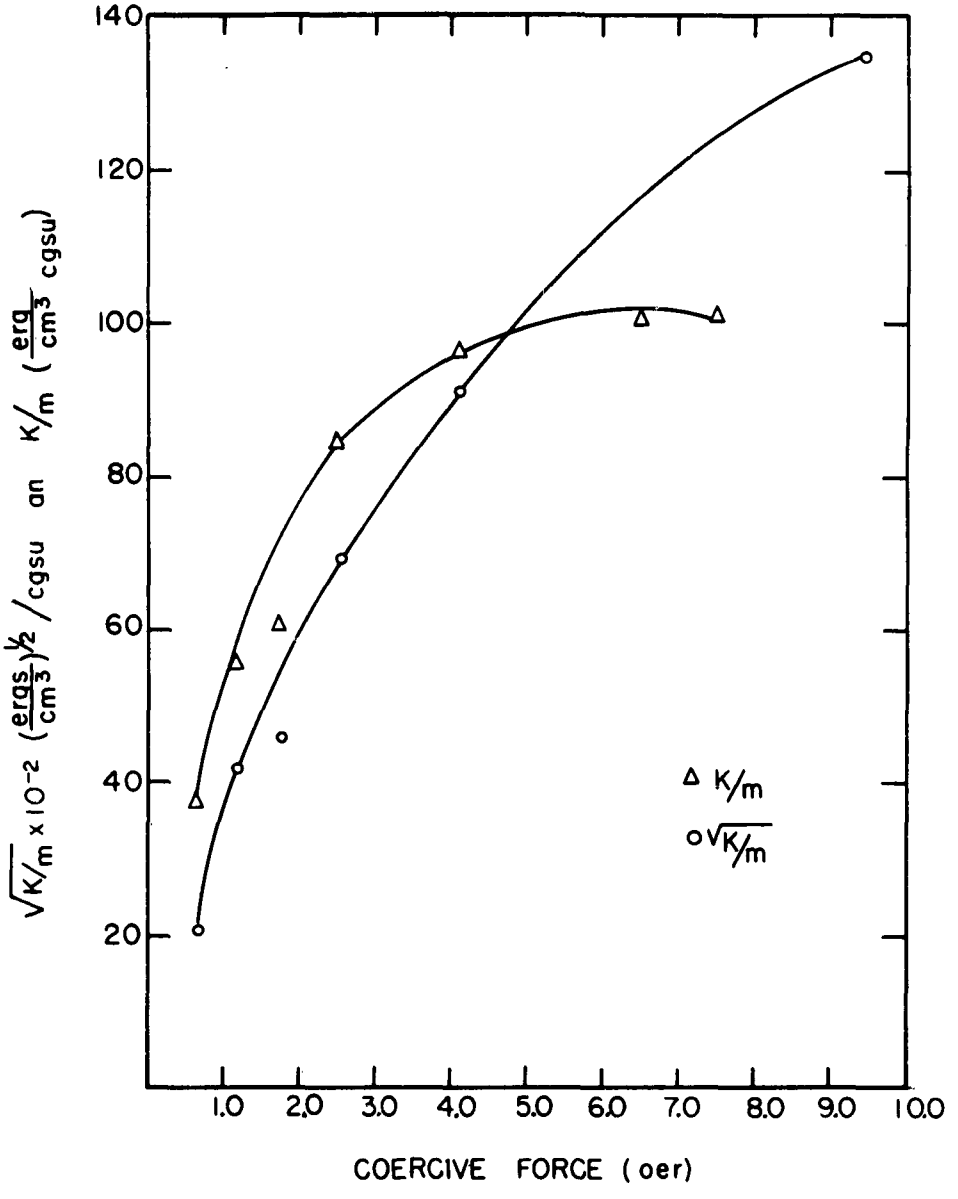

FIG. 4-4 $\sqrt{K/m}$ AND K/m AS A FUNCTION OF THE COERCIVE FORCE FOR VARIOUS IRON GARNETS

inspection of these curves shows that they have the general form of a continually rising characteristic in agreement with measurements by others (1, 2).

From this field dependence, a value of the switching parameter, S_w, i.e., $S_w = dH/d(1/t)$, may be obtained. In this report, this parameter is obtained by fitting the 1/t data with a straight line at the lowest field for which the reversed magnetization becomes constant as determined from the flux switched experiment. In almost all cases this region is easily found in the switching characteristic as a relatively marked change in slope. The intercept of this straight line on the field axis will be denoted by H_1.

Unfortunately, S_w is not an absolute constant of the material, even for a given switching field. In certain technically important regions it is dependent on the manner in which the core is reset to its opposite state (3, 4). The determination of S_w for these applications is probably best done by switching the core between its two magnetic states with the same value of current. On the other hand, when the switching properties of the core are to be studied, it is desirable to reset the core by applying a pulse of sufficient amplitude to cause the switching which is measured to initiate from a state which is independent of the switching current. The experimental data reported here was obtained in this manner. This state is determined experimentally by observing the switching as the reset field is varied. For a sufficiently high field no variation is seen, and the switching behavior is independent of the reset amplitude.

Figure 4-5 shows the field dependence of the inverse switching time as measured for yttrium, ytterbium, and erbium iron garnets, as well as yttrium-indium and yttrium-gallium iron garnets. Figures 4-6, 4-7, and 4-8 give the data for the mixed iron garnet systems: gadolinium-yttrium, samarium-yttrium, and holmium-yttrium respectively. The measurements for a nickel cobalt series are shown in Fig. 4-9. In Table 4-1 the values of S_w and H_1 for these specimens are given.

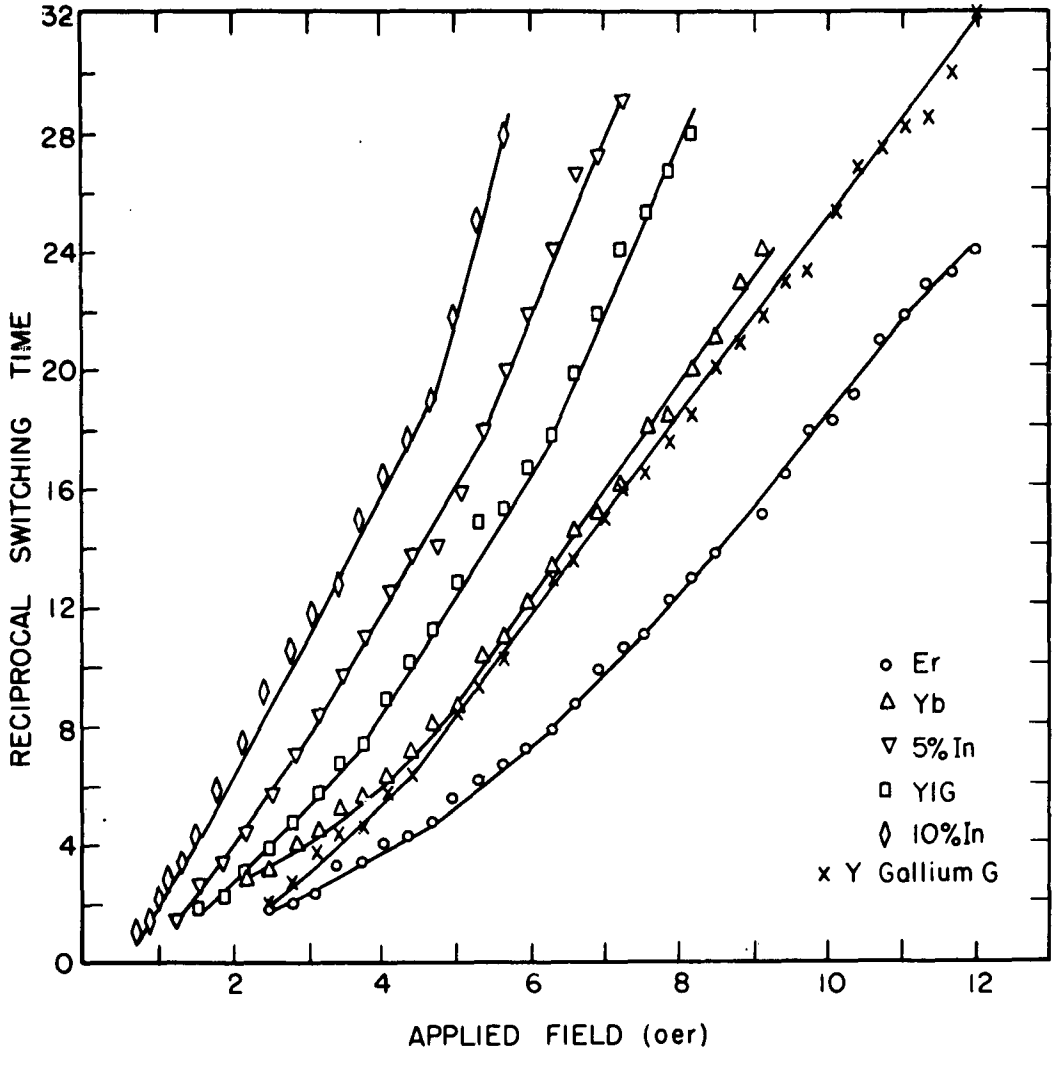

FIG. 4-5 SWITCHING CHARACTERISTIC FOR IRON GARNETS

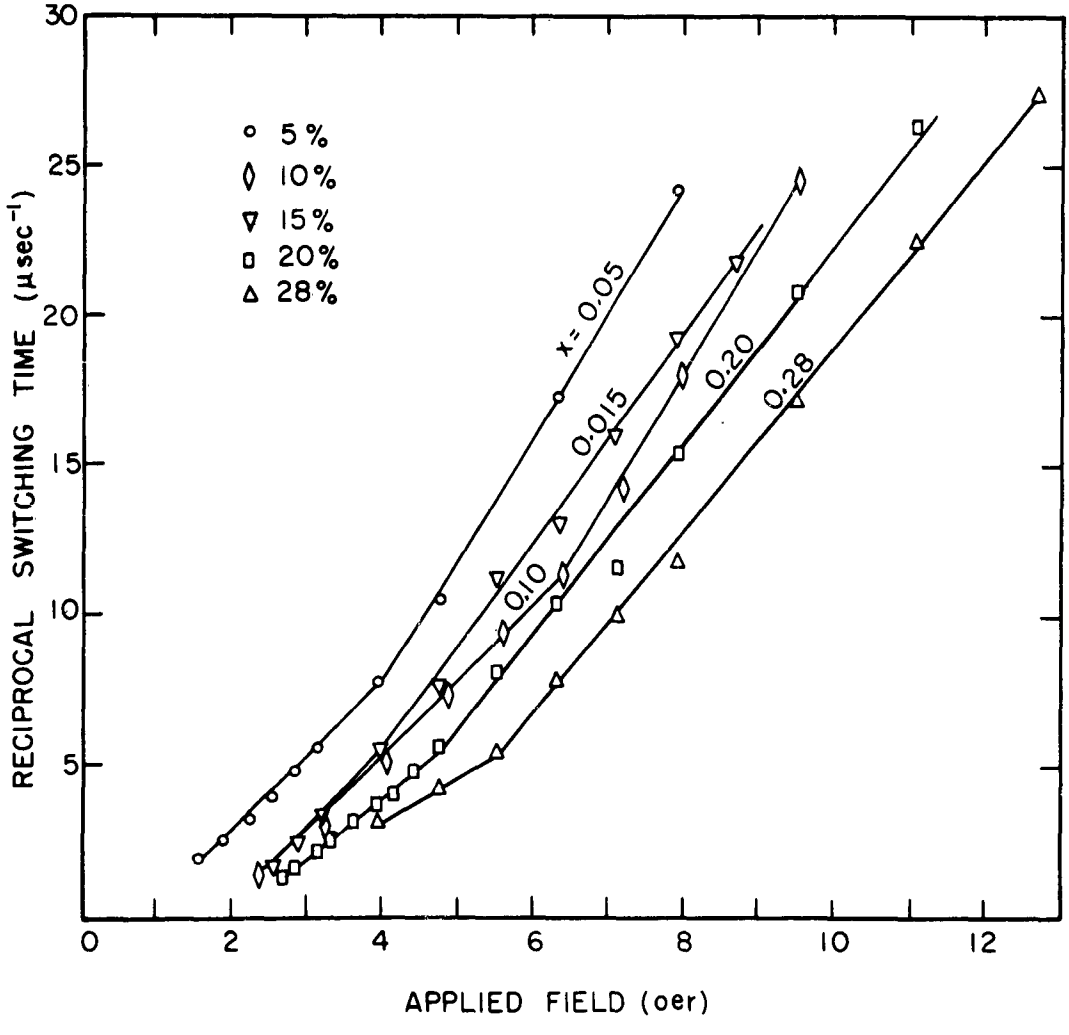

FIG. 4-6 SWITCHING CHARACTERISTIC FOR $3(1-x)Y_2O_3 \cdot 3x\,Gd_2O_3 \cdot 5Fe_2O_3$

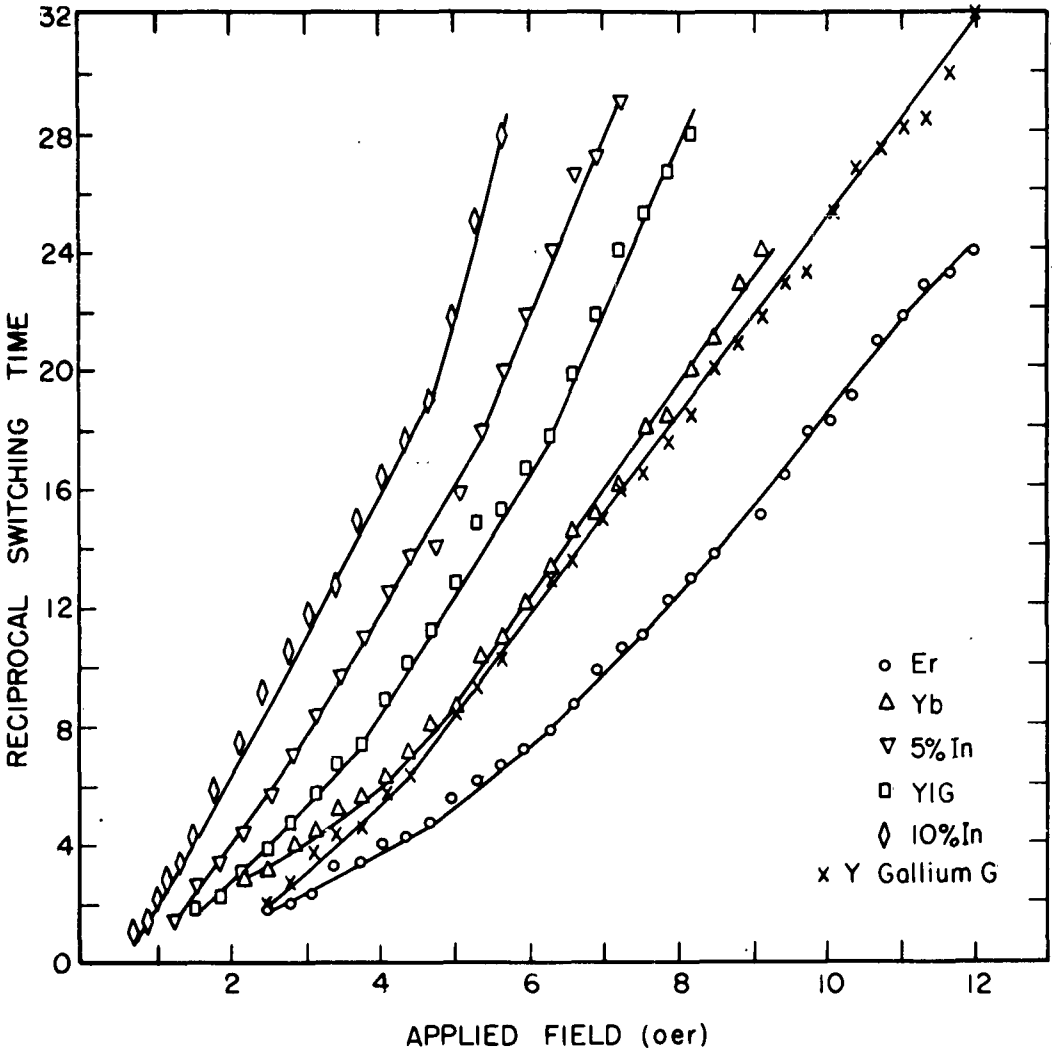

FIG. 4-5 SWITCHING CHARACTERISTIC FOR IRON GARNETS

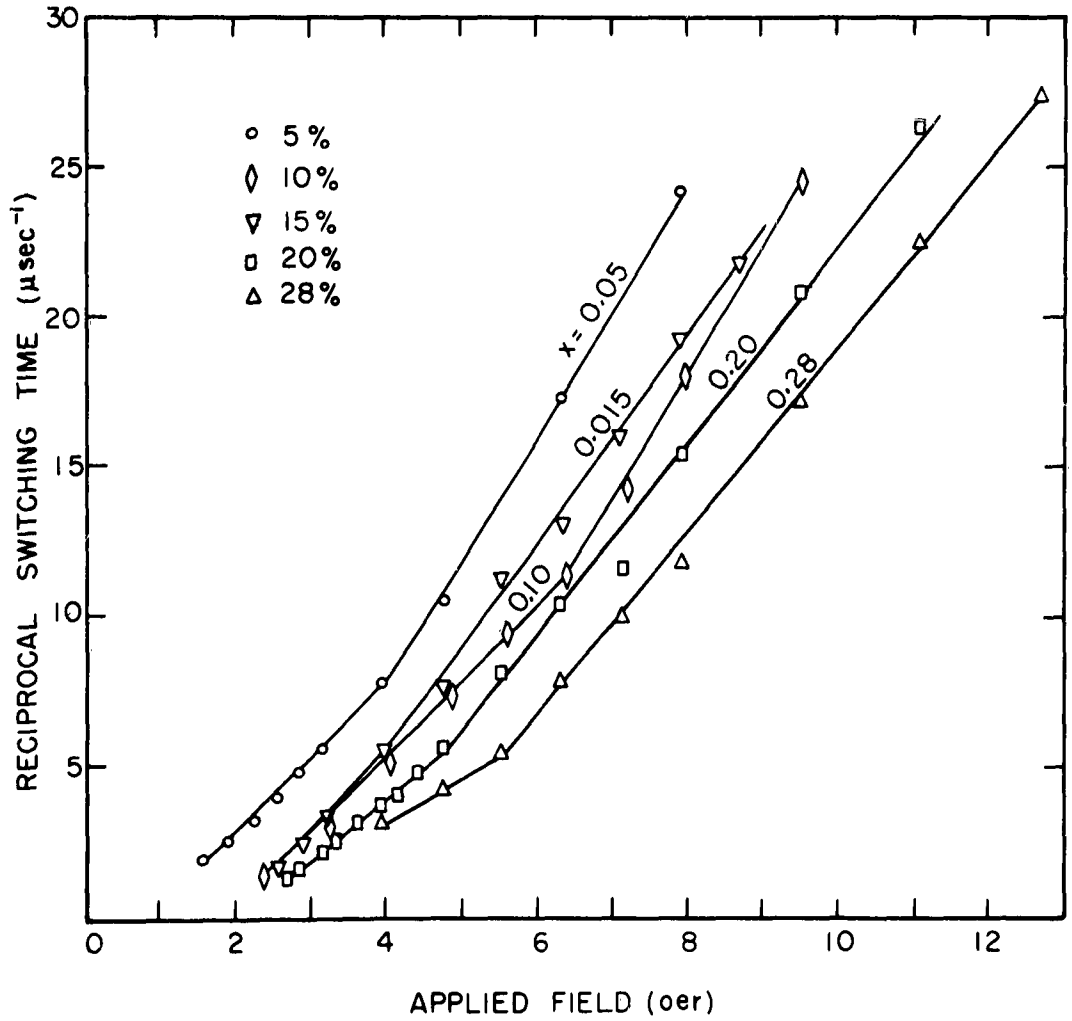

FIG. 4-6 SWITCHING CHARACTERISTIC FOR $3(1-x)Y_2O_3 \cdot 3x\,Gd_2O_3 \cdot 5Fe_2O_3$

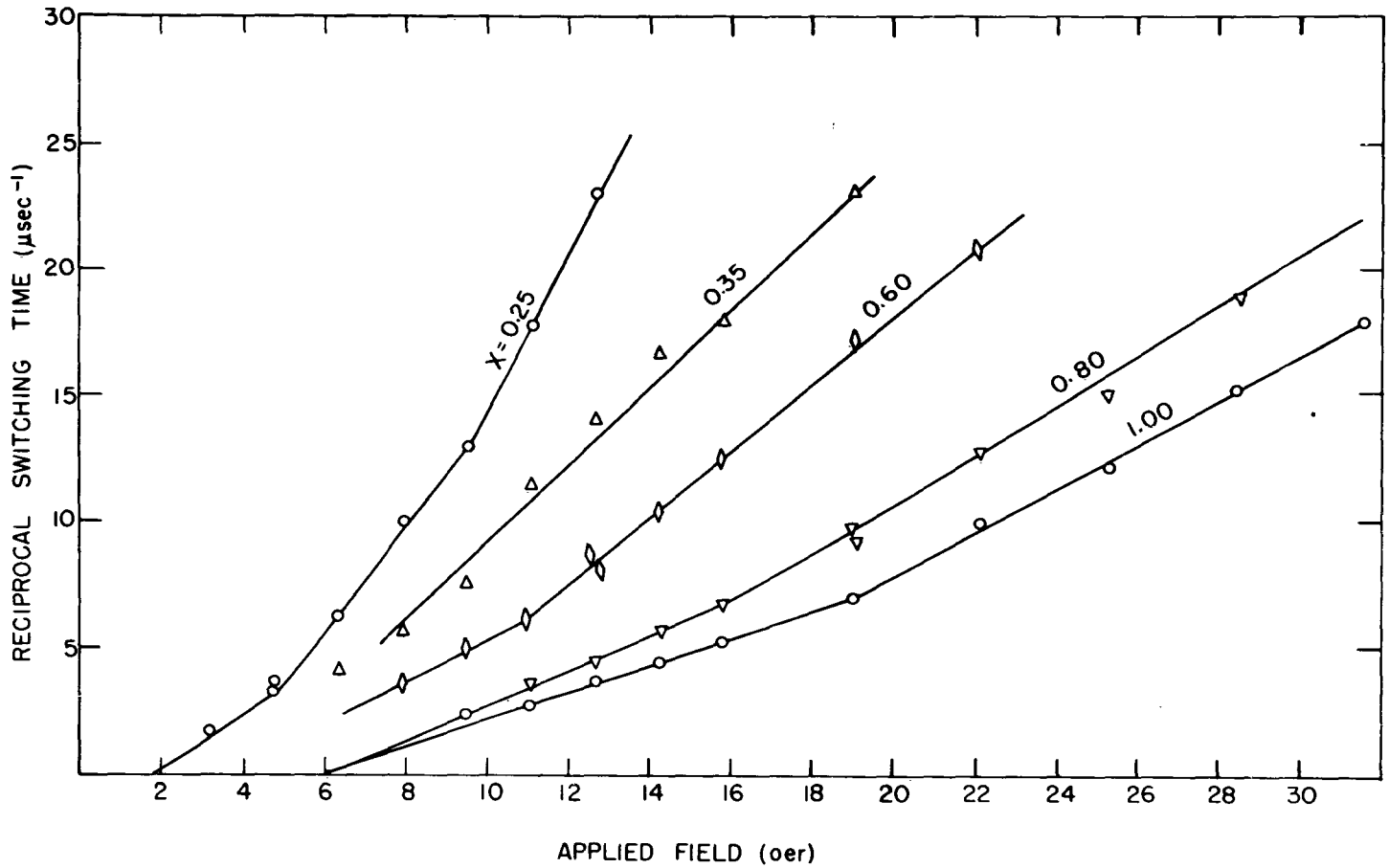

FIG. 4-7 SWITCHING CHARACTERISTIC FOR SAMARIUM SUBSTITUTED YTTRIUM IRON GARNETS $3(1-x)Y_2O_3 \cdot 3x\,Sm_2O_3 \cdot 5Fe_2O_3$

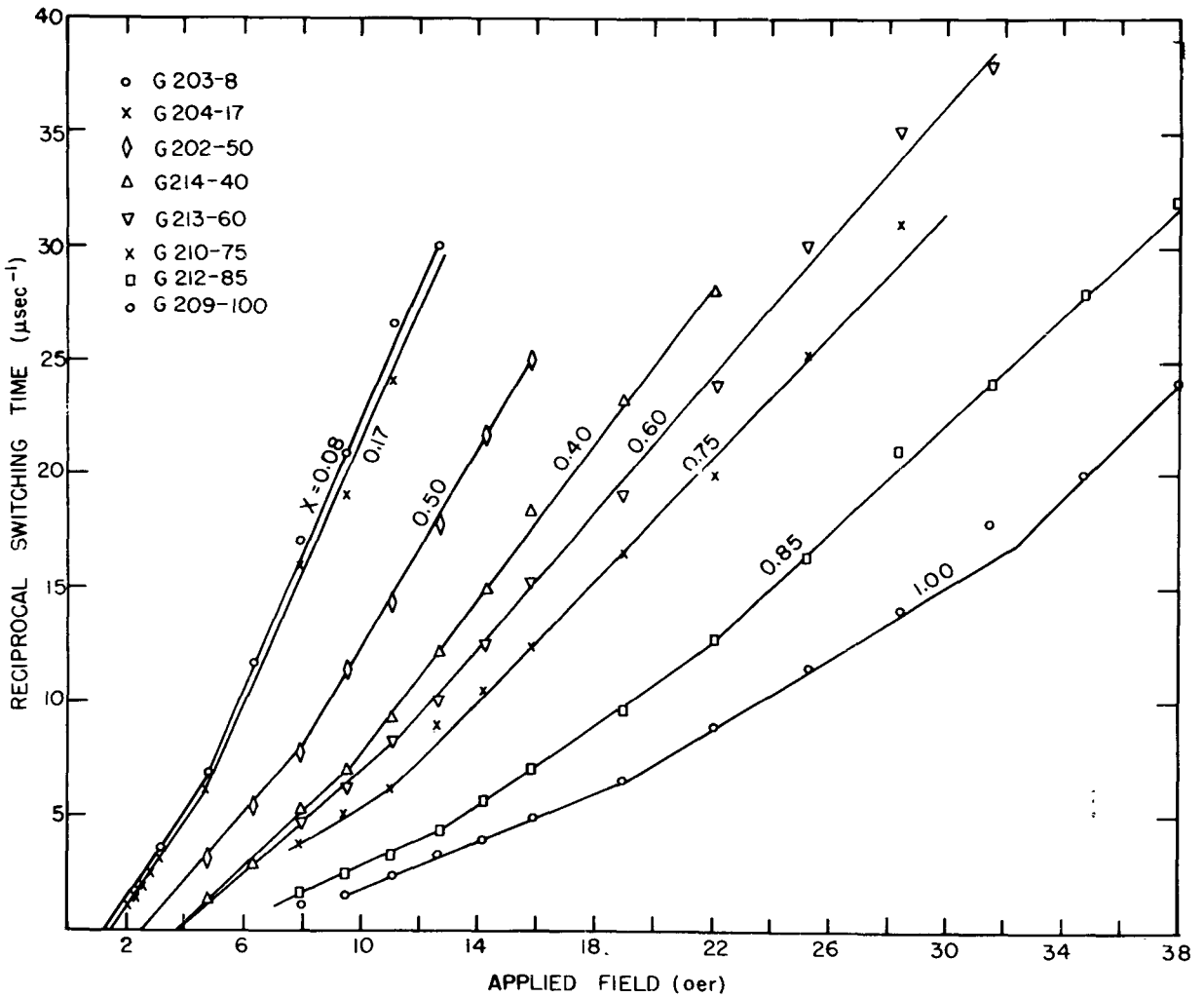

FIG. 4-8 SWITCHING CHARACTERISTIC FOR $3(1-x)Y_2O_3 \cdot 3x\,Ho_2O_3 \cdot 5Fe_2O_3$

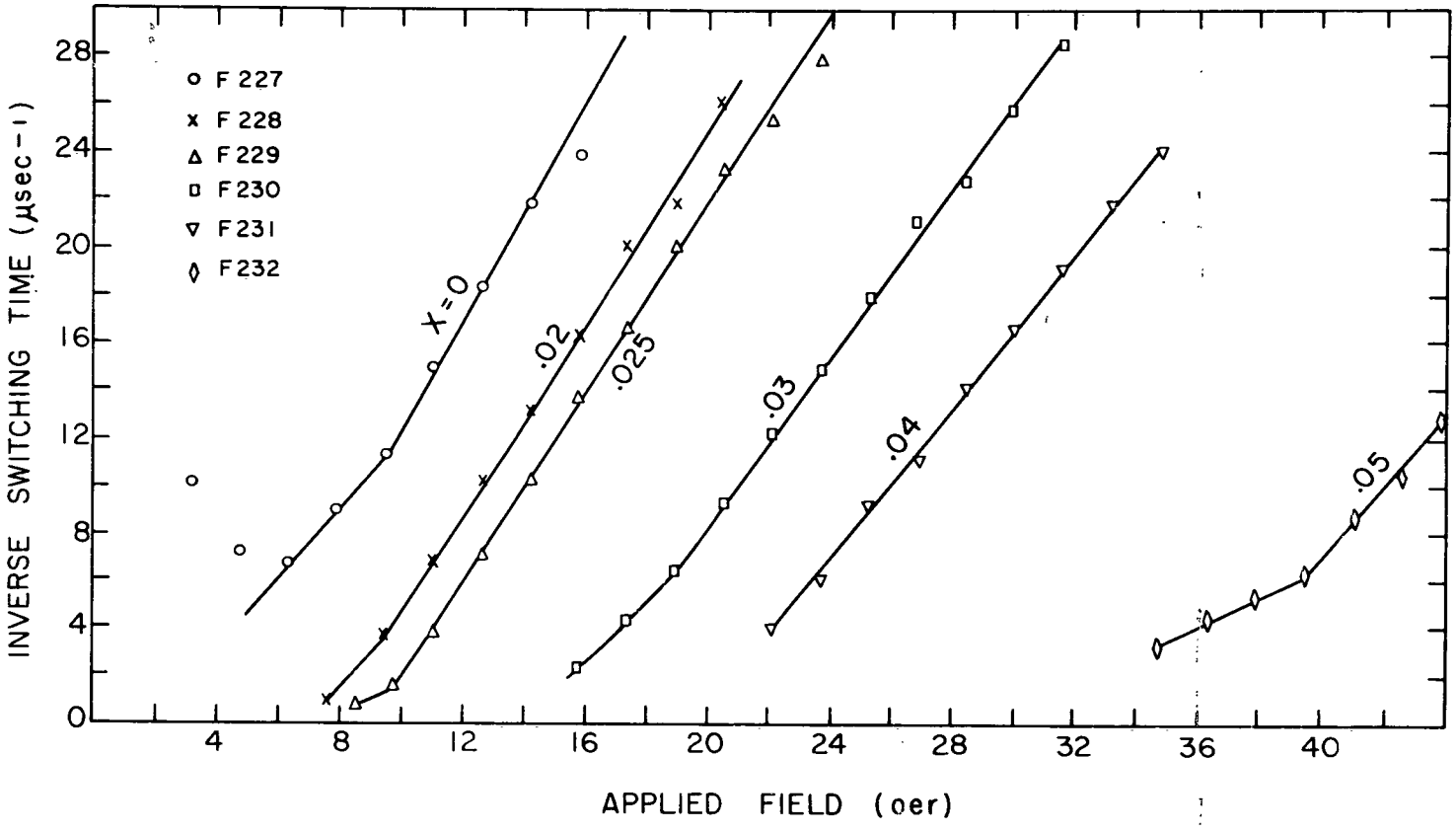

FIG. 4-9 SWITCHING CHARACTERISTIC, $Ni_{1-x}Co_x Mn_{.02} Fe_{1.9} O_4$

Table 4-1

Switching parameter, S_w, and H_1 for garnets and nickel cobalt ferrite. (Room temperature)

$Ni_{1-x}Co_xMn_{.02}Fe_{1.9}O_4$

x	S_w(oe μsec)	H_1(oe)
0	0.43	4.7
0.02	0.50	7.7
0.025	0.52	9.1
0.03	0.54	15.5
0.04	0.60	19.6
0.05	1.62	29.4

$3(1-x)Y_2O_3 \cdot 3xGd_2O_3 \cdot 5Fe_2O_3$

x	S_w(oe μsec)	H_1(oe)
5	0.40	0.9
10	0.40	1.8
15	0.44	1.7
20	0.48	4.0
28	0.66	4.0

$3(1-x)Y_2O_3 \cdot 3xHo_2O_3 \cdot 5Fe_2O_3$

x	S_w(oe μsec)	H_1(oe)
8	0.51	1.3
17	0.55	1.4
40	0.86	3.6
50	0.70	2.5
60	0.85	3.8
75	1.26	3.2
85	1.67	5.4
100	1.94	6.7

$3(1-x)Y_2O_3 \cdot 3xSm_2O_3 \cdot 5Fe_2O_3$

x	S_w(oe μsec)	H_1(oe)
25	0.47	3.3
35	0.66	4.3
60	0.76	6.3
80	1.01	9.3
100	1.15	10.8

Table 4-1 (Cont.)

Various Garnets

Garnet	S_w(oe μsec)	H_1(oe)
Yttrium	0.38	0.95
Yttrium-indium 5%	0.29	0.87
Yttrium-indium 10%	0.25	0.55
Yttrium-gallium 5%	0.44	1.74
Ytterbium	0.41	1.42
Erbium	0.78	1.26

Table 4-2

Switching parameter, S_w, and H_1 at 53°C for several garnets.

Garnet	S_w(oe μsec)	H_1(oe)
Yttrium	0.29	1.1
Ytterbium	0.29	1.9
Erbium	0.57	1.7
Samarium	0.82	11.1

Independent of the mechanism of reversal, we may generally expect that if the core is switched with a field that is insufficient to cause a complete reversal of the toroid's magnetization, the reversal will slowly be completed, since there then exist regions in which the excess driving force becomes vanishingly small. This is illustrated by the study in the Appendix to this chapter in which the effect of applying a field which is insufficient to switch the entire toroid is examined. It is this type of phenomenon which is important in the low field region, and it can be brought about by inhomogeneities of any kind which cause variations of the coercive force.

In Fig. 4-10, S_w is plotted as a function of the relaxation frequency, λ, which was taken from Tables 3-1 and 3-2 for yttrium, erbium, samarium, ytterbium, holmium and the gadolinium substituted iron garnets and the nickel cobalt ferrite series. This data shows that S_w remains relatively constant until $\lambda = 10^8$ cycles/sec and then increases abruptly. It seems that the switching process self imposes a limit on its speed which is independent of the small displacement damping. This is discussed further in Chap. VI.

In Fig. 4-11, the switching data taken at 55° for the lowest fields at which the magnetization reversed remains constant is shown. S_w and the field intercept from this data are given in Table 4-2. The switching of the single crystal toroid is shown in Fig. 4-12. Note the slowness of its switching. These topics will be further discussed in Chap. VI.

4. EFFECTS OF FABRICATION PARAMETERS

As has already been pointed out, the preparation procedure may have an effect on the switching performance of a material. A number of experiments were performed which attempted to assess these effects. The results of these experiments are reported here.

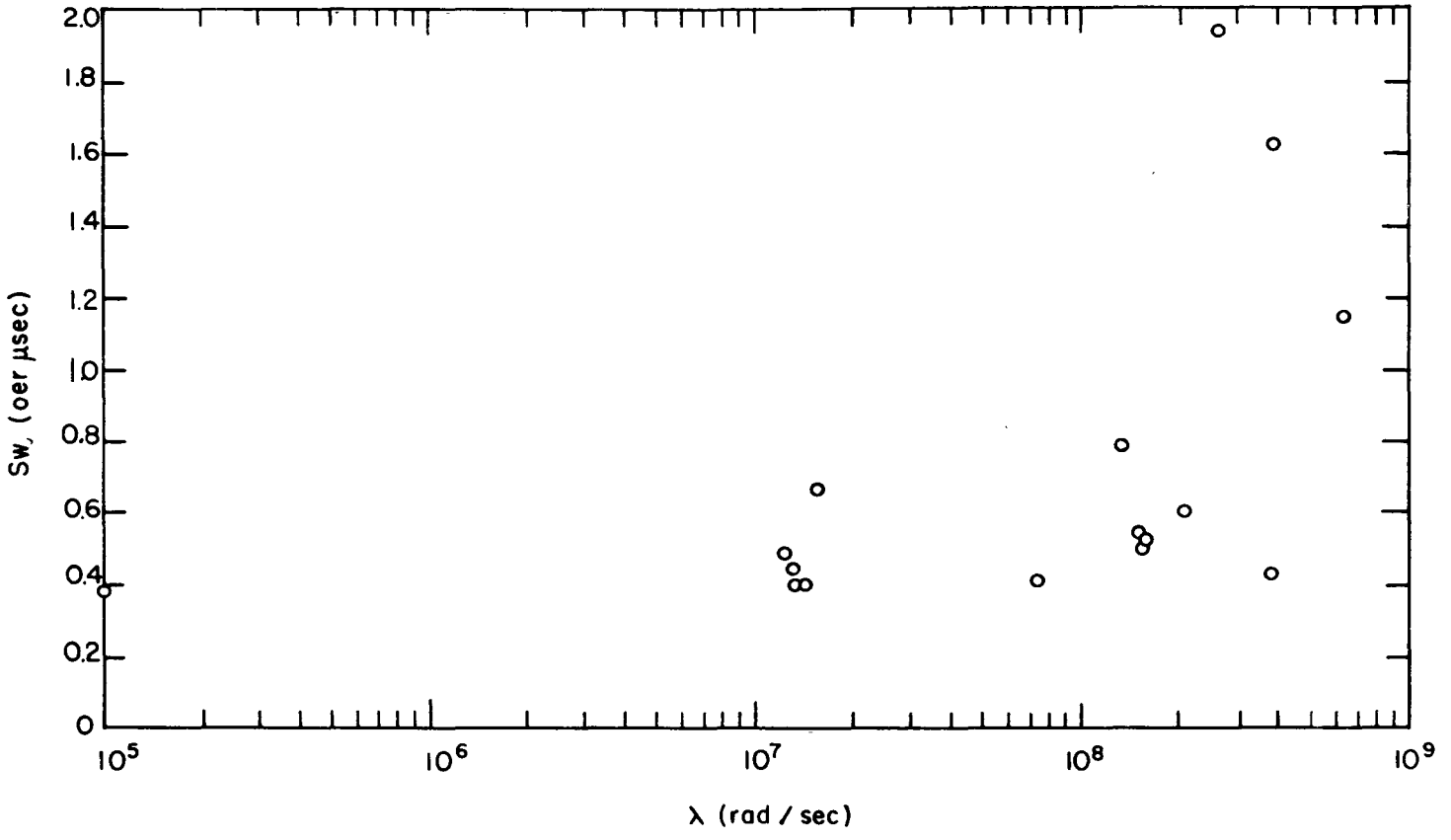

FIG. 4-10 SWITCHING PARAMETER AS A FUNCTION OF RELAXATION FREQUENCY

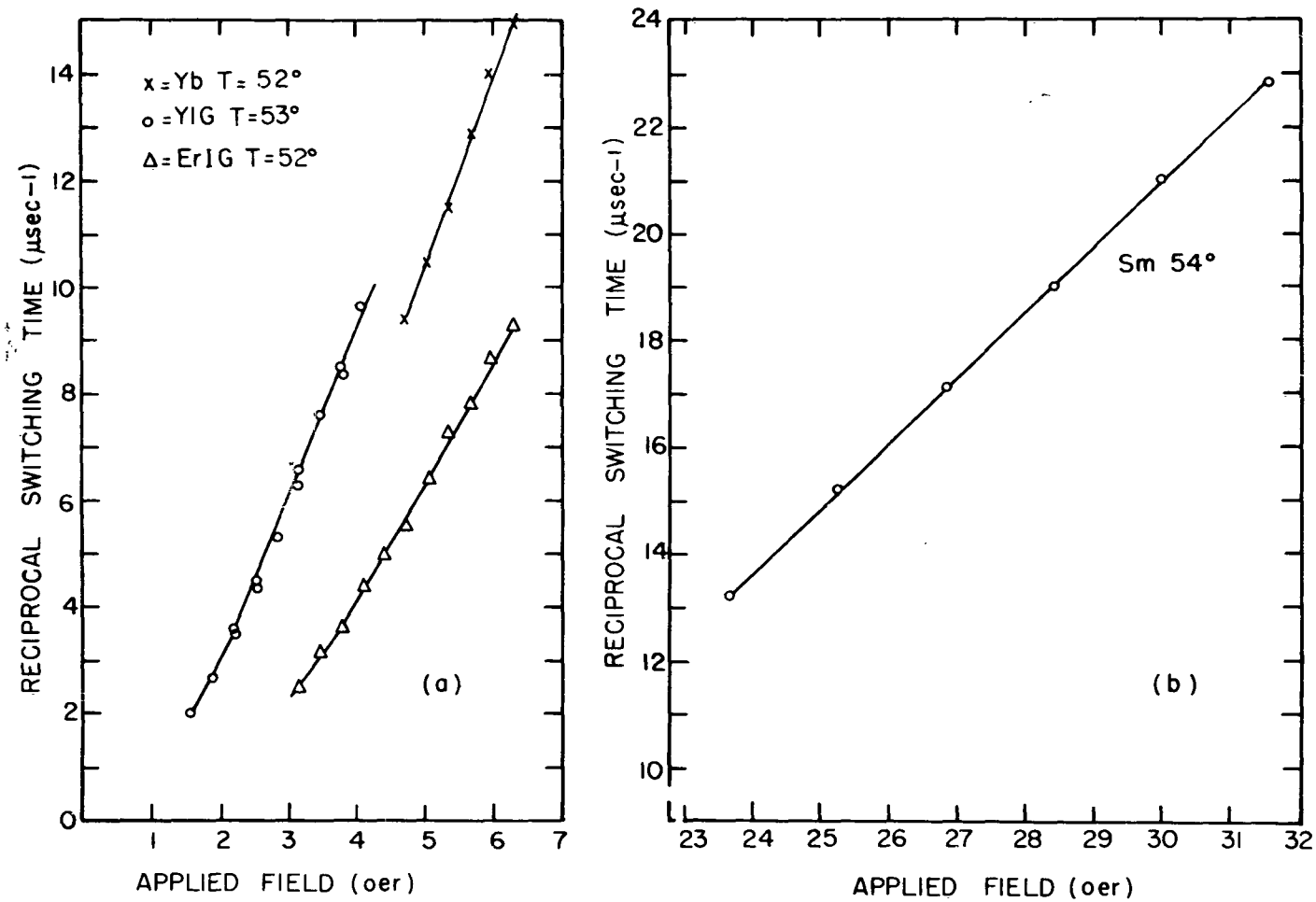

FIG 4-11 a+b SWITCHING CHARACTERISTIC AT INDICATED TEMPERATURE FOR Yb, Y, Er, Sm IRON GARNET.

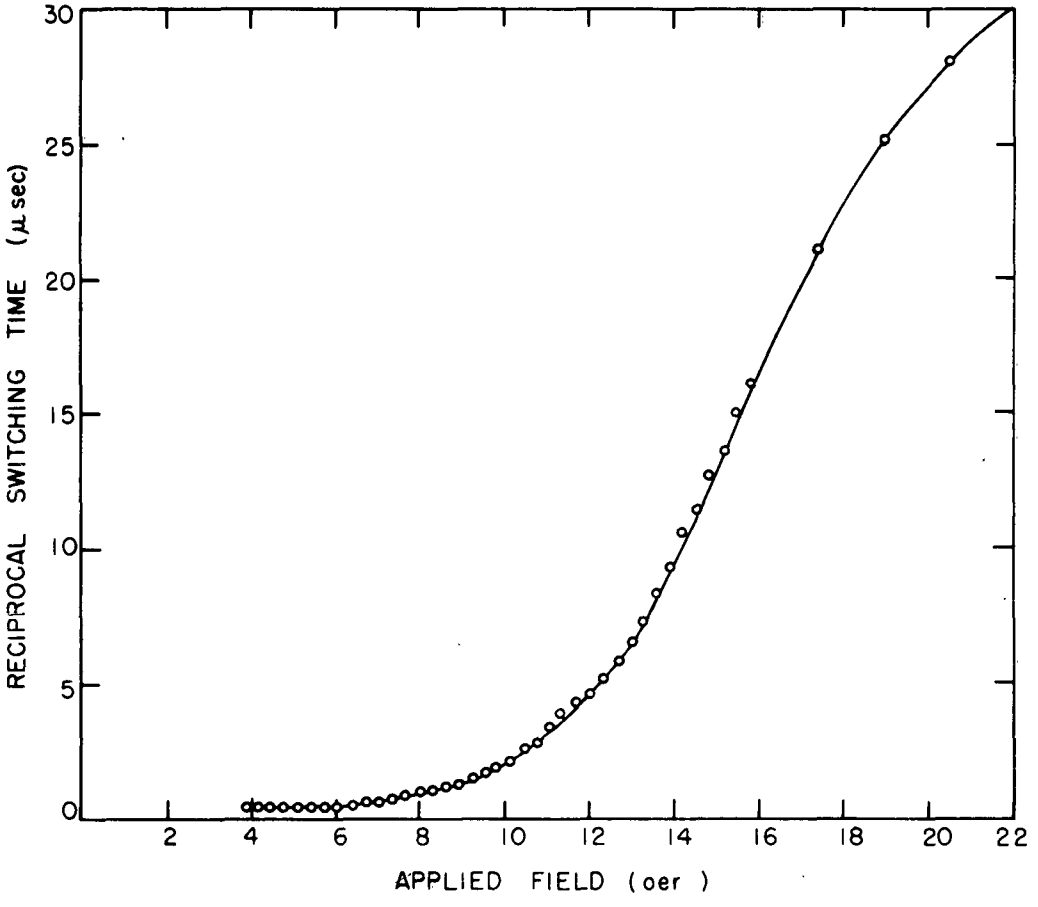

FIG. 4-12 SWITCHING CHARACTERISTIC SINGLE CRYSTAL YTTRIUM IRON GARNET WITH 0.5 % HOLMIUM.

a. Variation of core height

A number of cores of heights varying from 80 mils to 1/8 inch were pressed from a given oxide mix and fired simultaneously. This was done for both yttrium and samarium iron garnets. Measurements of the switching time were found to be independent of the core height for these materials. In fact, samples prepared from the same mix of oxides and fired at the same temperature, although not simultaneously, showed no deviations in their switching characteristics.

b. Variation of core thickness

The effect of core thickness is studied in the Appendix to this chapter in conjunction with the effect of the nonuniformity of the applied field. There it is shown that since the field decreases from the inner to the outer edge of the core and since it is the field at the slowest switching region which determines the switching time, increasing the core thickness will result in slower switching. No cores were fabricated to test this hypothesis because of the difficulty and expense of preparing the dies used to form them. The large values of S_w found for small fields tend to substantiate this conclusion in almost all cases.

c. Variation of dielectric loss

During the course of the preparation of these materials there appeared samples whose dielectric loss tangents were large. The dielectric loss tangents were measured at 20 megacycles. Although it was the objective of the materials' preparation to produce materials with loss factors of 0.005 or less, samples were produced which had substantially higher loss factors.

Microscopic examination of polished surfaces of these garnets showed the existence of regions (grains) of highly reflective material. From observations made by others in ferrites (5), it appears that these grains are an iron oxide – either magnetite or hematite. These grains probably result from poor mixing in the early stages of the preparation of the garnets.

The switching characteristics measured on the lossy materials and the counterpart non-lossy materials are presented in Fig. 4-13. In each case the material is yttrium iron garnet with a holmium substitution. The loss tangents for these materials are given in Table 4-3 together with a summary of their switching characteristics. The predominant effect, as seen in the higher loss materials, is to displace the switching characteristic towards higher fields as the loss increases. The inverse slope, S_w, is also seen to increase slightly. Each of these effects is probably attributable to the strain introduced by the second phase found in these materials. Since this strain increases the anisotropy, since S_w varies as $\sqrt{K}$, as will be shown in Chap. VI, and since the coercive force varies as K, the simultaneous increase of S_w and the coercive force found in these materials appears reasonable.

Table 4-3

Variation of switching parameters with dielectric loss.

$3(1-x)Y_2O_3 \cdot 3xHo_2O_3 \cdot 5Fe_2O_3$

x	Dielectric loss tangent	S_w(oe μsec)	H_1(oe)
75%	0.0180	1.3	3.1
75%	0.001	1.3	3.1
50%	0.003	0.72	2.4
50%	0.04	0.94	4.0
17%	0.001	0.55	1.1
17%	>1	0.79	3.2

If the size of the loss tangent is a measure of the amount of second phase present, then one may note that the effect of the second phase disappears when the dielectric loss tangent is about 0.02. All of the samples measured, unless

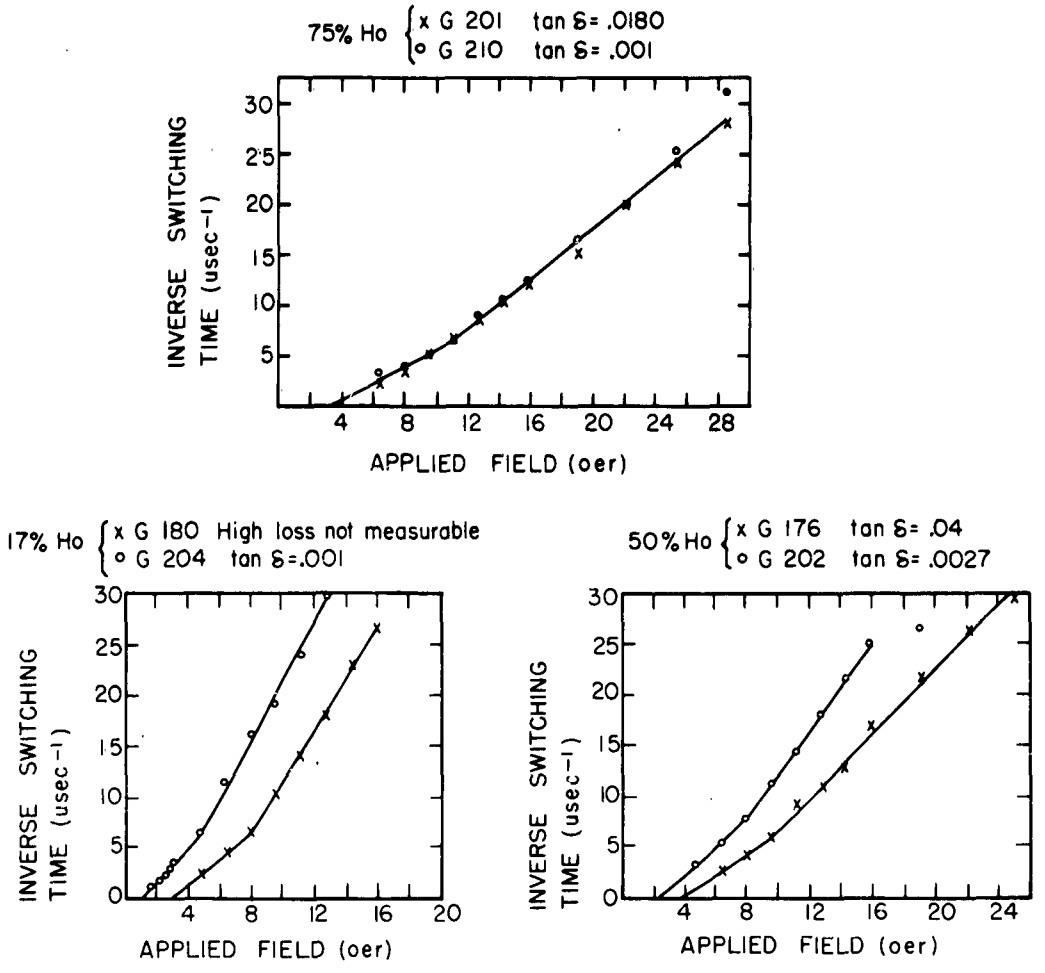

FIG. 4-13 SWITCHING CHARACTERISTIC OF YTTRIUM HOLMIUM GARNET WITH VARIOUS DIELECTRIC LOSS TANGENTS.

otherwise stated, had loss tangents less than 0.02. However, since the sample size was extremely small, the loss tangents were measured on larger samples which were pressed from the same mix and fired simultaneously.

d. Variation of sintering time

Another fabrication factor which may determine switching behavior is the duration of the sintering, since grain size (6) and oxygen retention (7) are affected by the length of the sintering cycle. To study these effects a number of samples of yttrium iron and samarium iron garnet were sintered for various times. For these materials it was found that, at the usual sintering temperature of 1400°C, no noticeable effects could be attributed to a variation of the sintering time from four to fifteen hours.

CHAPTER IV – BIBLIOGRAPHY

1. W. L. Shevel, Jr., J. Appl. Phys. 30, 47S (1959).

2. F. B. Humphrey and E. M. Gyorgy, J. Appl. Phys. 30, 935 (1959).

3. R. Vautier and A. Marais, Compt. Rend. 248, 660 (1959).

4. R. H. Tancrell and R. E. McMahon, J. Appl. Phys. 31, 762 (1960).

5. E. W. Gorter, Proc. I. R. E. 43, 1945 (1955).

6. J. Smit and H. P. J. Wijn, "Ferrites" (John Wiley and Sons, New York, 1959).

7. L. G. Van Uiteret, F. W. Swanekamp, S. W. Haszko, J. Appl. Phys. 30, 363 (1959).

APPENDIX

In this Appendix the effect of a nonuniform field on a toroidal core of finite thickness is studied. Although the results of this Appendix are obtained for a particular inhomogeneity, they should be applicable to any nonuniformity in the threshold field of a core.

If a toroidal core is switched by the field resulting from the current, I, flowing in a conductor coaxial with the toroid, as shown in Fig. 4A-1, then the field H at distance r from the conductor is in c.g.s. units

$$H = \frac{2I}{r} . \tag{4-1A}$$

From this equation it follows that the field which promotes switching decreases from inner to outer edge of the core. If we now assume that, after the field, H, is applied, the component of the magnetization along the field changes linearly at each point in the toroid as shown in Figure 4A-2, the toroid's switching time can be calculated. To this end, the relation between the switching time, t_r, of the magnetization at a distance r from the toroid's center is required. From eq. (1-18), this relation is

$$t_r = \frac{S_w}{H - H_c}, \tag{4-2A}$$

H_c is the toroid's coercive force.

If the current producing the field is such that the field at the inner radius, r_i, of the toroid is greater than H_c while the field at the outer radius, r_o, is less then H_c, then only that portion of the core will reverse that lies between r_i and $r_c = 2I/H_c$. The signal produced in a single turn pickup winding is given by the rate of change of flux and is proportional to

$$v = \frac{d}{dt} \int_{r_i}^{r_c} \frac{2M_o t}{S_w} \left(\frac{2I}{x} - H_c\right) dx \tag{4-3A}$$

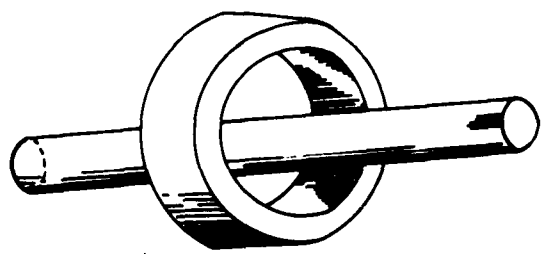

FIG. 4-A1 ARRANGEMENT FOR SWITCHING A TOROIDAL CORE.

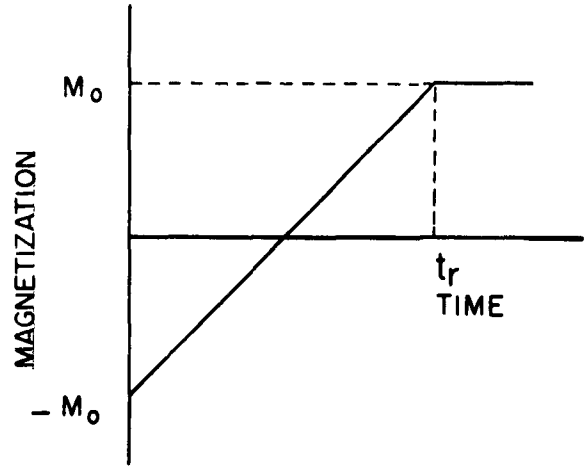

FIG. 4A-2 THE ASSUMED TIME VARIATION OF MAGNETIZATION. t_r IS THE TIME TAKEN BY THE MAGNETIZATION TO REVERSE AFTER A FIELD HAS BEEN APPLIED.

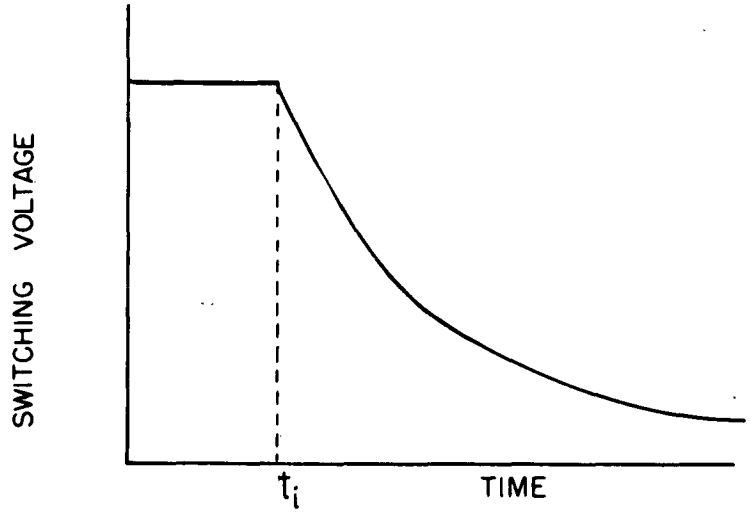

FIG. 4A-3 TYPICAL REVERSING SIGNAL FOR AN INCOMPLETELY SWITCHED CORE. t_i IS TIME TAKEN BY THE INNER DIAMETER TO SWITCH.

for $t < t_i$. t_i is the time required for magnetization at the inside diameter to reverse and is given by

$$t_i = \frac{S_w}{\frac{2I}{r_i} - H_c} \quad . \tag{4-4A}$$

At this time the reversal signal becomes

$$v = \frac{d}{dt} \int_{r(t)}^{r_c} \frac{2Mt}{S_w} \left(\frac{2I}{x} - H_c\right) dx + \frac{d}{dt} \int_{r_i}^{r(t)} 2M dx, \tag{4-5A}$$

with

$$r(t) = \frac{2It}{S_w + H_c t} \tag{4-6A}$$

locating the boundary between the reversed and reversing magnetization. Evaluation of these integrals gives

$$v = \text{constant}, \qquad t < t_i \tag{4-7A}$$

$$v' = \frac{v}{\frac{4MI}{S_w}} = \log(a+1) - \frac{a}{1+a}, \quad t \geq t_i \tag{4-8A}$$

with

$$a = S_w / H_c t. \tag{4-9A}$$

For small a, the expression for v' becomes

$$v' = \frac{1}{2} a^2. \tag{4-10A}$$

That this condition is pertinent to the present situation can be seen by noting

$$a < a_i = \frac{S_w}{H_c t_i} = \frac{r_o}{r_i} - 1. \tag{4-11A}$$

The dimensions of a typical core are $r_i \approx 35$ and $r_o < 50$ mils, so that α is less than 0.5

The reversal (switching) signal seen under these circumstances is shown in Fig. 4A-3. If the 10% rule is applied to this waveform to determine the switching time, then the switching time, t, would be the solution of the equation

$$0.1\, \alpha_i^2 = \alpha^2, \tag{4-12A}$$

after substituting Eqs. (4-11A) and (4-9A) in it. This solution is

$$\begin{aligned} t &= 3.2\, t_i \\ &= 3.2\, \frac{S_w}{\frac{2I}{r_i} - H_c} . \end{aligned} \tag{4-13A}$$

In the case where the applied field is sufficient to reverse the entire core, the reversal signal is again constant until the magnetization at the inner diameter reverses. At this time it becomes proportional to

$$v = \frac{4MI}{S_w} \left[\log \frac{r_o}{r(t)} - \frac{H_c}{H_o} \left(1 - \frac{r(t)}{r_o}\right) \right]. \tag{4-14A}$$

H_o is the field at the outer radius, r_o, of the core. This expression may be simplified by again using the fact that α is small. After writing

$$\begin{aligned} \log \frac{r_o}{r(t)} &= -\log \left[1 + \frac{r(t) - r_o}{r_o} \right] \\ &= -\left(\frac{r(t) - r_o}{r_o} \right) + \frac{1}{2} \left(\frac{r(t) - r_o}{r_o} \right)^2 , \end{aligned} \tag{4-15A}$$

the reversal signal can be written as

$$v = \frac{4MI}{S_w} \left[\left(1 - \frac{H_c}{H_o}\right)\left(1 - \frac{r(t)}{r_o}\right) + \frac{1}{2}\left(1 - \frac{r(t)}{r_o}\right)^2 \right]. \tag{4-16A}$$

For a sufficiently large field this becomes

$$v = \frac{4MI}{S_w}\left(1 - \frac{H_c}{H_o}\right)\left(1 - \frac{r(t)}{r_o}\right), \tag{4-17A}$$

while in the region where the field at the outside of the core is not much greater than H_c,

$$v = \frac{2MI}{S_w}\left(1 - \frac{r(t)}{r_o}\right)^2. \tag{4-18A}$$

This resembles the reversal signal obtained when the core was not completely switched.

In the case where $H_o > H_c$, the switching time based on the 10% rule is found to be

$$t = \frac{S_w}{\frac{2I}{0.9r_o + 0.1r_i} - H_c}. \tag{4-19A}$$

Since r_i is of the order of r_o, this may be further approximated to be

$$t = \frac{S_w}{\frac{2I}{r_o} - H_c}. \tag{4-20A}$$

This last formula is just the time required to switch the material at the outer portion of the core by the current, I.

The switching times for the case where $H_o \approx H_c$ may also be determined. But this will not be done here, since this solution is only valid over a small field interval. Under this condition, the solution is given by Eqs. (4-13A) and (4-19A) and shown in Fig. 4A-4. The ratio of the intercepts for the two linear regions is found to be r_i/r_o, while the inverse slopes have a ratio 3.2 times as great as this.

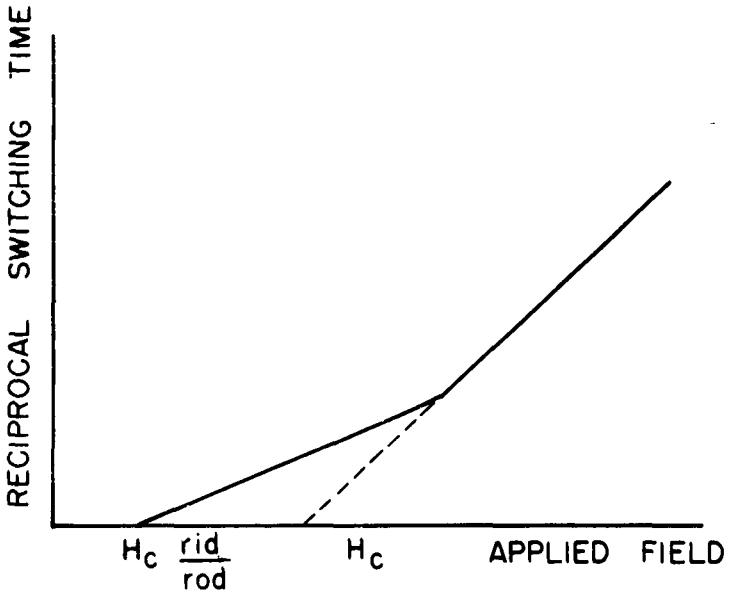

FIG. 4A-4 THE CALCULATED RECIPROCAL SWITCHING TIME AS A FUNCTION OF THE APPLIED FIELD FOR THE CASE OF A NONUNIFORM APPLIED FIELD. THE APPLIED FIELD IS THE FIELD AT THE OUTER DIAMETER.

From these results it can be seen that if the fields are computed at the outside diameter of the core, a value of S_W can be found for a material which is relatively independent of core size. It also can be seen from these results that, for a given current and inner radius, thin-walled toroids will switch faster than thick-walled toroids.

CHAPTER V: DOMAIN WALL MOTION

1. INTRODUCTION

In this chapter an expression will be found for the velocity of a 180° domain wall. An objective of this calculation is the determination of the domain wall velocity for materials which possess little or no damping. The domain wall velocity will also be calculated by a second method which yields an interpretation of the damping parameter in terms of wall collisions.

2. PRELIMINARY ASSUMPTIONS

The plane 180° domain wall whose velocity will be determined is assumed to exist within an infinite material prior to the application of an applied field. Its center is taken as the origin of a rectangular coordinate system, and the plane of the wall is taken parallel to the x-z plane. The domain which lies on the negative y side of this wall is magnetized in the positive z-direction, while the domain on the positive y side is magnetized in the negative z-direction. The wall remains at rest until a field $-\hat{z}H_z$ is applied. At this time the wall proceeds to move in the negative y-direction.

To describe the magnetization in the wall a spherical polar coordinate system whose polar axis lies along the y-direction is found convenient. The polar angle, θ, is measured from this axis, and the azimuthal angle, ϕ, is measured from the z-axis as shown in Fig. 5-1. Then, when the wall is static, $\theta = \pi/2$, everywhere, $\phi = 0$ for $y < 0$, and $\phi = \pi$ for $y > 0$.

The forces (or torques) which determine the motion of this wall are taken to arise from the applied field, the exchange and anisotropy interactions, and those magnetic fields which appear when the wall is in motion Except insofar as they may be taken into account by a reduction of the applied field, those fields which are responsible for the existence of the domain wall and which give rise to its coercive force have been neglected.

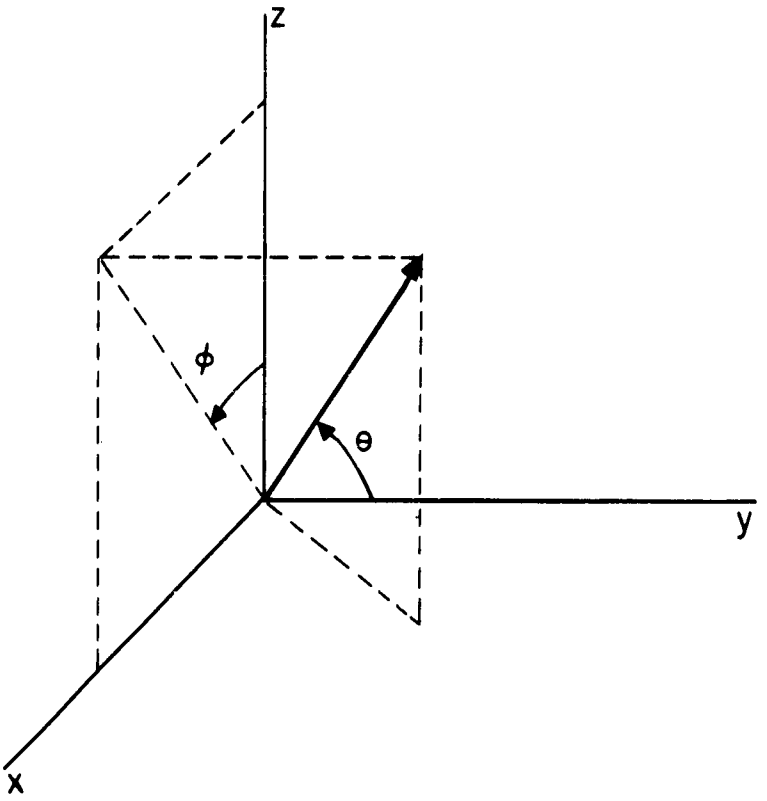

FIG. 5-1 COORDINATE SYSTEM FOR MAGNETIZATION ORIENTATION WITHIN A DOMAIN WALL. THE Z AXIS IS THE PREFERRED AXIS AND THE PLANE OF THE WALL IS THE X—Z PLANE.

3. EQUATION OF MOTION FOR THE MAGNETIZATION

The choice of an equation of motion presents some difficulty, since, at the moment, it is not known how the moving wall's magnetization is affected by the presence of thermal fluctuations. It was shown in Chap. I that, as a result of the average magnetization's interaction with thermally excited spin waves, the possibility exists that the average magnetization can be reduced in a resonance experiment, and the appropriate equation of motion should contain terms which allow for the occurrence of this phenomenon. Whether such effects occur during the motion of a domain wall is as yet unknown. Nevertheless, there are indications that these magnetization changes do not play an important role in domain wall motion. Indeed, the present picture of a static domain wall assumes that the magnetization within the wall does not fluctuate, and, as indicated in Chap. I, such a description seems to agree well with experimental data. Moreover, microwave experiments (1) aimed at the realization of a power limiting device which operates on the basis of transferring energy from the uniform precession to a spin wave, or a group of spin waves, indicate that the energy transfer requires a time of the order of $0.1\,\mu$sec. The exact time, however, is dependent on the magnitude of the excitation and decreases with increasing excitation. In addition, it is known that the transfer of energy into spin waves requires large excitations as the relaxation parameter increases. From these considerations and the anticipated result that a magnetic moment remains in a moving domain wall for times small compared to $0.1\,\mu$sec, it can be seen that the equation of motion need not always allow for a change in the amplitude of the magnetization. Further discussion of the applicability of this equation is given in Chap. VI, Sec. 5. For this regime, then, of the equations discussed in some detail in Chap. I, the choice is then between the Landau-Lifshitz equation and Gilbert's modification of it. Since, as has been shown previously, these two equations are related and approach each other as the damping parameter diminishes, the Landau-Lifshitz equation will be used.

When written in spherical polar coordinates this equation takes the form

$$M \frac{d\theta}{dt} = -\gamma M H_\phi + \lambda H_\theta \tag{5-1}$$

$$M \sin\theta \frac{d\phi}{dt} = \gamma M H_\theta + \lambda H_\phi \tag{5-2}$$

where H_θ and H_ϕ are the effective fields in the θ and ϕ directions respectively.

4. EFFECTIVE FIELDS

The effective fields which are to be used in Eqs. (5-1) and (5-2) arise from the interactions which have already been mentioned in Sec. 2. They can be most readily found from their respective energy densities.

In terms of the previously chosen spherical coordinate system the energy density, E_H, of the magnetization in the applied field and the exchange energy, E_A, are given by

$$E_H = MH \sin\theta \cos\phi \tag{5-3}$$

and

$$E_A = A \left[\left(\frac{\partial\theta}{\partial y}\right)^2 + \sin^2\theta \left(\frac{\partial\phi}{\partial y}\right)^2 \right]. \tag{5-4}$$

Although the materials to which these calculations are to be applied are cubic, for the purpose of obtaining results in this chapter the anisotropy is chosen as uniaxial. This is done to simplify the calculation and to avoid an indeterminancy (2) in the width and shape of domain walls in cubic materials. It will, however, turn out that the results obtained here do not critically depend on the anisotropy symmetry. The uniaxial anisotropy, E_K, for the wall described in Sec. 2 is then

$$E_K = -K \sin^2\theta \cos^2\phi . \tag{5-5}$$

When the wall is in motion, θ need not be $\pi/2$. A component $M_y = M \cos \theta$ will exist, and if θ is a function of y, then, since

$$\text{div } M = \frac{dM_y}{dy} = -M \sin \theta \frac{d\theta}{dy} \neq 0, \tag{5-6}$$

a field will exist in the wall. This field will satisfy the Maxwell equations

$$\nabla \cdot B = 0 \tag{5-7a}$$

and

$$\nabla \times H = 0, \tag{5-7b}$$

where the magnetic induction is

$$B = H + 4\pi M. \tag{5-8}$$

The evaluation of this field is difficult unless we assume that the plane of the wall is infinite and the magnetization within the wall is uniform. Under these conditions substitution of Eq. (5-8) into Eq. (5-7a) gives

$$\frac{\partial H_y}{\partial y} = -4\pi \frac{\partial M_y}{\partial y}$$

which becomes with Eq. (5-6)

$$\frac{\partial H_y}{\partial y} = 4\pi M \sin \theta \frac{\partial \theta}{\partial y}. \tag{5-9}$$

Integration then gives

$$H_y = -4\pi M \cos \theta \tag{5-10}$$

with the constant of integration vanishing since H_y vanishes when $\theta = \pi/2$. Equation (5-7b) can be used to show that H_y is a function of y alone.

The self demagnetizing energy becomes

$$E_{dem} = -2\pi M^2 \cos^2 \theta. \tag{5-11}$$

To determine the effective fields to use in the equations of motion, Eqs. (5-1) and (5-2), the four energies found above are operated on using the formulae found in Goldstein's (3) book on mechanics.

The effective θ and ϕ components of the magnetic field are then

$$H_\theta = \frac{-\partial E_H}{M\partial\theta} = -H\cos\theta\cos\phi \tag{5-12a}$$

and

$$H_\phi = -\frac{1}{M\sin\theta}\frac{\partial E_H}{\partial\phi} = H\sin\phi\ , \tag{5-12b}$$

where E_H is given in Eq. (5-3). Replacing E_H by E_K of Eq.(5-5) in the above equations permits the determination of the components of the effective anisotropy field. These are found to be

$$H_\theta = \frac{K}{M}\ 2\sin\theta\cos\theta\cos^2\phi \tag{5-13a}$$

and

$$H_\phi = -\frac{K}{M}\ 2\sin\theta\cos\phi\ \sin\phi\ . \tag{5-13b}$$

When E_H is replaced by E_{dem} given in Eq. (5-11), the effective components of the demagnetizing fields are

$$H_\theta = 4\pi M\cos\theta\sin\theta \tag{5-14a}$$

and

$$H_\phi = 0. \tag{5-14b}$$

The effective exchange fields, however, need to be handled in a different manner since these fields result from spacial changes in the magnetization. Here we have

$$H_\theta = \frac{1}{M}\left[\frac{d}{dy}\left(\frac{\partial E_A}{\partial(\frac{d\theta}{dy})}\right) - \frac{\partial E_A}{\partial\theta}\right] = \frac{2A}{M}\left[\frac{d^2\theta}{dy^2} - \sin\theta\cos\theta\,(\frac{d\phi}{dy})^2\right] \tag{5-15}$$

and

$$H_\phi = \frac{1}{M \sin\theta}\left[\frac{d}{dy}\left(\frac{\partial E_A}{\partial(\frac{d\phi}{dy})}\right) - \frac{\partial E_A}{\partial \phi}\right] = \frac{2A}{M}\left[\sin\theta \frac{d^2\phi}{dy^2} + \frac{4A}{M}\cos\theta \frac{d\phi}{dy}\frac{d\theta}{dy}\right] . \tag{5-16}$$

We then have for the total θ and ϕ fields

$$H_\theta = -H\cos\theta\cos\phi + \frac{2K}{M}\sin\theta\cos\theta\cos^2\phi + 4\pi M\cos\theta\sin\theta + \frac{2A}{M}\left[\frac{d^2\theta}{dy^2} - \sin\theta\cos\theta\left(\frac{d\phi}{dy}\right)^2\right] . \tag{5-17}$$

$$H_\phi = H\sin\phi - \frac{2K}{M}\sin\theta\cos\phi\sin\phi + \frac{2A}{M}\sin\theta\frac{d^2\phi}{dy^2} + \frac{4A}{M}\cos\theta\frac{d\phi}{dy}\frac{d\theta}{dy} . \tag{5-18}$$

If these fields were substituted into the equations of motion, the resulting equations would be far too complex for solution. To simplify the resulting equations, a number of approximations will be made.

5. WALL SHAPE ASSUMPTION

The first of these approximations consists of assuming that the wall moves so as to preserve the relative angular relationships that exist in a static wall. In the static domain wall the magnetization appears to rotate about an axis perpendicular to the plane of the wall as the wall is traversed along this axis. The assumption made here allows this axis, when the wall moves, to assume a position in the plane normal to the preferred axis.

As a result of this assumption we may further dismiss from consideration the torques (and fields) due to exchange and anisotropy interactions, since in the static wall the exchange and anisotropy torques balance each other. This is just the physical significance of the differential equation obtained in Chap. I in the determination of the shape of the domain wall (4). In Appendix I of this chapter this assumption is further justified.

The effective fields then assume the greatly simplified forms,

$$H_\theta = -H\cos\theta\cos\phi + 4\pi M\cos\theta\sin\theta \qquad (5\text{-}19)$$

and

$$H_\phi = H\sin\phi\,, \qquad (5\text{-}20)$$

and consist only of the applied field and the field which arises from the divergence of the magnetization across the wall.

6. EQUATION OF WALL MOTION

Now, if $\psi = \pi/2 - \theta$, ψ will measure the rotation of the magnetization from the static wall plane, and from energy considerations ψ will be shown to be small. As the magnetization changes from antiparallel to parallel to the applied field, its energy in the applied field is converted into demagnetizing energy in the absence of losses and when the exchange and anisotropy effects are neglected. The maximum change in Zeeman energy in this case is approximately 2MH, while the demagnetizing energy becomes $2\pi M^2\sin^2\psi$. Equating these energies gives an equation for the maximum ψ, ψ_{max}.

$$\sin\psi_{max} = 2\sqrt{\frac{H}{4\pi M}}\,. \qquad (5\text{-}21)$$

For the materials and experiments to which this discussion will be applied, $4\pi M > 1000$ gauss and the applied field is less than 40 oe, so that $\sin\psi_{max} = 0.4$. For $\psi < \psi_{max}$, $\sin\psi$ may be replaced by ψ and $\cos\psi$ by 1 with reasonable accuracy (less than 8 per cent error at $\psi = 0.4$ radians). The presence of loss improves this situation. With these approximations, the fields become

$$H_\theta = -H\psi\cos\phi + 4\pi M\psi\,, \qquad (5\text{-}22)$$

and

$$H_\phi = +H\sin\phi\,, \qquad (5\text{-}23)$$

and the equations of motion take the form

$$-M\frac{d\psi}{dt} = -\gamma MH\sin\phi + \lambda(4\pi M - H\cos\phi)\psi \qquad (5\text{-}24)$$

and

$$M\frac{d\phi}{dt} = \gamma M(-H\cos\phi + 4\pi M)\psi + \lambda H\sin\phi. \qquad (5\text{-}25)$$

These latter equations may be further simplified by noting that when these results are applied

$$H \ll 4\pi M. \qquad (5\text{-}26)$$

Thus, Eqs. (5-24) and (5-25) reduce to

$$-\frac{d\psi}{dt} = -\gamma H\sin\phi + \lambda 4\pi\psi \qquad (5\text{-}27a)$$

and

$$\frac{d\phi}{dt} = \gamma(4\pi M)\psi + \lambda\frac{H}{M}\sin\phi. \qquad (5\text{-}27b)$$

When ψ is eliminated from these equations, after again using Eq. (5-26), the equation of motion of the magnetization within a domain wall,

$$\ddot{\phi} + 4\pi\lambda\dot{\phi} - 4\pi\gamma^2 HM\left(1 + \frac{\lambda^2}{\gamma^2 M^2}\right)\sin\phi = 0, \qquad (5\text{-}28)$$

is found.

7. SOLUTIONS OF THE DOMAIN WALL MOTION EQUATION

In the study of the motion of a damped pendulum a differential equation identical to Eq. (5-28) is found. There the solution of this equation describes the pendulum's angular displacement as a function of the time, and it has been shown that, for λ less than some critical value, λ_c, the displacements are of a damped oscillatory type; the amplitude of the oscillations of the pendulum about its equilibrium decreases as a function of time. When $\lambda \geq \lambda_c$, this theory shows that the displacements asymptotically decay to the equilibrium position.

Here, these solutions describe the rotations of the magnetization about a normal to the wall as a function of the time, and it is these rotations which are the source of wall motion. The translation of the wall is accomplished through the rotation of the magnetization within the wall. And, since the rotation of the magnetization within the wall is given by the solutions of the pendulum equation, it may be expected that when the damping is small or absent, the magnetization will overshoot the new equilibrium to the extent of forming a new wall behind it. These overshoots and the resulting multiwall formation are, however, consequences of neglecting the anisotropy and exchange torques. As long as the magnetization does not overshoot the vicinity of its new equilibrium position, i.e., $\phi < \pi$, the exchange and anisotropy torques are oppositely directed, and they can cancel each other. Once the magnetization passes $\phi = \pi$ this possibility no longer exists. The exchange and anisotropy torques are then in the same direction and increase as the magnetization moves away from $\phi = \pi$ towards larger ϕ's and cause the magnetization to precess about its new equilibrium. The details of this motion need not concern us for we wish only to obtain the velocity of the moving wall, and, for this purpose, only the time taken by the magnetization to reverse, i.e., for ϕ to become π, need be obtained.

8. WALL VELOCITY

One further point should be discussed before the wall velocity is determined. In the theory of the domain wall given in Chap. I, Sec. 3b, the equation relating the magnetization direction, ϕ, with its position along the wall measured relative to the center of the wall was found to be (Eq. (1-33a))

$$\log \tan \frac{\phi}{2} = \frac{z}{\sqrt{A/K}} \tag{5-29}$$

for a 180° wall in a uniaxial anisotropic material. Examination of this

equation revealed that although it takes an infinite distance for the magnetization to completely reverse (rotate 180°), a large fraction of the rotation takes place in a finite distance. To avoid dealing with this type of infinity, the part of the wall for which $\pi/4 < \phi < 3\pi/4$ corresponding to a wall width, W,

$$W = 1.76 \sqrt{A/K}, \tag{5-30}$$

is considered. The wall velocity, v, is then defined as this distance divided by the time, t_o, for the magnetization in the wall to change from $\phi = \pi/4$ to $\phi = 3\pi/4$:

$$v = \frac{W}{t_o} . \tag{5-31}$$

To obtain t_o, the pendulum equation must be solved. Since this equation is a nonlinear type for which solutions in closed form are not obtainable, a piecewise linear approximation of the differential equation was made to obtain its solution. The details are given in Appendix II. In order to sufficiently generalize the result so that it may be applied as the parameters are varied, the equation was reduced to

$$\frac{d^2\phi}{d\tau^2} + \xi \frac{d\phi}{d\tau} - \sin\phi = 0 \tag{5-32a}$$

where

$$\tau = \omega_o t, \tag{5-32b}$$

$$\xi = 2\pi \lambda/\omega_o \tag{5-32c}$$

and

$$\omega_o = \gamma \left[4\pi MH \left(1 + \frac{\lambda^2}{\gamma^2 M^2}\right)\right]^{1/2} . \tag{5-32d}$$

In terms of these variables, τ_o, the reduced time for the wall to advance a distance, W, is given by

$$\tau_o = \omega_o t_o \tag{5-33}$$

and is shown in Fig. 5-2 as a function of ξ as obtained in Appendix II. It may be noted from this figure that τ_o is linear with ξ for large ξ. This corresponds to the solution of the reduced equation when the term containing the second derivative is neglected. The damping force is so large that the inertial force may be neglected. Under these conditions, the solution is readily found to be

$$\tau = \xi \log \tan \phi/2. \tag{5-34}$$

From this equation the reduced time for the magnetization to rotate through the central 90° is then

$$\tau_o = 1.76\,\xi, \tag{5-35a}$$

and t_o is then found from Eqs. (5-33), (5-32c) and(5-35a) to be

$$t_o = \frac{\tau_o}{\omega_o} = 1.76\,\frac{2\pi\lambda}{\omega_o^2}. \tag{5-35b}$$

Hence, for $\lambda \gg 0$, the wall velocity is found by substituting Eqs. (5-35b), (5-30) and (5-32d) in Eq. (5-31) and is

$$v = \frac{2H}{M}\,\frac{\lambda^2 + \gamma^2 M^2}{\lambda}\,\sqrt{A/K}. \tag{5-36}$$

For $\lambda = 0$, τ_o is found by using Fig. 5-2 to be 1.3. t_o is then

$$t_o = \frac{1.3}{\gamma(4\pi MH)^{1/2}}.$$

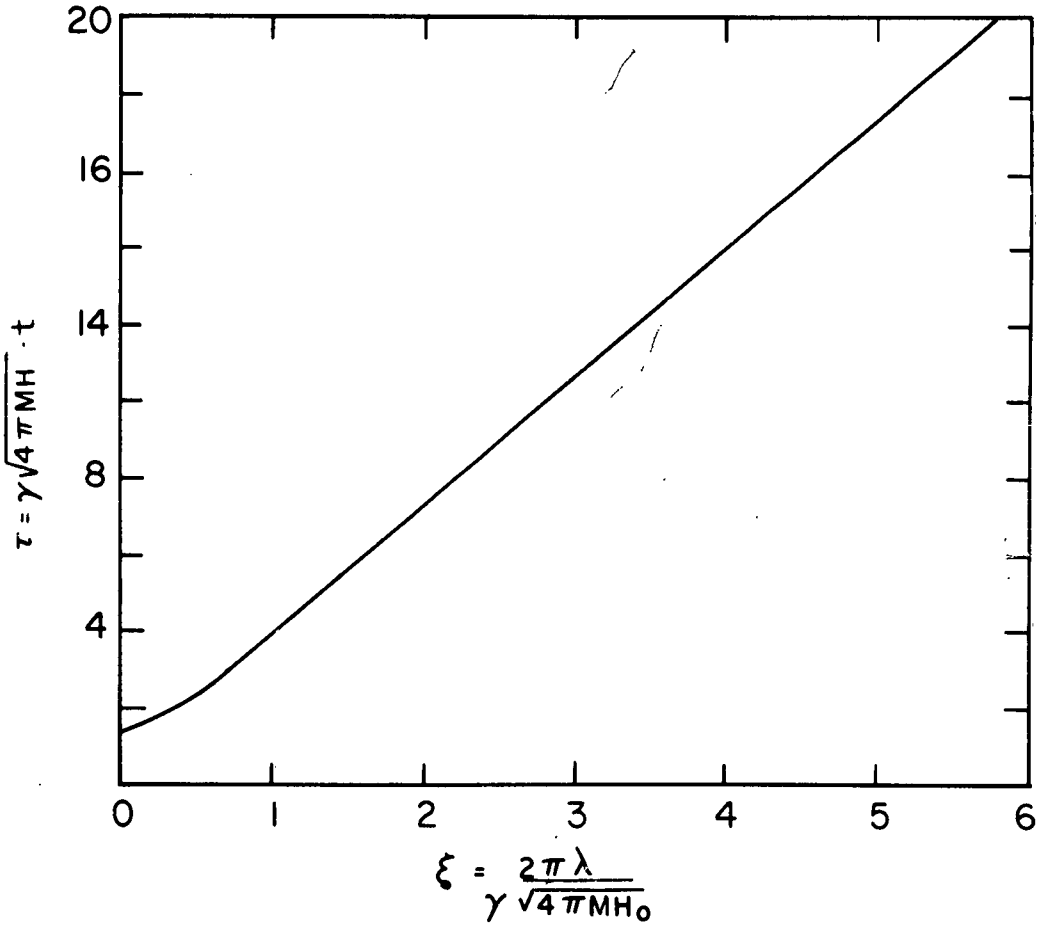

FIG. 5-2 RELATIVE SWITCHING TIME τ VS RELATIVE DAMPING PARAMETER.

Using this value in Eq. (5-31) and taking W again from Eq. (5-30), the wall velocity in the absence of losses is

$$v = 4.8\gamma\left(\frac{MHA}{K}\right)^{1/2} . \qquad (5\text{-}37)$$

Although the results contained in the wall velocity equations, Eqs. (5-36) and (5-37), were obtained for a model based on a material with uniaxial anisotropy, they can be applied to cubic materials as is seen by examination of the origin of the factors W and t_o of the wall velocity equations, Eq. (5-31), from which these results were obtained. Since in the calculation of t_o it was assumed that the domain wall does not distort when it moves, the anisotropy and exchange torques were neglected, and, consequently, the crystal symmetry did not enter into t_o's determination. The factor W which measures the wall width is somewhat differently obtained in cubic materials from the manner in which it is found in the uniaxial case. Here it is found that in order for a 180° wall to exist, magnetoelastic effects must be present. However, as Kittel (2) has shown, these effects only weakly determine the wall's energy and width, and W is proportional to $\sqrt{A/K}$. Hence, to within a factor of the order of 1, Eqs. (5-36) and (5-37) are applicable to cubic materials.

The value obtained for the wall velocity by utilizing the equations derived here is probably too large. For should any wall distortions occur, they will take up energy which otherwise would be available to the demagnetizing field. Hence in the presence of wall distortion the demagnetizing field will decrease, which in turn will decrease the rate of reversal.

9. VARIATIONS IN WALL VELOCITY WITH DAMPING

In Fig. 5-3 a plot of t_o, the time for the magnetization at a given position in the wall to reverse, is given. Since the wall velocity is inversely proportional to t_o, it is seen from this figure that the domain wall velocity has a maximum as the damping parameter is decreased to zero, a minimum when the damping parameter is γM, and the wall velocity increases without bound as the damping parameter becomes very large. This latter effect is attributable to the choice of the damping term in the equation describing the motion of the magnetization. In Chap. I, the damping term, λ, in the Landau-Lifshitz equation was shown to measure the rate of loss of energy. Hence it is to be expected that increasing λ, increases the wall velocity.

10. COMPARISON WITH PREVIOUS RESULTS

Comparison of the wall velocity determined here with previous calculations shows that it is equivalent to the results obtained by Landau and Lifshitz (5) for large damping. Here this wall velocity calculation has been extended to cover the case of small damping. The Landau and Lifshitz calculation was restricted to large damping by virtue of their assumption that the velocity is proportional to the applied field. They made no attempt to obtain the wall velocity for small damping. Others, such as Kittel (6), Becker (7), and Galt (8), who have calculated the wall velocity and obtained the Landau-Lifshitz result, placed no restriction on the damping, although their calculations assume that the domain wall dissipates all of its energy before it moves a distance greater than its own width.

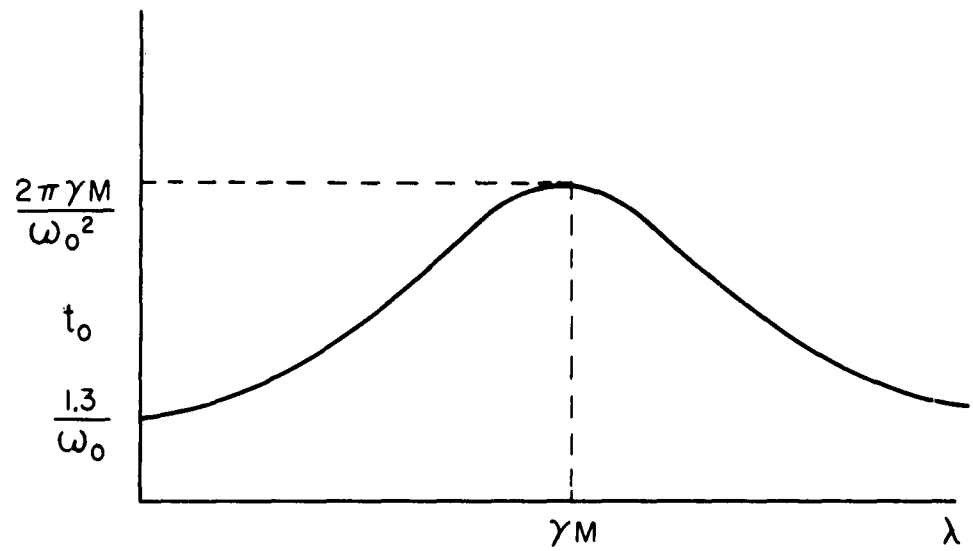

FIG. 5-3 THE TIME, "t_0", FOR THE MAGNETIZATION AT A GIVEN POSITION WITHIN THE WALL TO REVERSE AS A FUNCTION OF THE DAMPING, λ.

11. WALL COLLISIONS

Relationships for the wall velocity similar to Eqs. (5-36) and (5-37) may be found from another damping model. This model also provides a physical picture of the reason the wall velocity will not decrease indefinitely with the reduction of the damping parameter.

In this model the wall is assumed to move without any damping until it makes a collision. The wall then loses its entire velocity in a time very small compared to other times between collisions. To determine the wall's velocity Eqs. (5-27a) and (5-27b), with $\lambda = 0$, are used to describe the motion between collisions.

For small times Eq. (5-27a) may be integrated to give

$$\psi = + \gamma H t \sin \phi . \tag{5-38}$$

Substituting this in Eq. (5-27b) gives

$$\frac{d\phi}{dt} = \gamma^2 (4\pi MH) t \sin \phi . \tag{5-39}$$

From Eq. (1-33) the spacial derivative of the angular variation within the static wall is

$$\frac{d\phi}{dz} = \sqrt{K/A} \sin \phi = \frac{1}{\delta} \sin \phi . \tag{5-40}$$

If the time, t, is sufficiently short, the moving wall's structure will resemble the static wall's structure sufficiently well so that Eq. (5-40) still holds. Then the wall's velocity, v, may be determined from

$$v = \frac{\frac{d\phi}{dt}}{\frac{d\phi}{dz}} . \tag{5-41}$$

Using Eqs. (5-39) and (5-40) in Eq. (5-41), the wall velocity is

$$v = \gamma^2 (4\pi MH)\, t\, \delta . \tag{5-42}$$

Taking $\bar{t}$ as the average time between collisions, the average attained velocity, $\bar{v}$, is

$$\bar{v} = \gamma^2 MH\, 2\pi \bar{t}\, \delta . \tag{5-43}$$

If $\Omega = (2\pi\bar{t})^{-1}$, $\bar{v}$ becomes

$$\bar{v} = (\gamma^2 MH/\Omega)\sqrt{A/K}\,, \tag{5-44}$$

a form very similar to Eq. (5-36).

Eq. (5-42) shows that the wall velocity increases with time. However, this is not entirely correct, even if Eq. (5-38) were to hold for all t. Once the time between collisions is sufficiently long so that ϕ changes from 0 to π, the instantaneous wall velocity can no longer increase. The wall velocity then varies linearly with time until $t = t_o$, the time for the magnetization at one point within the wall to reverse, at which time it remains constant.

When the time between collisions, $\bar{t}$, is greater than t_o,

$$v = \frac{4\pi}{\bar{t}} \left(\bar{t} - \frac{t_o}{2}\right) t_o \gamma^2 MH\delta . \tag{5-45}$$

t_o may be estimated from Eq. (5-39). Taking $\frac{d\phi}{dt} = \frac{\pi}{t_o}$ and $\sin\phi \approx 1/2$ and solving Eq. (5-39), t_o is

$$t_o = (2\gamma^2 MH)^{-1/2} . \tag{5-46}$$

In the case of very long collision times, Eq. (5-45) reduces to

$$\bar{v} = 4\pi\gamma^2 MH t_o \delta .$$

This becomes

$$\bar{v} = \frac{4\pi}{\sqrt{2}} \gamma \sqrt{MH}\ \sqrt{A/K}\,, \tag{5-47}$$

when the value for t_o found in Eq. (5-46) is introduced. Equation (5-47) is to be compared with the previously determined velocity, Eq. (5-37), for the small damping case. Here again the $\sqrt{H}$ dependence is found.

CHAPTER V – BIBLIOGRAPHY

1. G.S. Uebele, I.R.E. Trans. MIT 7, 18 (1959).
2. C. Kittel, Rev. Mod. Phys. 21, 563 (1949).
3. H. Goldstein, "Classical Mechanics" (Addison Wesley Press, Inc., 1951) p. 350.
4. R.W. DeBlois, J. Appl. Phys. 29, 459 (1959).
5. L. Landau and E. Lifshitz, Physik. Z. Sowjetunion 8, 153 (1935).
6. C. Kittel, Phys. Rev. 80, 918 (1950).
7. R. Becker, J. Phys. radium 12, 332 (1951).
8. J.K. Galt, B.S.T.J. 33, 1023 (1954).

APPENDIX I

JUSTIFICATION OF THE DOMAIN WALL SHAPE ASSUMPTION

In this appendix, the domain wall shape assumption made in Sec. 5 where the domain wall velocity was calculated is treated in greater detail. There it was postulated that the magnetization in the moving domain wall maintains the same angular distribution with the easy axis as it does in the static wall, and, as a result, the exchange and anisotropy fields could be neglected. Although it can be anticipated that the changes in the angular distribution will be small, the sizes of the fields which do arise from these changes are unknown. Since the exchange interaction is large and usually has associated with it large fields, a large field could arise from this source and dominate the reversal process. It is shown here that this does not happen.

For large damping the present solution for the wall velocity, Eq. (5-36) is consistent with the domain wall shape assumption. This may be seen by comparing Eq. (5-34) which relates the angle which the magnetization at a particular point within the wall makes with the easy direction with the time and Eq. (5-29) which gives the wall shape. Since these relations are expressed by the same function, it follows that in this case there is no wall deformation. The same conclusion is obtained by noting that when the damping is large any energy which would be available to distort the wall is quickly dissipated.

When the damping is small, these considerations no longer apply and a more detailed examination must be made. If the wall moves after the application of the applied field (i.e., the field is larger than the coercive force of the material), the angle between the applied field and the magnetization within the wall must change. In order that this angle change, there must exist a field normal to both the applied field and the magnetization.

In the nondeforming wall model, this field has been taken as the demagnetizing field arising from rotations of the magnetization out of the plane of the wall. If the wall does deform, then a field may arise from exchange effects which can rotate the magnetization. It cannot arise from anisotropic considerations here as a consequence of assuming uniaxial anisotropy. For this type of anisotropy can only bring about a precession about the preferred axis, which here is also the direction of the applied field.

We now estimate the size that this exchange field may take in order to show that no serious error exists in its neglect. In order to do this, the coordinate system shown in Fig. 5-1A is adopted. This coordinate system differs from the one previously used only in that the polar axis is changed from the y-axis to the negative z-axis. Again the plane of the wall is the x-z plane. In this coordinate system, the effective exchange field which is reponsible for changes in θ is

$$H_{ex} = \frac{-2A}{M} \left[\sin\theta \frac{d^2\phi}{dy^2} + 2 \cos\theta \frac{\partial\phi}{\partial y} \frac{d\theta}{dy} \right] .$$

We note that if the moving wall bears any resemblance to the stationary wall then

$$\frac{d\theta}{dy} = 0$$

at $\theta = \pi$ or 0, and $d\theta/dy$ is maximum at the center of the wall where $\theta = \pi/2$. Hence the second term for H_{ex} has its largest value in the vicinity of $\theta = 3\pi/4$, being zero at $\theta = \pi/2$ and π; identical considerations hold for the region between 0 and $\pi/2$. On the other hand because of the $\sin\theta$ term, the first term will be large at $\theta = \pi/2$.

The maximum values of the ϕ derivatives in the above formula may be estimated as follows.

The maximum value of ϕ, ϕ_m, is obtained, as in Eq. (5-21), from magnetostatic considerations. If ϕ monotonically increases to this value as the wall is traversed, then an upper bound on the first derivative is

$$\frac{d\phi}{dy} \approx \frac{\phi_m}{\delta}, \tag{5-1A}$$

where $\delta = \sqrt{A/K}$ is the distance measured from the center of the wall in which the magnetization of a static wall rotates by $\pi/4$ radians. This upper bound will be taken as an estimate of the maximum of $d\phi/dy$. Similarly, an upper bound for the second derivative is found to be

$$\frac{d^2\phi}{dy^2} = \frac{\phi_m}{\delta^2}. \tag{5-2A}$$

Now, if H_{ex} be written as

$$H_{ex} = H_1 + H_2 \tag{5-3A}$$

with

$$|H_1| = 4\frac{A}{M}\frac{d\phi}{dy}\frac{d\theta}{dy}\cos\theta \tag{5-4A}$$

and

$$|H_2| = 2\frac{A}{M}\frac{d^2\phi}{dy^2}\sin\theta, \tag{5-5A}$$

then the maximum value of H_{ex} will be less than the sum of the maximum values of $|H_1|$ and $|H_2|$, for, as has been shown above, these maximums do not occur simultaneously.

The maximum values of H_1 and H_2 are found by using Eqs. (5-1A) and (5-2A) in Eqs. (5-4A) and (5-5A). These values are

$$H_{1max} = 4\frac{K}{M}\phi_m \tag{5-6A}$$

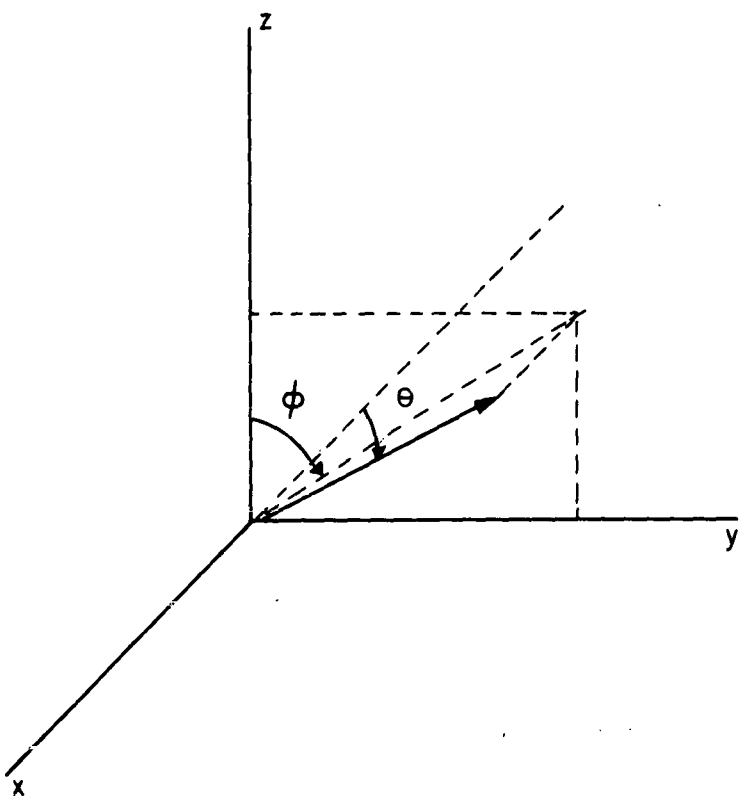

FIG. 5A-1 COORDINATE SYSTEM FOR USE WITH APPENDIX I THE z AXIS IS THE EASY AXIS AND THE DOMAIN WALL PLANE IS x — z PLANE.

and

$$H_{2max} = 2\frac{K}{M}\phi_m, \tag{5-7A}$$

giving for the maximum value of H_{ex}

$$H_{ex_{max}} = 6\frac{K}{M}\phi_m. \tag{5-8A}$$

The maximum demagnetizing field is

$$H_{dem} = 4\pi M\phi_m. \tag{5-9A}$$

Comparison of H_{dem} with $H_{ex\ max}$ shows that H_{dem} will be larger if $4\pi M^2$ is greater than 6K.

For most soft magnetic materials this is indeed true; in particular, for the cases in which we need to apply this result, it holds. Hence, we see that, in the limit of zero damping, the demagnetizing field is the only field responsible for the rotations in the wall.

One further point deserves consideration. In the argument given above we have assumed that the increase in energy which the magnetization could have is obtained only from its own decrease in magnetostatic energy. It also may obtain the magnetostatic energy released by virtue of the wall shrinking. But this should be small, for, in order for the wall to shrink, it would have to increase its exchange energy which depends on $d\theta/dy$.

APPENDIX II

NUMERICAL SOLUTION OF THE EQUATION OF DOMAIN WALL MOTION

In this appendix, the numerical method used to calculate the reduced time for the magnetization within the wall to rotate through its central 90° when the wall moves to reverse the magnetization is described.

The calculation proceeds from Eq. (5-32a) which is the equation which governs this motion. We first approximate the sine term in this equation by a relation of the form

$$\sin\phi = a\phi + b, \tag{5-1B}$$

where

$$\begin{array}{lll} a = 1 & b = 0 & 0 \leq \phi \leq \pi/4 \\ a = 0.374 & b = 0.414 & \pi/4 \leq \phi \leq \pi/2 \\ a = -0.374 & b = 1.586 & \pi/2 \leq \phi \leq 3\pi/4. \end{array} \tag{5-2B}$$

Using these relations in Eq. (5-32a), the set of equations

$$\frac{d^2\phi}{d\tau^2} + \xi \frac{d\phi}{d\tau} - a\phi = b \tag{5-3B}$$

is obtained. Here a and b are again given by Eq. (5-2B). Equation (5-3B) replaces Eq. (5-32a) with three linear equations, each of which is valid in a different interval.

The solutions of these equations can be obtained by well known methods. The solution for the first interval evaluated at $\phi = \pi/4$ furnishes initial conditions for the second interval, which in turn furnishes initial conditions for the third interval. Since the solution of Eq. (5-3B) is a transcendental function of the time, it is impossible to solve analytically for the time at which a certain ϕ occurs, and so a graphical solution was used. This value of time is required in order to obtain the initial value of $d\phi/d\tau$.

The initial conditions for the first interval are somewhat more complicated, as may be seen from the considerations which follow. Two variables which can describe the orientation of the magnetization are ϕ and ψ. In terms of these variables a reasonable initial condition appears to be $\phi = 0$ and $\psi = 0$. When these values are used in Eq. (5-27b), $d\phi/d\tau$ is found to vanish. If $d\phi/d\tau$ and ϕ simultaneously vanish, then Eq. (5-32a) has only the solution which shows no motion of the magnetization. However, it is clear that $\phi = 0$, $\psi = 0$ is a point of unstable equilibrium, and when a field is applied to move a wall and reverse the magnetization, any displacement of the magnetization from this orientation will initiate the reversal. Thus we assume for initial conditions that ϕ has some value near zero but retain the zero value for $d\phi/d\tau$.

In the calculations the initial value of ϕ was taken as 10°, or 0.17 radians, and ξ was varied in steps of 0.05. The results are shown in Fig. 5-2.

CHAPTER VI: INTERPRETATION OF EXPERIMENTAL DATA

1. INTRODUCTION

The purpose of this chapter is to interpret the measurements of the garnets and ferrites described in Chap. IV. A model will be established which unites the measurements of the garnets and which gives a basis on which the measurements for the nickel cobalt ferrites will be discussed.

This will be done using as a foundation the calculations of Chap. V. The paths traversed by the domain walls during the reversal will be discussed, and the effective parameters for the multi-sublattice magnetic systems which concern us here will be found and used with wall velocity calculations. These calculations will then be applied to the garnets and compared with the switching measurements. The switching will also be examined in the light of nonlinear losses. Following a discussion of the nickel cobalt results, the higher field regions will be treated using a field dependent relaxation frequency.

2. DOMAIN WALL PATH

If the domain configurations acquired by the magnetization during its reversal were known, then the distance through which the domain walls moved during the reversal could be determined and then combined with the wall velocities found in Chap. V to calculate the time required to switch a ferromagnetic material. However, in order to theoretically determine these domain configurations a number of factors (grain sizes, shapes, and relative orientations, stress and imperfection distribution, etc.) which are not accessible must be known. Hence, to obtain information concerning the wall paths, direct experimental observations are necessary.

Consequently, an attempt was made to observe domain walls in yttrium iron garnet specimens. Although this observation is possible (1) it is difficult for a number of reasons. Since the specimens are fine grained, large

magnifications are required to discern the magnetic domains within the grains, and, therefore, of the available methods of domain observation the choice is restricted to the Bitter technique (2) which was described in Chap. I, Sec. 3c. The concentration of colloid which is formed over the domain walls in the application of this technique is proportional to the magnetic pole density (3) which results from the intersection of the magnetization within the wall with the specimen's surface. This pole concentration is then inversely proportional to the domain wall width and directly proportional to the material's magnetization. Since all iron garnets have broad walls due to their relatively small anisotropy, and since their magnetization is low, the pole density over the walls is small. Coupled with this is the fact that as a result of the high magnification which is required the contrast in the image of the aggregate of particles is decreased, and this decrease in contrast is all the worse when the density of particles is low. Thus it may be seen that the observation of domain walls in the garnets is difficult and that under these conditions it is relatively easy to overlook their presence.

The results of observations on yttrium iron garnet, an example of which is shown in Fig. 2-8, nevertheless, did show the existence of domain walls in these materials. Whenever they were found, no more than two existed in a grain. In contrast with the periodic and simple shaped domain patterns (4, 5) observed in large grained or single crystal materials, here highly irregular shaped and isolated domains were seen. These shapes were probably due to the irregular stress and demagnetizing field distributions which can exist in fine grained materials and which can overcome the order usually established by the magnetocrystalline anisotropy. These observations are consistent with those of Knowles (6) and others (7) who have examined other fine grained ferrites.

However, attempts to track the motion of these walls as the magnetization was reversed did not prove fruitful. The presence of domain walls at a particular location within the sample was unpredictable. Cycling a toroid around its hysteresis loop did not seem to return walls to their initial position. This may be due to the fact that the energy wells in which the walls may reside are all approximately the same depth. A field which then frees a wall from one of these wells will free it from all of them. However, occasionally the walls will stick in one of these energy troughs.

When a portion of a wall's motion during the reversal was observed as the applied field was increased, the wall was seen to stretch while being held fast at certain point impediments (somewhat like a clothesline in a wind) before breaking loose and disappearing.

Knowles, as discussed in Chap. I, Sec. 5e2, observed the domain configurations in a polycrystalline ferrite as a function of applied field. The grains of this ferrite were much larger than ours. From his observations, it may be concluded that the initial and final states of the magnetization reversal process are remanent states, i.e., states which are multidomain. This is in agreement with hysteresis and switching data presented by Wijn and Smit (8). Their hysteresis data obtained by d.c. measurements and their switching data show that the quantity of magnetization which is reversed in each experiment is the same and that the reversals are between remanent states, not saturated states. The magnetization change, as observed by these authors, is approximately half that which would be obtained if the reversals were between saturated states.

From these observations the conclusion can be drawn that the domain configurations involved in the magnetization reversal process are independent of the time required for the field to attain its final value. However, the domain configurations are dependent on the final value of the field until this field is somewhat greater than the material's coercive force. For these

large field values the domain configurations are almost independent of the applied field.

In other words, the distance, d, which a domain wall moves in a reversal of the magnetization is a function of the applied field and increases with increasing applied field. However, the rate of increase decreases and d takes on a relatively constant value, d_o, when the applied field is in excess of the major hysteresis loop's coercive force. The size of this field will depend not only on the chemistry of the sample but also on its preparation.

Estimates of d_o may be obtained from these observations by noting that d_o must be less than a grain dimension. Since the switching time of a core is determined by the slowest switching elements which exist in sufficient quantity, it will be determined by the larger grains. To be precise, the grain size for determining d should be chosen on a statistical basis. However, since the grain sizes in a typical garnet sintered at 1400°C vary from around 2 to 15 microns with a predominance at about 10 microns, it is felt that this is unnecessary. In these grains the walls probably do not traverse the entire grain, and so the size of d should be between 5 and 10 microns.

The time, t, required for the magnetization to reverse is then

$$t = \frac{d}{v} \quad , \tag{6-1}$$

where d is the average distance which a domain wall moves, and v is its velocity. For large enough damping this leads to the relation, using Eq. (5-36),

$$t = \frac{dM}{2H} \frac{\lambda}{(\lambda^2+M^2\gamma^2)} \sqrt{K/A} \quad , \tag{6-2a}$$

while in the absence of damping, using Eq. (5-37),

$$t = \frac{d}{4.8\gamma} \left(\frac{K}{MHA}\right)^{1/2} \tag{6-2b}$$

From Eq. (6-2a) the switching parameter, S_w, which was introduced in Eq. (1-84), may be found.

$$S_w = \frac{d}{2} \frac{\lambda M}{\lambda^2 + \gamma^2 M^2} \sqrt{K/A} \quad . \tag{6-3a}$$

When $\lambda \ll \gamma M$, this becomes

$$S_w = \frac{d}{2} \frac{\lambda}{\gamma^2 M} \sqrt{K/A} \quad . \tag{6-3b}$$

Whenever in this chapter (unless otherwise modified) S_w, which has been determined from experimental results, is discussed, the value of S_w is taken from that region of the switching characteristic for which it has been found that the amount of flux reversed has become constant. This is done in order to make sure that the entire core is switching and that d is not varying as the field is increased. In the Appendix to Chap. IV it was shown how partial switching of the core can increase the measured S_w.

3. EQUIVALENT ONE LATTICE MODEL

Discussions in Chaps. I and III pointed out that the ferrites' and garnets' magnetic properties arise from a number of magnetic sublattices. In this section, these multilatticed systems will be shown to be reducible to an equivalent single lattice system for domain wall velocity calculations. When this is done, the results obtained in Chap. V may be used. By employing this procedure, it is possible that certain processes unique to a multilatticed system may not be uncovered. However, this approximation should not introduce a serious error, since the processes unique to a multilatticed system generally require large energies to excite.

Since the results in Chap. V arise from properties of the static domain wall and an equation of motion, the necessary equivalent lattice parameters are those which specify these entities. In the following, the relationships between these equivalent parameters and the parameters of the individual sublattices will be found. They then may be used in Eqs. (6-2a), (6-2b), (6-3a) or (6-3b).

a. Domain walls

To discuss static domain walls in a multilatticed system, domain walls in a two sublattice linear system will be considered. The results obtained from this case will then be generalized to the three sublattice system of the garnets. Here the exchange stiffness constant will be shown to be independent of the rare earth lattice.

Consider the two sublattice arrangement of magnetic moments in Fig. 6-1 where the moments marked 1 comprise the first sublattice, while those marked 2 comprise the second sublattice. The moments within sublattice 1 are distant $d_{11}a$ from each other and $d_{12}a$ from those in sublattice 2 which, in turn, are distant $d_{22}a$ from each other. a is the lattice constant. In this particular arrangement $d_{11}a = d_{22}a = a$. However, in order to keep the discussion general, the da notation is employed. If J_{11}, J_{22}, and J_{12} are taken as the exchange integrals for interactions within the first sublattice, within the second sublattice, and between the two sublattices respectively, then the exchange energy, F_A, is

$$F_A = -2\Sigma J_{11} S_{1,i} S_{1,i+2} - 2\Sigma J_{22} S_{2,i+1} S_{2,i+3} - 2\Sigma J_{12} S_{2,i+1} S_{1,i} \quad . \tag{6-4}$$

Here $S_{1,i}$ and $S_{2,i}$ denote the magnetic moments on the sites of lattice 1 and 2 respectively, and the sums are taken over the entire lattice. The numbering system of the moments was chosen so that the sites of the combined lattices are serial numbered.

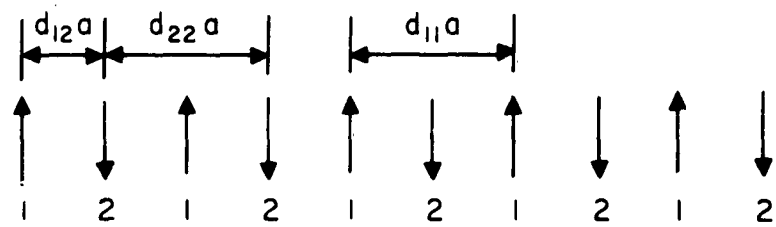

FIG. 6-1 HYPOTHETICAL LINEAR TWO LATTICE SPIN SYSTEM. THE DISTANCES BETWEEN THE MAGNETIC MOMENTS HAVE BEEN CHOSEN TO PERMIT GENERALIZATION OF THE MODEL.

Since domain wall problems are more tractable on a continuous basis, Eq. (6-4) will be transformed to such a basis. In Chap. I it was shown that in order to reduce the magnetostatic energy associated with a domain wall the magnetization within the wall rotates about an axis perpendicular to the wall. This condition simplified the domain wall problem, for only one variable, θ, was required to specify the orientation of the magnetization. Identical considerations hold here. So, again, only θ need be given as a function of x, the distance measured normal to the domain wall, to describe the wall. Thus in transforming Eq. (6-4) to a continuous model only contributions due to a θ variation need be taken into account.

In terms of θ, Eq. (6-4) becomes

$$F_A = -\Sigma 2J_{11}S_1^2 \cos\Delta\theta_{i,i+2} - \Sigma 2J_{22}S_2^2 \cos\Delta\theta_{i+1,i+3} - \Sigma 2J_{12}S_1S_2\cos\Delta\theta_{i,i+1} \quad , \tag{6-5}$$

where

$$\Delta\theta_{i,j} = \theta_i - \theta_j \quad . \tag{6-6}$$

The difference in energy from the aligned condition, E_A, is then

$$E_A = \Sigma(J_{11}S_1^2(\Delta\theta)^2_{i,i+2} + J_{22}S_2^2(\Delta\theta)^2_{i+1,i+3} + J_{12}S_1S_2(\Delta\theta)^2_{i,i+1}) \quad . \tag{6-7}$$

Taking

$$\Delta\theta_{i,j} = \frac{d\theta}{dx}\Big|_{i,j} d_{ij}a$$

and noting that θ changes slowly over the unit cell so that

$$\frac{d\theta}{dx}\Big|_{i,i+1} = \frac{d\theta}{dx}\Big|_{i,i+2} = \frac{d\theta}{dx}\Big|_{i+1,i+3} \quad ,$$

Eq. (6-7) becomes

$$E_A = \Sigma(J_{11}S_1^2 d_{11}^2 + J_{22}S_2^2 d_{22}^2 + J_{12}S_1S_2d_{12}^2)\, a^2 \left(\frac{d\theta}{dx}\right)^2 \Big|_{i,\,i+1} \tag{6-8}$$

To complete the transformation, the energy represented by the summand is reduced to an energy density by averaging over the unit cell. On the continuous model, the exchange energy is then

$$E_A = \int A \left(\frac{d\theta}{dx}\right)^2 dv \tag{6-9}$$

with

$$A = \frac{J_{11}S_1^2 d_{11}^2 + J_{22}S_2^2 d_{22}^2 + J_{12}S_1S_2d_{12}^2}{a} \tag{6-10}$$

If the sublattices have a uniaxial anisotropy, K_1 and K_2, and if the zero of θ is taken as the easy axis, the anisotropy energy can be written as

$$E_K = \int (K_1 \sin^2\theta + K_2 \sin^2\theta)\, dv ,$$

and since θ changes little between consecutive atoms,

$$E_K = \int (K_1 + K_2) \sin^2\theta \, dv = \int K \sin^2\theta \, dv \quad . \tag{6-11}$$

Here $K = K_1 + K_2$ is the usual anisotropy constant.

Comparison of Eqs. (6-9) and (6-11) with similar equations that arise in the theory of a conventional wall shows that the results of that theory may be used for multisublatticed systems. When this is done, the anisotropy constant is taken as the anisotropy of the individual lattices, and the exchange stiffness constant may be taken in the form of Eq. (6-10).

When Eq. (6-10) is to be used to determine the exchange stiffness constant, it must be altered to take account of the three dimensional

character of the sublattices. We then find that our result is identical with that of Harris (9) in his determination of the spin wave spectrum of yttrium iron garnet. The general form is not specifically given here, as it is not used.

In applying Eq. (6-10) to the rare earth garnets additional terms are required, for, as Pauthenet (10) has shown, there exist three magnetic sublattices. Using Pauthenet's values to estimate these terms, it is seen that they may be neglected. This was to be anticipated on the basis of the lack of variation in the Curie temperatures of the rare earth garnets.

b. Equation of motion

The equation of motion for the magnetization which was used in Chap. V where domain wall velocities were calculated applies only to a ferromagnet. However, under circumstances occurring in switching, the same equation of motion can be shown to apply to a ferrimagnet by following a procedure similar to that which was used to obtain the equation of motion for the ferromagnet. This comes about since it may be assumed in a switching experiment that the magnetization in each of the sublattices when in motion retains its relative static orientation. As a consequence of these conditions, the magnetization will not be acted upon by any interlattice exchange torques. Then, for the total magnetization,

$$M = M_1 + M_2 \tag{6-12a}$$

with total angular momentum,

$$J = \frac{M_1}{\gamma_1} + \frac{M_2}{\gamma_2} \quad , \tag{6-12b}$$

the equation of motion,

$$\dot{M} = \gamma_{eff} (M \times H) + \frac{\lambda}{M^2} (M \times M \times H) \quad , \tag{6-13}$$

can be written, and the effective gyromagnetic ratio is simply given by

$$\gamma_{eff} = \frac{M}{J} = \frac{M}{\frac{M_1}{\gamma_1} + \frac{M_2}{\gamma_2}} \quad . \tag{6-14}$$

Equations (6-13) and (6-14) have been derived by Wangsness (11) and others in connection with ferrimagnetic resonance. Kittel (12) and Van Vleck (13) have shown on the basis of different models that the free ion gyromagnetic ratios cannot be used for γ_1 and γ_2 in Eqs. (6-13) and (6-14). They must be determined by considering the atoms in their crystal environment.

The significance of the damping term in Eq. (6-13) has been discussed in Chap. I. Its evaluation in terms of the contributions from each of the sublattices is deferred to Sec. 4c of this chapter.

In the case of the rare earth garnets, the equation of motion must be applied to a material with three sublattices. The above results could be extended to three sublattices, or, since the character of the two iron sublattices is the same and since the iron sublattices are so tightly coupled through strong exchange fields, these materials can be considered to consist of only two sublattices - one containing the iron and the other the rare earth ions.

c. The switching parameter, Sw

From the discussions of Secs. a and b above, the equations for the switching parameter of a ferromagnetic material, Eqs. (6-3a) and (6-3b), are seen to hold for ferrimagnetic materials since the relations underlying their derivations are identical. The parameters which enter into these equations are related to the parameters of the individual sublattices by the formulae given in these sections.

4. DISCUSSION OF THE EXPERIMENTAL DATA

a. Non rare earth garnets and gadolinium substituted garnets

The materials whose experimental data are examined in this section are yttrium-indium, yttrium-gallium, and yttrium-gadolinium iron garnets. Their magnetic properties are given in Table 3-2, and their switching properties are listed in Table 4-1 and shown in Figs. 4-5 and 4-6.

If, for any of these garnets, λ is found from the ferromagnetic resonance linewidth and Eq. (3-11) and is substituted in Eq. (5-32c) to determine the reduced damping parameter, ξ, then the resulting ξ will be much less than 1. All of these systems should then exhibit a characteristic for the reciprocal switching time which is given by Eq. (6-2b) and is of the form

$$\frac{1}{t} = \frac{c}{\sqrt{H}}, \tag{6-15}$$

where c is a material dependent constant. Inspection of the measured switching characteristics, Figs. 4-5 and 4-6, shows that this is not the case. These characteristics have a continually increasing slope; a feature not exhibited by Eq. (6-15). If they are considered to be piecewise linear, these characteristics are better represented by Eq. (6-2a) which shows that the reciprocal switching time is linearly dependent on the applied field.

If Eq. (6-2a) describes the results of the switching experiment, then λ obtained from low power resonance experiments is not applicable. This is not too surprising; it is already known from resonance experiments that λ is a parameter which depends on the particulars of the dynamic process. This point is further discussed in this and the following section of this chapter.

Examination of Eq. (6-3b) shows that if λ is regarded as smaller than γM (equivalent in the case of resonance to the half linewidth being smaller

than the resonant field) and has the same value independent of composition, S_w should vary inversely with the magnetization. To test this inference the switching parameters of the yttrium-gadolinium iron garnets which were measured have been plotted as a function of 1/M in Fig. 6-2. This series of garnets was shown in Chap. III to differ only in magnetization, when the relaxation frequency is excepted. The switching parameters are taken from the two lowest field linear regions. Also shown in the figure is the calculated variation. The agreement is within 3% for the larger S_w's and within 5% for the lower values.

As a further test of this hypothesis the switching parameters for the gallium and indium substituted garnets can be compared with the predictions of Eq. (6-3b). The situation here is of greater complexity than that of the gadolinium substituted garnets, since now not only does the magnetization but also the exchange stiffness and the magnitude of the anisotropy vary. From Eq. (6-3b) the ratio of the switching constants for two materials which differ in these respects is determined to be

$$\frac{S_{w_1}}{S_{w_2}} = \frac{M_2}{M_1} \sqrt{\frac{K_1}{K_2} \frac{A_1}{A_2}}. \tag{6-16}$$

The subscripts in Eq. (6-16) denote the materials being compared.

As discussed in connection with Eq. (1-8), A can be taken proportional to the Curie temperature, T_c, and Eq. (6-16) becomes with the aid of this proportionality

$$\frac{S_{w_1}}{S_{w_2}} = \frac{M_2}{M_1} \sqrt{\frac{K_1}{K_2} \frac{T_{c_1}}{T_{c_2}}}. \tag{6-17}$$

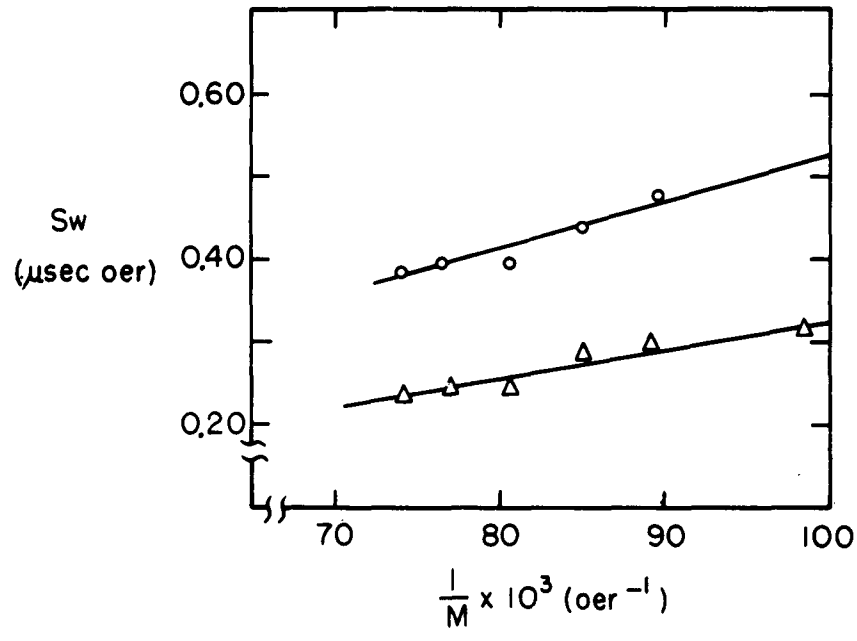

FIG. 6-2 SWITCHING PARAMETER, Sw, FOR YTTRIUM-GADOLINIUM SERIES AS A FUNCTION OF $\frac{1}{M}$ WHERE M IS THE MAGNETIZATION. THE CIRCLED POINTS ARE EXPERIMENTAL. THE SOLID LINES ARE CALCULATED. THE UPPER CURVE IS FOR THE FIRST LINEAR REGION, WHILE THE LOWER CURVE IS FOR THE NEXT HIGHEST (IN FIELD) LINEAR REGION.

If one of the materials is taken as the gallium or indium substituted garnet and the other as yttrium iron garnet, then the values shown in Table 6-1 are obtained from Eq. (6-17). Together with these results the experimentally determined ratios are given. A comparison of these calculated and experimental values of S_{w_1}/S_{w_2} shows a maximum deviation of 13% and lends further validity to the use of Eqs. (6-3a) and 6-3b) in explaining these results and to the assumption that λ has substantially the same value in all these materials.

Table 6-1

Ratio of the switching parameters of indium and gallium substituted garnets to those of yttrium iron garnet.

	S_{w_1}/S_{w_2} (calculated)	S_{w_1}/S_{w_2} (experimental)
Y-In 5%	0.77	0.86
Y-In 10%	0.67	0.72
Y-Ga 5%	1.15	1.32

From Eq. (6-3b), the experimental value for S_w, the magnetic parameters listed in Table 3-1, and a value of A taken from Shinozaki (14), λ can be determined for yttrium iron garnet. Using the value 0.44×10^{-6} ergs/cm for A, a relaxation frequency of about 5×10^8 cycles/sec is found. A comparison of this value with the relaxation frequencies listed in Table 3-1 and determined from magnetic resonance shows that only the samarium iron garnet's relaxation frequency exceeds this value.

b. Single crystal

Next we turn our attention to the yttrium iron garnet single crystal toroid whose switching characteristic is shown in Fig. 4-12. It is apparent from this figure that this toroid switches slower than its polycrystalline

counterpart. To compare the data quantitatively the number of domain walls participating in the single crystal's reversal process must be known. The toroidal shape of the specimen, as shown in Chap. I, permits the magnetization to be distributed without the formation of domains. In this distribution the magnetic moments are parallel to the surface of the toroid. It is possible, in this case, to have this distribution since the anisotropy energy of yttrium iron garnet is small. Since this distribution removes the driving force for domains, they need not exist at remanence. However, stray fields associated with imperfections in the crystal, or on its surface, probably cause a domain structure to exist about these imperfections, and this structure could provide the domain walls for reversing the magnetization. Domain nucleation may also take place when a field is applied to reverse the magnetization because of the gradual change in direction which the magnetization makes with the easy direction in encircling the toroid. But it does not appear that any, or all, of these causes can produce as large a number of walls as appear in the polycrystalline reversal. This reduction in the number of walls increases the distance traversed by each wall in bringing about the reversal. If all other things remained the same, an increased S_w could be anticipated. Since this increase is found experimentally, we have here another justification for the domain wall motion model. The possibility does exist that the relaxation frequency is smaller in the single crystal than the polycrystalline material. This would offset the increase in S_w somewhat. However, the difference in relaxation frequency cannot be very large, for then the switching characteristic would take on the shape described by Eq. (6-2b).

It is of interest to note that there exists a possibility that only a few walls contribute to the switching. Suppose that a wall is formed at the inside edge of the specimen and is parallel to the curved sides of the toroid

and that it is this wall which reverses the toroid's magnetization when it moves from the inside to the outside. In accomplishing this the wall moves through the thickness of the toroid which is about 370 microns. In the polycrystal, the distance a wall moves has been anticipated as 5 microns, as indicated in Sec. 2 above. It would then be expected that, if all the other pertinent material parameters were the same, the ratio of switching parameters would be about 75. From the experimental results, S_w for the single crystal is 7.0 oe μsec, and the switching parameter ratio is approximately 20. The small difference in these ratios indicates that a few walls do reverse the magnetization; the difference probably results from the lack of precise information on the damping parameter and the distance of wall travel.

c. Rare earth garnet behavior – theoretical preliminaries

The replacement of yttrium ions with rare earth ions was noted in Chap. I, Sec. 6 to result in a marked increase in the width of the ferromagnetic resonance line. It was also shown there that the mechanism which brings about this line broadening should enter into the determination of the relaxation frequency, λ, in switching experiments. Since the phenomenon which underlies this mechanism is associated with the coupling of the magnetic moment of the ion to the vibrating lattice, the effects of this mechanism are strongest in those ions whose spin magnetic moments are coupled to the orbital magnetic moment (15). Since the magnetic ions of the materials which were considered in the earlier parts of this section do not have an orbital magnetic moment, this effect is absent. However, in the other rare earth garnets measured here orbital magnetic moments do exist, and, therefore, an additional loss mechanism is expected to play a role in the switching process.

The effects of this mechanism on the switching may be estimated in either of two ways. On the one hand, use may be made of Callen's work (16) which led to an equation of motion discussed in Chap. I, Sec. 6. In this study, Callen showed that if there exist two loss mechanisms, one in which energy is lost directly to the lattice and the other in which energy is transferred within the magnetization system itself, then the relaxation frequencies of these mechanisms add. On the other hand, this result may be obtained from a treatment of ferromagnetic resonance given by Wangsness (11). In this treatment, relations are found which show the contributions made by the individual sublattices to the total loss. Although the general relationship amongst the effective loss parameters is extremely complicated, as long as the loss parameters are not extremely large, the theory shows that the losses in the various sublattices augment each other. If the mechanism responsible for the losses of the materials discussed in part a of this section is taken to result from the iron sublattices (taken as one sublattice) and the mechanism referred to above as an attribute of the rare earth sublattice, a relaxation frequency which is larger than that of the iron lattices may be anticipated. Equation (6-3a) then indicates that S_w should increase over that of yttrium iron garnet, and this, indeed, is what is found. In the following this is examined in greater detail for ytterbium, erbium, holmium, and samarium iron garnets as well as for the holmium and samarium substituted series.

To place the discussion on a quantitative basis, the Wangsness result for the effective relaxation frequency,

$$\lambda = M^2 \frac{\frac{\lambda_1}{2} + \frac{\lambda_2}{2}}{\left(\frac{M_1}{\gamma_1} + \frac{M_2}{\gamma_2}\right)^2} \frac{\gamma_1 \quad \gamma_2}{}, \qquad (6\text{-}18)$$

will be employed. In this expression the quantities carrying the subscript 1 denote the iron sublattice, while those carrying 2 denote the rare earth sublattices.

When $\gamma_1 = \gamma_2$, Eq. (6-18) becomes

$$\lambda = \lambda_1 + \lambda_2. \tag{6-19}$$

Since in the series of the gadolinium substituted garnets which were discussed in part a the gyromagnetic ratios of iron and rare earth lattices are equal, this equation should apply. When the rare earth sublattice is only sparsely filled as it is in these garnets, $\lambda_2 << \lambda_1$, and Eq. (6-19) becomes

$$\lambda = \lambda_1. \tag{6-20}$$

This is just the manner in which λ was chosen in the treatment of the gadolinium series.

The inequality leading to Eq. (6-20) can be understood by remembering that λ represents the rate of loss of magnetic energy. (See Chap. I, Sec. 5c.) It follows from this description of λ that λ is related to the strength of the coupling between the magnetic system and that system to which the energy is lost. Examples of such systems were given in Chap. I. If now each rare earth ion represents a channel for the loss of magnetic energy as is indicated by the assignment of a loss constant to its lattice, the number of channels and, therefore, the coupling will depend on the concentration of rare earth ions. Thus λ can be expected to increase with increasing numbers of rare earth ions. For the particular case of gadolinium, the coupling per ion is probably much the same as that of the iron ions, since the ions of both are in S states. (In resonance, losses due to S states are usually small. However, as evidenced by yttrium iron garnet, this is not the case in switching.) Since the relative number of

gadolinium ions is small in the compositions considered here, λ_2 will be much smaller than λ_1.

For the other rare earth garnets which were measured here Kittel (12) and Van Vleck (13) have shown that γ_2 is large. Thus the effective gyromagnetic ratio, Eq. (6-14), for the combined sublattices becomes

$$\gamma = \gamma_1 \frac{M}{M_1} \quad , \tag{6-21}$$

and Eq. (6-18) can be written as

$$\lambda = \gamma^2 \left[\frac{\lambda_1}{\gamma_1^2} + \frac{\lambda_2}{\gamma_2^2} \right] \quad . \tag{6-22}$$

From this equation it may be seen that λ consists of two parts. One, λ_1', has its origin in the iron lattices, the other, λ_2', in the rare earth lattice.

$$\lambda = \lambda_1' + \lambda_2' \quad . \tag{6-23}$$

As shown in Sec. c, λ_1' is large; λ_2' has been discussed above and should be obtainable from resonance by application of the relation, Eq. (3-11), between the relaxation frequency and linewidth, ΔH, at the dc field, H, required for resonance.

$$\lambda_2' = \frac{\gamma M}{2} \quad \frac{\Delta H}{H} \quad . \tag{6-24}$$

To determine S_w, Eq. (6-23) must be used in Eq. (6-3a).

Three additional relations are required in order to treat the substituted systems. With these relationships a dependence of S_w on the degree of substitution can be established. The first of these is taken from

de Gennes et al (15) and the reasoning given above in connection with the gadolinium garnet. It gives the relative linewidth, $(\Delta H/H)_x$, as a function of the atomic fraction, x, of the yttrium sites occupied by rare earth ions:

$$(\frac{\Delta H}{H})_x = x\frac{\Delta H}{H} . \tag{6-25}$$

Here $\Delta H/H$ is the relative linewidth for complete substitution ($x = 1$).

If ΔM represents the change in magnetization for a fully substituted rare earth lattice from that of yttrium iron garnet, the magnetization at a concentration x is

$$M_x = \frac{M_1 + x\Delta M}{M_1}, \tag{6-26}$$

and, from Eq. (6-21), the gyromagnetic ratio at a concentration x is

$$\gamma = \gamma_1 \frac{M_1 + x\Delta M}{M_1} . \tag{6-27}$$

ΔM is usually negative.

Equations (6-25), (6-26), and (6-27) together with Eqs. (6-3a) and (6-24) then determine S_w as a function of x.

d. Rare earth garnet behavior – comparison with experiment

As yet, the distance, d, that a domain wall moves has not been determined beyond indication of its expected size. Unless it can be determined, we cannot compare the results of the previous section with our experimental values. Fortunately, by obtaining a best fit to the experimental data for either the holmium or samarium substituted iron garnet systems, a value of d can be obtained. In the discussions of d in Sec. 2, it was concluded that d should be relatively independent of composition and should depend strongly on grain structure. Therefore, the value of d found for one of these systems should be useful in predicting

the experimental values of d for other structurally similar materials. The successful predictions that result justify this method of interpreting the measurements.

The procedure used for the curve fitting is given here. From Eqs. (6-23) and (6-3a) the switching parameter can be written as

$$S_w = \frac{1}{2} \frac{\lambda_1' + \lambda_2'}{\gamma^2 M} \frac{d}{\delta} F, \tag{6-28}$$

where

$$\delta = \sqrt{A/K} \tag{6-29}$$

and

$$F = (1 + \lambda^2/\gamma^2 M^2)^{-1}. \tag{6-30}$$

δ through its dependence on the anisotropy constant, K, is composition sensitive.

Calling

$$S'_{w_A} = \frac{1}{2} \frac{\lambda_1'}{\gamma^2 M} \frac{d}{\delta} \tag{6-31}$$

and

$$S'_{w_B} = \frac{1}{2} \frac{\lambda_2'}{\gamma^2 M} \frac{d}{\delta}, \tag{6-32}$$

S'_w may be written as

$$S'_w = S'_{w_A} + S'_{w_B}. \tag{6-33}$$

S'_{w_A} orginates from interactions within the iron lattices and S'_{w_B} from the rare earth lattice. Therefore, Eq. (6-33) permits the determination of S'_w

(and consequently S_w) from its constituents. The primes indicate that the factor, F, given by Eq. (6-30) has not as yet been taken into account in finding the S_w's.

S'_{w_A} can be determined without obtaining a value for d by assuming that d and λ'_1 are independent of composition; as in Sec. 4a, Eq. (6-17) applies. Here, however, the Curie temperature, too, is independent of composition, and so in the notation of this section Eq. (6-17) becomes

$$S'_{w_A} = \frac{M_1}{M} \sqrt{\frac{K}{K_1}}\, S_{w_1} . \tag{6-34}$$

The subscript 1 again refers to yttrium iron garnet. Direct substitution in Eq. (6-32) is used to determine S'_{w_B}, with λ'_2 taken from microwave resonance experiments and d taking on various values. The factor F is found by noting that

$$\frac{\lambda}{\gamma M} = \frac{S'_{w_A} + S'_{w_B}}{S''_{w_B}} \frac{\lambda'_2}{\gamma M} . \tag{6-35}$$

Using trial values of d = 5, 6, and 7 microns, a best fit was determined by comparison with the experimental values of the holmium series. The results are shown in Fig. 6-3. For the 6 micron case, the type A and B contributions are also shown. Using d = 6 microns, the experimental results are compared with our calculated values for samarium in Fig. 6-4. Here, also, the A and B contributions are given. Table 6-2 summarizes the results found using d equal to 5 and 6 microns for the rare earth garnets. From this table it is seen that the major contributions to S_w for erbium and ytterbium garnets arise from the type A process.

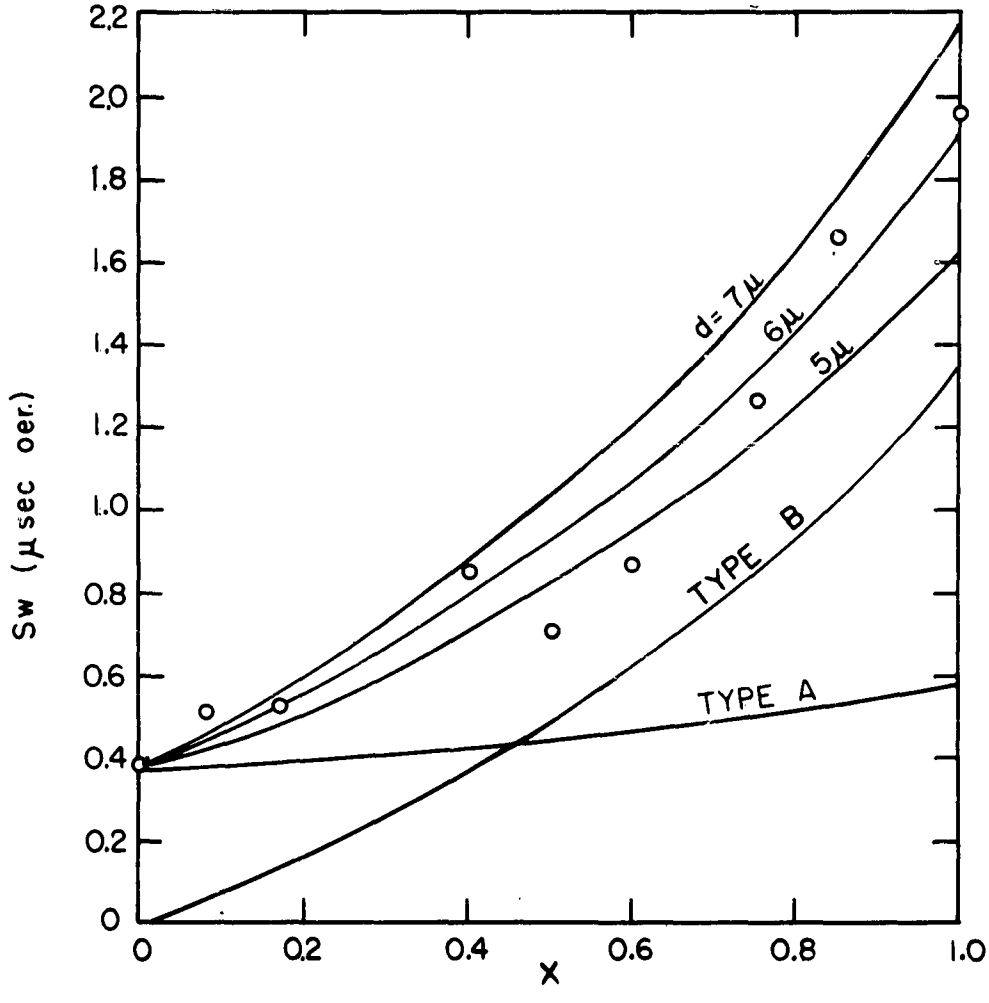

FIG. 6-3 SWITCHING PARAMETER, Sw, AS A FUNCTION OF FRACTION X OF HOLMIUM IRON GARNET IN YTTRIUM IRON GARNET ($3(1-x)Y_2O_3 \cdot 3xHo_2O_3 \cdot 5Fe_2O_3$) THE CIRCLED POINTS ARE EXPERIMENTAL. THE SOLID CURVES ARE CALCULATED. THE CALCULATED CONTRIBUTIONS OF THE A AND B MECHANISMS TO Sw FOR d= 6μ ARE ALSO SHOWN.

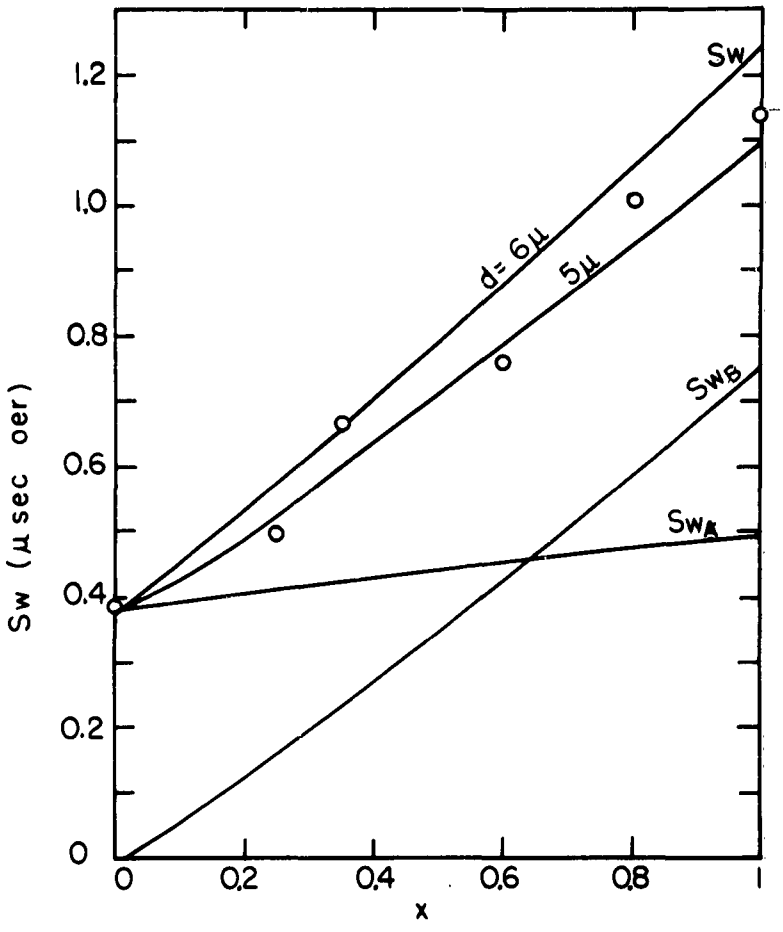

FIG. 6-4 SWITCHING PARAMETER, Sw, AS A FUNCTION OF X IN $3(1-x)\ Y_2\ O_3 \cdot 3x\ Sm_2\ O_3 \cdot 5\ Fe_2\ O_3$. THE CIRCLED POINTS ARE EXPERIMENTAL. THE SOLID CURVES ARE CALCULATED. THE TYPE A AND B CONTRIBUTIONS TO Sw ARE SHOWN FOR $d = 6\mu$.

In all cases the agreement between the calculated values and the experimentally determined ones is good and somewhat better, perhaps, than the combined uncertainties in the values of the parameters would lead us to expect.

Table 6-2

Comparison of S_w measured with S_w calculated for d = 5 and d = 6 microns. Data taken at room temperature.

Garnet	S_w (oe μsec) experimental	calculated d=6	calculated d=5
Ytterbium	0.41	0.43	0.43
Erbium	0.77	0.79	0.73
Samarium	1.15	1.22	1.06
Holmium	1.94	1.91	1.64

e. Garnets at 55°C

The measurements of the garnets made at 55°C are compared in this section with the predictions obtained from the results given in Sec. c above. The values of the magnetic parameters for these materials can be found in Table 3-4; the experimental data is shown in Fig. 4-11, summarized in Table 4-2, and also listed in Table 6-3 together with the calculated values. As in the last section, the agreement is good. The value of d found there also fits this data. Determination of λ from the room temperature and 55°C yttrium iron garnet switching data shows that the relaxation frequencies at these temperatures are equal within experimental error. A 2% decrease with temperature was actually found.

f. Nickel cobalt ferrites

Nickel cobalt ferrite, as indicated in Chap. III, was chosen to observe the effects on switching of a variation of the magnetocrystalline anisotropy.

Table 6-3

Comparison of S_w measured with S_w calculated for d=5 and d=6 microns. Data taken at 53°C.

Garnet	S_w (oe μsec) experimental	calculated d=6	calculated d=5
Ytterbium	0.29	0.29	0.28
Erbium	0.57	0.59	0.55
Samarium	0.82	0.88	0.76
Yttrium	0.29	—	—

The macroscopic anisotropy constant as calculated for this ferrite changes sign, i.e., the preferred easy direction changes from <111> to <100> as the cobalt content is increased (17). This effect has been observed in microwave resonance (18), which is a rotational magnetization process in the sense that the entire magnetization takes on a coherent motion. However, the data contained in Fig. 4-9 and summarized in Fig. 6-5 indicates the absence of this type of behavior. According to either Eq. (6-2a) or Eq. (6-2b) the switching time should become exceedingly short in the vicinity of K = 0. Instead, a steady increase in both switching time and coercive force is observed. These effects can be attributed to domain wall motion.

At most, the nickel ferrites used here contain 5% cobalt ferrite, and, if the cobalt is distributed randomly, the domain walls will consist of predominantly nickel ferrite. Since the exchange interaction is much stronger than the anisotropy interaction of the cobalt ion, the nickel ion anisotropy will dominate the wall shape. In other words, the occasional cobalt ions will not, on the average, have other cobalt ions as nearest magnetic ion neighbors, and so their orientation will be determined through

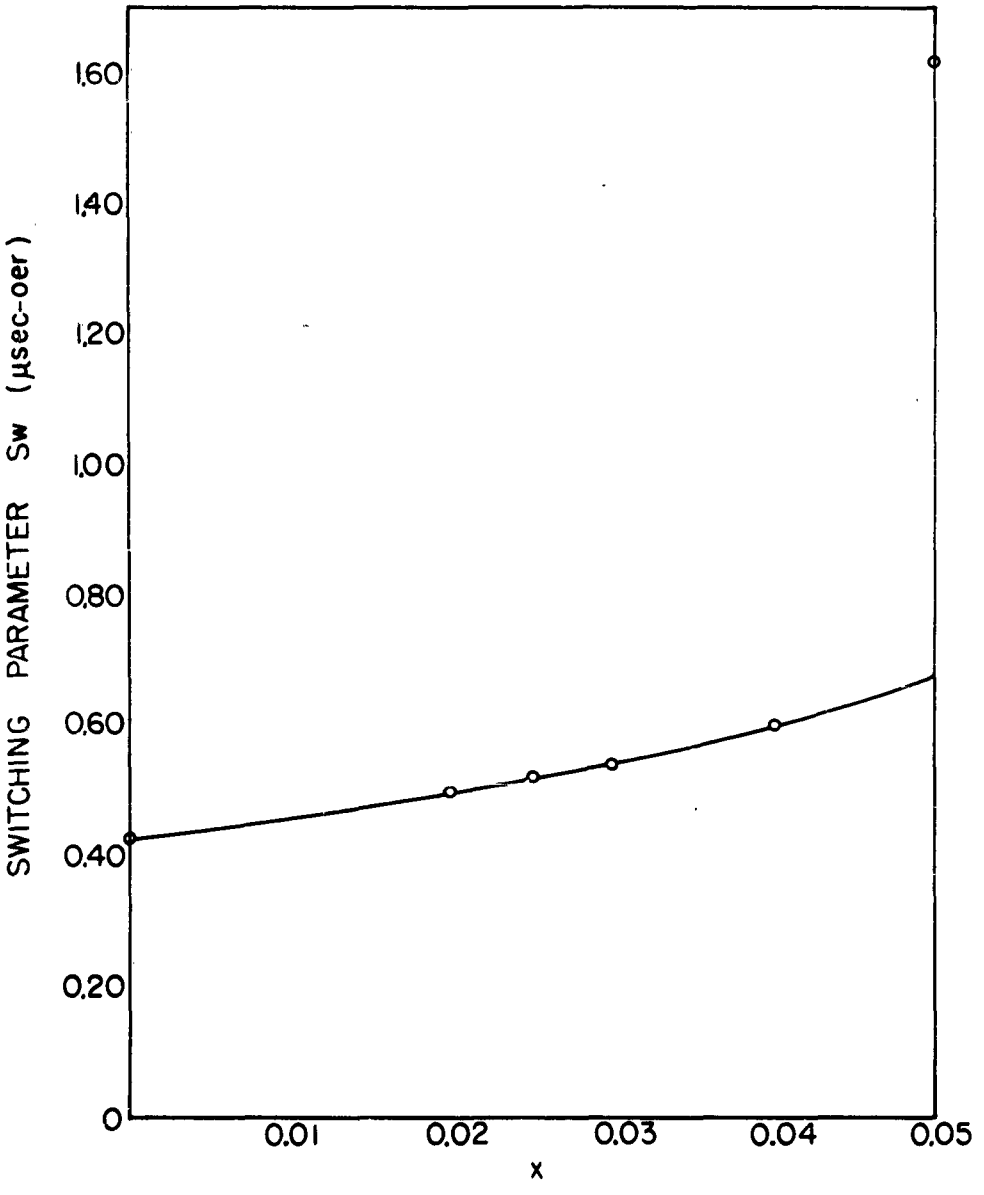

FIG. 6-5 SWITCHING PARAMETER, Sw, AS A FUNCTION OF x, THE FRACTIONAL AMOUNT OF COBALT FERRITE IN NICKEL FERRITE. ($Ni_{1-x}Co_x Mn_{.02}Fe_2O_4$)

an exchange interaction with their nickel neighbors, not by their anisotropy field. The cobalt ions, then, act as an impurity in the wall* which will increase the wall's coercive force. They will also bring about an increase in the relaxation frequency since the spin orbit coupling in these ions is large (19).

Pippin and Hogan (20) have studied the initial permeabilities of these ferrites. On the basis of the variation of the initial permeability with porosity, they concluded that wall motion was responsible for the magnetization change which they measured. They also found no evidence of a decrease in the anistropy and attributed their results to a wall motion model similar to that used above.

The grain size in the nickel ferrite used here was found to be about 2 microns. From this it may be inferred that the domain walls which are responsible for the magnetization reversal will move about 1 micron. S_w may be estimated for this ferrite if a value for λ can be obtained. Taking λ from linewidth measurements of polycrystals, S_w is again found to be smaller than the calculated value by two orders of magnitude.

A comparison of the λ's calculated from the switching data for nickel ferrite and yttrium iron garnet shows that the former's damping parameter is about 10 times larger than the latter's. At least two effects account for this. The more important one arises from the direct coupling of the nickel ions' magnetic moment to the lattice through spin orbit coupling. This coupling provides a means for the magnetic energy to pass directly to the lattice. The other arises as a result of the random positions taken by the magnetic ions in the nickel ferrite crystal as opposed to the well defined positions they occupy in the garnet crystal. This undoubtedly leads to a violation of the uniform plane wall assumption made in Chap. IV. As was noted there, if this occurs, one can expect increased switching times which in effect bring about an increase in λ.

---

* Since the cobalt ions have an easy direction distinct from that of the nickel ions, and since their anisotropy energy is much larger than that of the nickel ions, the wall will try to form so that the cobalt ions occupy certain positions within the wall which will allow them to point in their easy direction.

5. NONLINEAR RELAXATION IN SWITCHING

In a material such as yttrium iron garnet where the magnetization is due to the uncompensated spins of an ion which has no orbital angular momentum (and consequently no spin orbit interaction), the magnetization exists in relatively poor contact with the lattice, and one would expect that any disturbance in the magnetization would require a relatively long time to decay. Indeed, this is found in resonance experiments on yttrium iron garnet employing small amplitude microwave fields, and the processes which determine this material's exceedingly narrow linewidth appear to be the result of transfers of energy within the magnetic system which are brought about by such nonuniformities as porosity, anisotropy dispersions, and thermal fluctuations.

On the other hand, from the data obtained in our switching experiments, yttrium iron garnet has been shown to have a relatively large relaxation frequency. In view of the weak interaction of the iron ions with the lattice it appears reasonable to assume that the relaxation frequency here also is determined predominantly by interactions within the magnetic system. When the microwave field in a resonance experiment is increased beyond a certain size, the rate at which energy is lost is considerably increased as a result of nonlinear interactions within the magnetic system (see Chap. I, Sec. 6), and the possibility exists that a similar nonlinear process determines the large relaxation frequency found in switching.

The large losses found in the high power resonance experiments have been shown to originate from the existence of a nonlinear coupling between the uniform precession and spin waves which is a function of their amplitudes. Ordinarily this coupling is negligible since the spin wave amplitude is small, and the transfer of energy by this process can be neglected. However, as the amplitude of the uniform precession increases, a point is reached at which

energy is transferred to the spin waves more rapidly than they can dissipate it. As a result, certain spin waves become unstable, their amplitudes become large, and this coupling becomes an important mechanism for the dissipation of energy in the uniform precession.

In the moving domain wall, conditions appear to exist which make possible a similar nonlinear process as a means of energy transfer. By identifying the component of the magnetization which rotates in the plane of the wall with the precessing magnetization of the resonance experiment, an analogy between switching and resonance may be established. In the picture of domain wall motion developed in Chap. V this rotating component is large, and, therefore, a nonlinear interaction appears possible in yttrium iron garnet. When rare earth ions are added to this garnet, means are provided for the magnetic energy to readily pass to the lattice, as discussed in Sec. 4d. This should have the effect of rapidly removing energy from the spin waves, and, therefore, it will reduce their susceptibility to instability. In this manner the large coupling of energy to the spin waves which arose from their instability is removed.

When these nonlinear effects occur in microwave experiments they are accompanied by changes in the magnetization. The equation of motion used in Chap. V does not allow for this and it would follow that the results of that chapter are no longer applicable. However, large amounts of energy may be transferred to spin waves without an appreciable change in magnetization as a consequence of the spin wave energy containing a term in the exchange energy. And, only small deviations in the magnetization are needed to bring about a large increase in this energy. Thus it appears that even in the presence of such nonlinear effects, the results of Chap. V are good approximations.

One of the implications of the above discussion is that the analysis of the experimental results in Secs. 4d and 4e should be revised to take account

of the effect of the rare earth lattice on the relaxation frequency of the iron lattice. In those sections, the relaxation frequencies, λ_1 and λ_2, were treated as independent quantities. In the extreme case where the damping introduced by the rare earth lattice is so large that it completely prevents the transfer of energy by the nonlinear coupling process, the possibility exists that the relaxation frequency of the iron lattice can be neglected; the rare earth lattice alone determining the relaxations. Of course this conclusion presumes that this mechanism is the only one responsible for the relaxation of the iron lattices. In the absence of either a mathematical model or further experimental results the relation of the various loss processes is difficult to determine. Nevertheless, it appears from the data taken here that if the rare earth ions decrease the iron ions' contribution to the relaxation, the contribution made by them must more than compensate for this decrease, since the addition of rare earths consistently brings about an increase in λ.

6. HIGH FIELD BEHAVIOR

To study high field behavior, consider Eq. (3-11) which relates the resonance linewidth and the relaxation frequency.

$$\lambda = \frac{\gamma M}{2} \frac{\Delta H}{H} . \tag{6-36}$$

H is the field required for resonance. Although it is recognized that microwave resonance relaxation processes cannot be identical with wall motion relaxation processes, they must depend on similar effects.

The first observation we make is to note that measurements reported by Buffler (18) on the frequency dependence of the linewidth of single crystal and polycrystal yttrium iron garnets show that the linewidth remains substantially constant, independent of frequency. This then implies, through Eq. (6-36), that λ is field dependent. If λ is then written as

$$\lambda = \frac{\gamma M (\Delta H)_o}{2H} , \tag{6-37}$$

where $(\Delta H)_o$ is a constant which may be material dependent, and this is substituted in Eq. (6-2a), the inverse switching time is found to be, if $\lambda << \gamma M$,

$$\frac{1}{t} = \frac{4\gamma H^2}{d(\Delta H)_o} \sqrt{\frac{A}{K}} \quad . \tag{6-38}$$

This inverse switching time is proportional to H^2. To test the validity of this relation, $\sqrt{1/t}$ has been plotted for yttrium iron garnet and is shown in Fig. 6-6. The fit is good. However, it should be noted that the line intercepts the H-axis at a negative H. Hence our expression (6-38) should be written as

$$\frac{1}{t} = \frac{4\gamma (H + H_i)^2}{d(\Delta H)_o} \sqrt{\frac{A}{K}} \quad . \tag{6-39}$$

The significance of H_i is not clear. Its origin may lie in the fact that the total internal field is composed of the applied field, a demagnetizing field, and, possibly, the fields which are responsible for the material's coercive force.

To compare this result with the work of Sec. 3 above, the quantity S_w which was central there must be computed.

$$S_w = \frac{dH}{d(1/t)} = \frac{d(\Delta H)_o}{8\gamma (H + H_i)} \sqrt{\frac{K}{A}} \quad . \tag{6-40}$$

If the 1/t curve is actually parabolic, then the straight line drawn to fit the low field region is an approximation of the curve in that region. Hence, if H_o is an average value for the field in the low field region, the switching parameter becomes

$$S_w = \frac{d(\Delta H)_o}{4\gamma H_o} \sqrt{\frac{K}{A}} \quad . \tag{6-41}$$

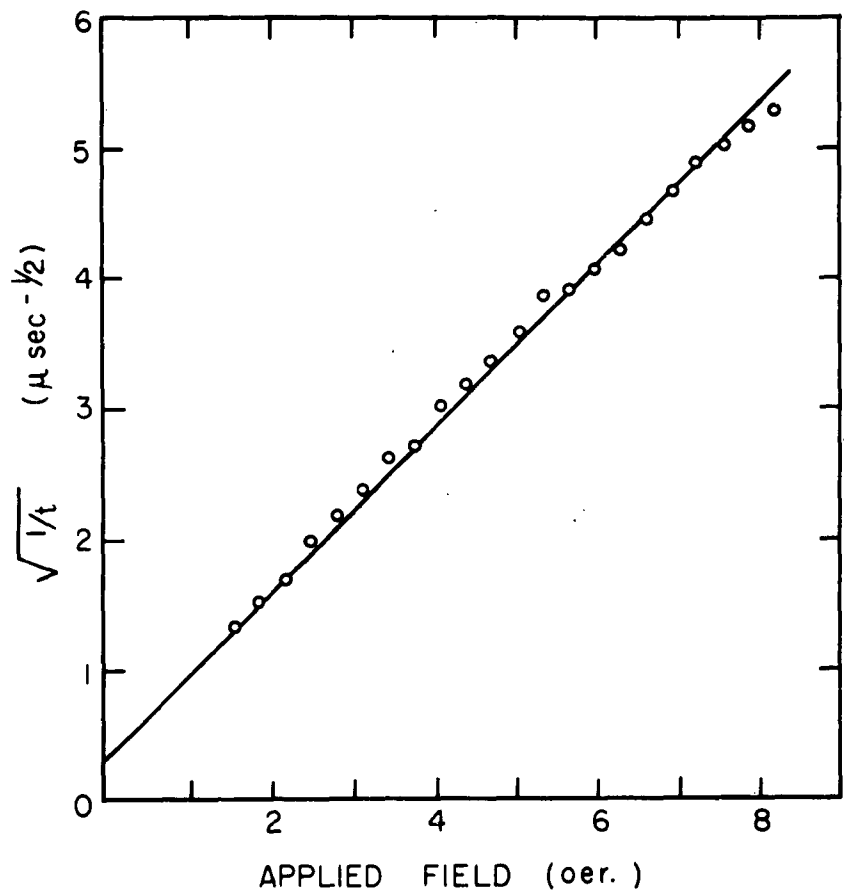

FIG. 6-6 THE SQUARE ROOT OF THE INVERSE SWITCHING TIME AS A FUNCTION OF THE APPLIED FIELD FOR YTTRIUM IRON GARNET.

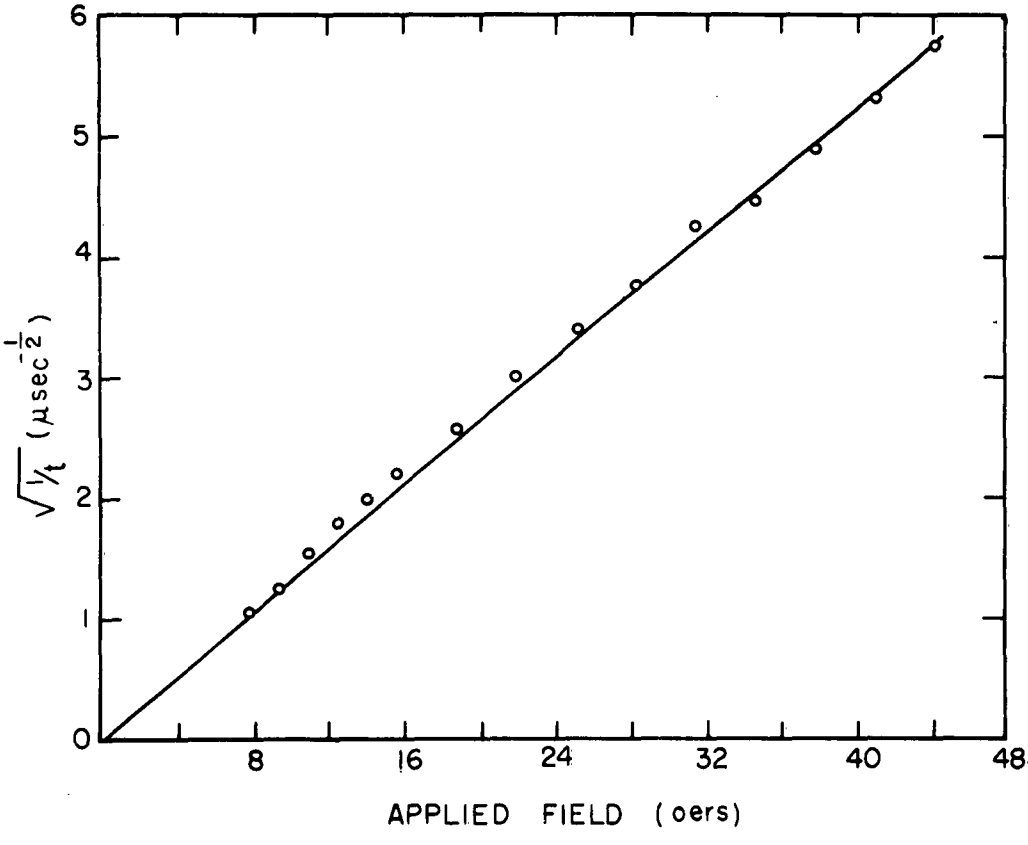

FIG. 6-7 THE SQUARE ROOT OF THE INVERSE SWITCHING TIME AS A FUNCTION OF THE APPLIED FIELD FOR HOLMIUM IRON GARNET.

In studying the nonrare earth garnets, it was found that S_w varied inversely with the magnetization. If Eq. (6-41) is to account for this result, then

$$(\Delta H)_o = \frac{c}{M} \tag{6-42}$$

For yttrium iron garnet Eq. (6-41) gives $(\Delta H)_o = 2.4$ oe when $H_o = 3$ oe, S_w is the experimental value, and the other parameters are taken as given in Chap. III. This value is remarkably close to the typical single crystal linewidths which are about 1 oe.

In Fig. 6-7 the switching characteristic for holmium iron garnet is shown in $\sqrt{1/t}$ versus H form. The resulting linear curve shows that here again Eq. (6-39) can be used to describe the switching characteristic.

CHAPTER VI – BIBLIOGRAPHY

1. C.E. Fuller, R.W. Teale, and R.F. Pearson, Sheffield Conference on Magnetism Report, Brit. J. Appl. Phys. 11, 307 (1960).
2. C. Kittel and J.K. Galt, "Solid State Physics", 3 (Academic Press, New York, 1956) p. 491.
3. C. Kittel, Phys. Rev. 76, 1527 (1949).
4. H.J. Williams, R.M. Bozorth and W. Shockley, Phys. Rev. 75, 155 (1949).
5. T.G. Nilan and W.S. Paxton, Phys. Rev. 97, 834 (1955).
6. J.E. Knowles, Proc. Phys. Soc. 75, 885 (1960).
7. D.J. Craik, Sheffield Conference on Magnetism (see Ref. 1 above).
8. J. Smit and H.P.J. Wijn, "Ferrites" (John Wiley and Sons, New York, 1959) p. 304 and p. 339.
9. A.B. Harris (to be published).
10. R. Pauthenet, Ann. Phys. 3, 424 (1958).
11. R.K. Wangsness, Phys. Rev. 111, 813 (1958).
12. C. Kittel, Phys. Rev. 115, 158 (1959).
13. J. Van Vleck, Phys. Rev. (1961).
14. S. Shinozaki, Phys. Rev. 122, 388 (1961).
15. C. Kittel, J. Appl. Phys. 31, 11S (1960).
    P.G. de Gennes, C. Kittel and A.M. Portis, Phys. Rev. 116, 323 (1959).
16. H.B. Callen, J. Phys. and Chem. Solids 4, 256 (1958).
17. J.E. Pippin and C.L. Hogan, Gordon McKay Lab. Sci. Rpt. #10 Harvard Univ. (1957).
18. C.R. Buffler, Gordon McKay Lab. Sci. Rpt. #3 (Series 2), Harvard Univ. (1960).
19. C. W. Hass and H. B. Callen, J. Appl. Phys. 32, 157S (1961).
20. J. E. Pippin and C. L. Hogan, Gordon McKay Lab. Sci. Rpt. #1, Harvard Univ. (1959).

AF19(604)-5487 DISTRIBUTION LIST*

APGC (PGAPI)
Elgin AFB, Florida

RADC (RAYLD)
Attn: Documents Library
Griffiss AFB, New York

RADC (RCE)
Attn: Dr. John S. Burgess
Griffiss AFB, New York

AF Missile Dev. Center (MDGRT)
Holloman AFB, New Mexico

Director of Resident Training
3380th Technical Training Group
Keesler AFB, Mississippi
Attn: OA-3011 Course

SAC (Operations Analysis Office)
Offutt AFB, Nebraska

AUL
Maxwell AFB, Alabama

AF Missile Test Center
Patrick AFB, Florida
Attn: AFMTC, Tech. Library
MU-135

USAF Security Service (CLR)
San Antonio, Texas

Technical Information Office
European Office, Aerospace Research
Shell Building, 47 Cantersteen
Brussels, Belgium

OAR (RROS, Col. John R. Fowler)
Tempo D
4th and Independence Ave.
Washington 25, D. C.

AFOSR, OAR (SRYP)
Tempo D
4th and Independence Ave.
Washington 25, D. C.

Hq. USAF (AFOAC-S/E)
Communications-Electronics
Directorate
Washington 25, D. C.

Hq. OAR (RROSP, Maj. Richard
W. Nelson)
Tempo D
4th and Independence Avenue
Washington 25, D. C.

ASD (ASAPRD-Dist.)
Wright-Patterson AFB, Ohio

WADD (WCLRSA, Mr. Portune)
Wright-Patterson AFB, Ohio

ASD (ASRNRE-3)
Attn: Mr. Paul Springer
Wright-Patterson AFB, Ohio

Director, Electronics Division
Air Technical Intelligence Center
Attn: AFCIN-4El, Col. H. K. Gilbert
Wright-Patterson AFB, Ohio

WADD (WWDRTR, Mr. A. D. Clark)
Directorate of System Engineering
Dyna Soar Engineering Office
Wright-Patterson AFB, Ohio

Lt. Col. Jensen (SSRTW)
Space Systems Division
Air Force Unit Post Office
Los Angeles 45, California

Director
Evans Signal Laboratory
Belmar, New Jersey
Attn: Mr. O. C. Woodyard

Commanding General
USASRDL
Ft. Monmouth, New Jersey
Attn: Tech. Doc. Ctr.
SIGRA/SL-ADT

---

*One copy to each address unless otherwise specified by numbers in brackets

Department of the Army
Office of the Chief Signal Officer
Washington 25, D. C.
Attn: SIGRD-4a-2

Massachusetts Institute of Technology
Signal Corps Liaison Officer
Cambridge 39, Massachusetts
Attn: A. D. Bedrosian, Rm. 26-131

Commanding General
USASRDL
Fort Monmouth, New Jersey
Attn: Mr. F. J. Triola

Office of Chief Signal Officer
Engineering and Technical Division
Washington 25, D. C.
Attn: SIGNET-5

Director
U. S. Army Ordnance
Ballistic Research Laboratories
Aberdeen Proving Ground, Maryland
Attn: Ballistic Measurements
Laboratory

Ballistic Research Laboratories
Aberdeen Proving Ground, Maryland
Attn: Technical Information Branch

Guided Missile Fuze Library
Diamond Ordnance Fuze Laboratories
Washington 25, D. C.
Attn: R. D. Hatcher, Chief Microwave
Development Section

Commanding General
USASRDL
Fort Monmouth, New Jersey
Attn: SIGFM/EL-AT

Redstone Scientific Information Center
U. S. Army Missile Command
Redstone Arsenal, Alabama (5)

Commanding General, SIGFM/EL-PC
USASRDL
Fort Monmouth, New Jersey
Attn: Dr. Horst H. Kedesdy
Deputy Chief, Chem-Physics Branch

ASTIA (TIPAA)
Arlington Hall Station
Arlington 12, Virginia (10)

Library
National Bureau of Standards
Boulder Laboratories
Boulder, Colorado (2)

Defence Research Member
Canadian Joint Staff
2450 Massachusetts Ave., N. W.
Washington 8, D. C. (Unclassified
only)

National Bureau of Standards
U. S. Department of Commerce
Washington 25, D. C.
Attn: Mr. A. G. McNish

National Bureau of Standards
U. S. Department of Commerce
Washington 25, D. C.
Attn: Gustave Shapiro, Chief,
Engineering Electronics Section
Electricity and Electronics Div.

Office of Scientific Intelligence
Central Intelligence Agency
2430 E Street, N. W.
Washington 25, D. C.

Director
National Security Agency
Fort George G. Meade, Maryland
Attn: C3/TDL

National Aeronautical Space Agency
Langley Aeronautical Research
Laboratory
Langley, Virginia
Attn: Mr. Cliff Nelson

AFCRL, OAR(CRXRA-Stop 39)
L. G. Hanscom Field
Bedford, Massachusetts (10)
(To be shipped under separate cover as reports to to our Documents Section)

AFCRL, OAR (CRRD)
Attn: Contract Files
L. G. Hanscom Field (2)
Bedford, Massachusetts

AFCRL, OAR (CRRD)
Attn: Carlyle J. Sletten
L. G. Hanscom Field (3)
Bedford, Massachusetts

Hq. ESD(ESDRW, Maj. J. J. Hobson)
L. G. Hanscom Field
Bedford, Massachusetts

Electronic Systems Division(AFSC)
Technical Information Services Division (ESAT)
L. G. Hanscom Field
Bedford, Massachusetts

Hq. AFCRL, OAR(CRXR, J. R. Marple)
L. G. Hanscom Field
Bedford, Massachusetts

Chief, Bureau of Ships
Department of the Navy
Washington 25, D. C.
Attn: Code 690

Chief, Bureau of Naval Weapons
Department of the Navy (2)
Washington 25, D. C.
Attn: DLI-31

Commander
U. S. N. Air Missile Test Center
Point Mugu, California
Attn: Code 366

U. S. Naval Ordnance Laboratory
White Oak
Silver Spring 19
Maryland
Attn: The Library

Commander
U. S. Naval Ordnance Test Station
China Lake, California
Attn: Code 753

Librarian
U. S. Naval Postgraduate School
Monterey, California

National Aeronautics and Space Administration
Attn: Antenna Systems Branch
Goddard Space Flight Center
Greenbelt, Maryland

Director
U. S. Naval Research Laboratory
Washington 25, D. C. (2)
Attn: Code 2027

Dr. J. I. Bohnert
Code 5210
U. S. Naval Research Laboratory
Washington 25, D. C.

Commanding Officer and Director
U. S. Navy Underwater Sound Laboratory
Fort Trumbull, New London
Connecticut

Chief of Naval Research
Department of the Navy
Washington 25, D. C.
Attn: Code 427

Commanding Officer
U. S. Navy Air Development Center
Johnsville, Pennsylvania
Attn: NADC Library

ONR, Branch Office, London
Navy 100, Box 39 (10)
F. P. O., New York, New York

Commanding Officer and Director
U. S. Navy Electronics Laboratory
(Library)
San Diego 52, California

Commander
U. S. Naval Air Test Center
Patuxent River, Maryland
Attn: ET-315, Antenna Branch

Material Laboratory, Code 932
New York Naval Shipyard
Brooklyn1, New York
Attn: Mr. Douglas First

Commanding Officer
U. S. Naval Ordnance Laboratory
Corona, California
Attn: Documents Librarian

Chief, Bureau of Ships
Department of the Navy
Washington 25, D. C.
Attn: Code 817B

AFSC Scientific and Technical
Liaison Office
c/o Department of the Navy
Room 2305, Munitions Building
Washington 25, D. C.

Aero Geo Astro Corp.
1200 Duke Street
Alexandria, Virginia
Attn: Library

Aerospace Corporation
Box 95085
Los Angeles 45, California
Attn: Library

Airborne Instruments Laboratory, Inc.
Division of Cutler Hammer
Walt Whitman Road
Melville, L. I. New York
Attn: Library

Aircom, Inc.
48 Cummington Street
Boston, Massachusetts

Andrew Alford, Consulting
Engineers
299 Atlantic Avenue
Boston 10, Massachusetts

Technical Operations, Inc.
South Street
Burlington, Massachusetts
Attn: Joseph I. Masters

ACF Electronics Division
Bladensburg Plant
52nd Avenue and Jackson St.
Bladensburg, Maryland
Attn: Librarian
Mailing Address for
classified:
3355 52nd Avenue
Hyattsville, Maryland

Battelle Memorial Institute
505 King Avenue
Columbus 1, Ohio
Attn: Wayne E. Rife, Project
Leader
Electrical Engineering
Division

Bell Aircraft Corporation
Post Office Box One
Buffalo 5, New York
Attn: Eunice P. Hazelton,
Librarian

Bell Telephone Laboratories
Murray Hill
New Jersey

Bell Telephone Laboratories, Inc.
Technical Information Library
Whippany Laboratory
Whippany, New Jersey
Attn: Technical Reports Librarian

Bendix Pacific Division
11600 Sherman Way
North Hollywood, California
Attn: Engineering Library

Bendix Radio Division
Bendix Aviation Corporation
E. Joppa Road
Towson 4, Maryland
Attn: Dr. D. M. Allison, Jr.
Director Engineering
and Research

Bjorksten Research Laboratories, Inc.
P. O. Box 265
Madison, Wisconsin
Attn: Librarian

Boeing Airplane Company
Pilotless Aircraft Division (2)
P. O. Box 3707
Seattle 24, Washington
Attn: R. R. Barber, Library
Supervisor

Boeing Airplane Company
Wichita Division Engineering Library
Wichita 1, Kansas
Attn: Kenneth C. Knight, Library
Supervisor

Brush Beryllium Company
4301 Perkins Avenue
Cleveland 3, Ohio
Attn: N. W. Bass

Chance Vought Corporation
9314 West Jefferson Boulevard
Dallas, Texas
Attn: A. D. Pattullo, Librarian

Chance Vought Corporation
Vought Electronics Division
P. O. Box 5907
Dallas 22, Texas

Chu Associates
P. O. Box 387
Whitcomb Avenue
Littleton
Massachusetts

Collins Radio Company
855 35th Street, N. E.
Cedar Rapids, Iowa
Attn: Dr. R. L. McCreary

Convair, A Division of
General Dynamics Corporation
Fort Worth, Texas
Attn: K. G. Brown, Division
Research Librarian

Convair, A Division of
General Dynamics Corporation
3165 Pacific Highway
San Diego 12, California
Attn: Mrs. Dora B. Burke
Engineering Librarian

Cornell Aeronautical Lab., Inc.
4455 Genesee Street
Buffalo 21, New York
Attn: Librarian

Dalmo Victor Company
A Division of Textron, Inc.
1515 Industrial Way
Belmont, California
Attn: Mary Ellen Addems
Technical Librarian

Dorne and Margolin, Inc.
29 New York Avenue
Westbury, Long Island
New York

Aircraft Division
Douglas Aircraft Co., Inc.
3855 Lakewood Boulevard
Long Beach, California
Attn: Technical Library

Douglas Aircraft Co., Inc.
3000 Ocean Park Boulevard
Santa Monica, California
Attn: Peter Duyan, Jr., Chief
Electrical/Electronics Sect.

Douglas Aircraft Company, Inc.
2000 North Memorial Drive
Tulsa, Oklahoma
Attn: Engineering Librarian, D-250

The Electrada Corporation
11244 Playa Street
Culver City, California
Attn: S. Stanley Locus, Section Head
Microwave Engineering

Electromagnetic Research Corporation
5001 College Avenue
College Park, Maryland
Attn: Mr. Martin Katzin

Electronics Communication
1830 York Road
Timonium, Maryland

Ferrotec, Inc.
Attn: P. D. Rutledge
217 California Street
Newton 58, Massachusetts

Watkins-Johnson Company
333 Hillview Avenue
Palo Alto, California
Attn: Dr. H. R. Johnson

Hq. AFCRL, OAR
(CRRCSP, Dr. Ernest R. Czerlinsky)
L. G. Hanscom Field
Bedford, Massachusetts

Electronic Specialty Company
5121 San Fernando Road
Los Angeles 39, California
Attn: Donald L. Margerum
Chief Engineer, Radiating
Systems Division

Emerson and Cuming, Inc.
59 Walpole Street
Canton, Massachusetts
Attn: Mr. W. Cuming

Emerson Electric Mfg. Co.
8100 West Florissant Avenue
St. Louis 21, Missouri
Attn: Mr. E. R. Breslin,
Librarian

Emerson Radio-Phonograph
Corporation
Emerson Research Laboratories
701 Lamont Street, N. W.
Washington 10, D. C.
Attn: Mrs. R. Corbin,
Librarian

Fairchild Aircraft-Missiles
Division
Fairchild Eng. and Airplane
Corporation
Hagerstown, Maryland
Attn: Library

ITT Federal Laboratories
Technical Library
500 Washington Avenue
Nutley 10, New Jersey

Gabriel Electronics Division
Main and Pleasant Streets
Millis, Massachusetts
Attn: Dr. Edward Altshuler

General Electric Company
Electronics Park
Syracuse, New York
Attn: Documents Library
B. Fletcher,
Building 3-143A

General Electric Company
Missile and Space Vehicle
Department
3198 Chestnut Street
Philadelphia, Pennsylvania
Attn: Documents Library

General Electric Company
3750 D. Street
Philadelphia 24, Pennsylvania
Attn: Mr. H. G. Lew
Missile and Space Vehicle
Department

General Precision Laboratory, Inc.
63 Bedford Road
Pleasantville, New York
Attn: Librarian

Goodyear Aircraft Corporation
1210 Massillon Road
Akron 15, Ohio
Attn: Library, Plant G

Granger Associates
Electronic Systems
974 Commercial Street
Palo Alto, California
Attn: John V. N. Granger, President

Grumman Aircraft Engineering
Corporation
Bethpage, Long Island, New York
Attn: Engineering Librarian,
Plant No. 5

Hallicrafters Company
4401 West 5th Avenue
Chicago 24, Illinois
Attn: LaVerne LaGioia, Librarian

The Hallicrafters Company
5th and Kostner Avenues
Chicago 24, Illinois
Attn: Henri Hodara, Head of Space
Communication

Hoffman Electronics Corporation
3761 South Hill Street
Los Angeles 7, California
Attn: Engineering Library

Hughes Aircraft Company
Antenna Department
Building 12, Mail Station 2714
Culver City, California
Attn: Dr. W. H. Kummer

Hughes Aircraft Company
Florence Ave. and Teale Streets
Culver City, California
Attn: Louis L. Bailin, Manager,
Antenna Department

Hughes Aircraft Company
Attn: Mr. L. Stark, Microwave
Department
Radar Laboratory
P. O. Box 2097
Building 600, Mail Station C-152
Fullerton, California

International Business Machines
Corporation
Space Guidance Center--
Federal Systems Division
Oswego, Tioga County, New York
Attn: Technical Reports Center

International Resistance Company
401 N. Broad Street
Philadelphia 8, Pennsylvania
Attn: Research Library

ITT Laboratories
3700 East Pontiac Street
Fort Wayne 1, Indiana
Attn: Technical Library

Jansky and Bailey, Inc.
1339 Wisconsin Avenue, N. W.
Washington 7, D. C.
Attn: Mr. Delmer C. Ports

Dr. Henry Jasik, Consulting
Engineer
298 Shames Drive
Brush Hollow Industrial Park
Westbury, New York

Lockheed Aircraft Corporation
2555 N. Hollywood Way
California Division Engineering
Library
Department 72-25, Plant A-1,
Building 63-1
Burbank, California
Attn: N. C. Harnois

Lockheed Aircraft Corporation
Missiles and Space Division
Technical Information Center
3251 Hanover Street
Palo Alto, California (2)

The Martin Company
P. O. Box 179
Denver 1, Colorado
Attn: Mr. Jack McCormick

The Martin Company
Baltimore 3, Maryland
Attn: Engineering Library
Antenna Design Group

Mathematical Reviews
190 Hope Street
Providence 6, Rhode Island

The W. L. Maxson Corporation
475 10th Avenue
New York, New York,
Attn: Miss Dorothy Clark

McDonnell Aircraft Corporation,
Department 644
Box 516
St. Louis 66, Missouri
Attn: C. E. Zoller
Engineering Library

McMillan Laboratory, Inc.
Brownville Avenue
Ipswich, Massachusetts
Attn: Security Officer, Document
Room

Melpar, Inc.
3000 Arlington Boulevard
Falls Church, Virginia
Attn: Engineering Technical
Library

Microwave Associates, Inc.
South Avenue
Burlington, Massachusetts

Microwave Development Labs, Inc.
92 Broad Street
Wellesley 57, Massachusetts
Attn: N. Tucker, General Manager

The Mitre Corporation
244 Wood Street
Lexington, Massachusetts, 73
Attn: Mrs. Jean E. Claflin,
Librarian

Motorola, Inc.
8201East McDowell Road
Phoenix, Arizona
Attn: Dr. Thomas E. Tice

National Research Council
Radio and Electrical Engineering
Division
Ottawa, Ontario, Canada
Attn: Dr. G. A. Miller, Head
Microwave Section

North American Aviation, Inc.
12214 Lakewood Boulevard
Downey, California
Attn: Technical Information Center
(495-12)
Space and Information Systems
Division

North American Aviation, Inc.
Los Angeles International Airport
Los Angeles 45, California
Attn: Engineering Technical File

Page Communications Engineers, Inc.
2001 Wisconsin Avenue, N. W.
Washington 7, D. C.
Attn: Mrs. Ruth Temple, Librarian

Northrop Corporation
Norair Division
1001 East Broadway
Hawthorne, California
Attn: Technical Information 3924-31

Philco Corporation
Research Division
Union Meeting Pond
Blue Bell, Pennsylvania
Attn: Research Librarian

Pickard and Burns, Inc.
103 Fourth Avenue
Waltham 54, Massachusetts
Attn: Dr. Richard H. Woodward

Polytechnic Research and
Development Company
202 Tillary Street
Brooklyn 1, New York
Attn: Technical Library

Radiation Engineering Laboratory
Main Street
Maynard, Massachusetts
Attn: Dr. John Ruze

Radiation, Inc.
Melbourne, Florida
Attn: RF Systems Division
Technical Information Center

Radiation Systems, Inc.
440 Swann Avenue
Alexandria, Virginia
Attn: Library

RCA Laboratories
David Sarnoff Research Center
Princeton, New Jersey
Attn: Miss Fern Cloak, Librarian

Radio Corporation of America
Defense Electronic Products
Building 10, Floor 7
Camden 2, New Jersey
Attn: Mr. Harold J. Schrader, Staff
Engineer, Organization of
Chief Technical Administrator

Radio Corporation of America
Missile Control and Electronics Division
Bedford Street
Burlington, Massachusetts
Attn: Librarian

Radio Corporation of America
Surface Communications Systems
Laboratory
75 Varick Street
New York 13, New York
Attn: Mr. S. Krevsky

Radio Corporation of America
West Coast Missile and Surface
Radar Division
Engineering Library, Building 306/2
Attn: L. R. Hund, Librarian
8500 Balboa Boulevard
Van Nuys, California

Radio Corporation of America
Defense Electronic Products
Advanced Military Systems
Princeton, New Jersey
Attn: Mr. David Shore

Director, USAF Project RAND
Via: AF Liaison Office
The Rand Corporation
1700 Main Street
Santa Monica, California

The Rand Corporation
1700 Main Street
Santa Monica, California
Attn: Technical Library

Rantec Corporation
23999 Ventura Boulevard
Calabasas, California
Attn: Grace Keener, Office
Manager

Raytheon Company
State Road, Wayland Laboratory
Wayland, Massachusetts
Attn: Mr. Robert Borts

Raytheon Company
Wayland Laboratory
Wayland, Massachusetts
Attn: Miss Alice G. Anderson,
Librarian

Raytheon Company
Missile Systems Division
Hartwell Road
Bedford, Massachusetts
Attn: Donald H. Archer

Remington Rand UNIVAC
Division of Sperry Rand
Corporation
P. O. Box 500
Blue Bell, Pennsylvania
Attn: Engineering Library

Republic Aviation Corporation
Farmingdale, Long Island, New York
Attn: Engineering Library
Thru: AF Plant Repre.
Republic Aviation Corp.
Farmingdale, Long Island
New York

Ryan Aeronautical Company
2701 Harbor Drive
Lindbergh Field
San Diego 12, California
Attn: Library

Sage Laboratories, Inc.
3 Huron Drive
Natick, Massachusetts

Sanders Associates, Inc.
95 Canal Street
Nashua, New Hampshire
Attn: Mr. Norman R. Wild

Sandia Corporation
P. O. Box 5800
Albuquerque, New Mexico
Attn: Records Management and
Services Department

Scanwell Laboratories, Inc.
6601 Scanwell Lane
Springfield, Virginia

STL Technical Library
Document Acquisitions
Space Technology Laboratories, Inc.
P. O. Box 95001
Los Angeles 45, California

Sperry Gyroscope Company
Great Neck, Long Island, New York
Attn: Florence W. Turnbull
Engineering Librarian

Stanford Research Institute
Documents Center
Menlo Park, California
Attn: Acquisitions

Sylvania Electric Products, Inc.
100 First Avenue
Waltham 54, Massachusetts
Attn: Charles A. Thornhill,
Report Librarian
Waltham Laboratories
Library

Sylvania Electric Products, Inc.
Electronic Defense Laboratory
P. O. Box 205
Mountain View, California
Attn: Library

Sylvania Reconnaissance Systems
Laboratory
Box 188
Mountain View, California
Attn: Marvin D. Waldman

TRG, Inc.
400 Border Street
East Boston, Massachusetts
Attn: Dr. Alan F. Kay

A. S. Thomas, Inc.
355 Providence Highway
Westwood, Massachusetts
Attn: A. S. Thomas, President

Texas Instruments, Inc.
6000 Lemmon Avenue
Dallas 9, Texas
Attn: John B. Travis
Systems Planning Branch

Trans-Tech, Inc.
P. O. Box 346
Rockville, Maryland
Attn: Mr. A. C. Blankenship
Chief Electronics Engineer

Westinghouse Electric Corporation
Electronics Division
Friendship Int'l Airport
Box 1897
Baltimore 3, Maryland
Attn: Engineering Library

Library Geophysical Institute of the
University of Alaska
College, Alaska

Brown University
Department of Electrical Engineering
Providence, Rhode Island
Attn: Dr. C. M. Angulo

California Institute of Technology
Jet Propulsion Laboratory
4800 Oak Grove Drive
Pasadena, California
Attn: Mr. I. E. Newlan

California Institute of Technology
1201 E. California Street
Pasadena, California
Attn: Dr. C. Papas

Space Sciences Laboratory
Leuschner Observatory
University of California
Berkeley 4, California
Attn: Dr. Samuel Silver, Director,
Space Sciences Laboratory

University of California
Electronics Research Laboratory
332 Cory Hall
Berkeley 4, California
Attn: J. R. Whinnery

University of Southern California
University Park
Los Angeles, California
Attn: Dr. Raymond L. Chuan
Director, Engineering
Center

Case Institute of Technology
Electrical Engineering Department
10900 Euclid Avenue
Cleveland, Ohio
Attn: Prof. Robert Plonsey

Columbia University
Department of Electrical Engineering
Morningside Heights
New York, New York
Attn: Dr. Schlesinger

University of Southern California
University Park
Los Angeles 7, California
Attn: Z. A. Kaprielian, Associate
Professor of Electrical
Engineering

Cornell University
School of Electrical Engineering
Ithaca, New York
Attn: Prof. G. C. Dalman

University of Florida
Department of Electrical
Engineering
Gainesville, Florida
Attn: Prof. M. H. Latour,
Library

Library
Georgia Technology Research
Institute
Engineering Experiment Station
722 Cherry Street, N. W.
Atlanta, Georgia
Attn: Mrs. J. H. Crosland,
Librarian

Harvard College Observatory
60 Garden Street
Cambridge 39, Massachusetts
Attn: Dr. Fred L. Whipple

Harvard University
Technical Reports Collection
Gordon McKay Library
303 Pierce Hall
Oxford Street
Cambridge 38, Massachusetts
Attn: Librarian

University of Illinois
Documents Division Library
Urbana, Illinois

University of Illinois
College of Engineering
Urbana, Illinois
Attn: Dr. P. E. Mayes, Department of Electrical Engineering

Illinois Institute of Technology
3301 S. Dearborn Street
Chicago 16, Illinois
Attn: Dr. George I. Cohn

Illinois Institute of Technology
Technology Center
Department of Electrical Engineering
Chicago 16, Illinois
Attn: Paul C. Yuen, Electronics Research Laboratory

The Johns Hopkins University
Homewood Campus
Baltimore 18, Maryland
Attn: Dr. Donald E. Kerr, Department of Physics

The Johns Hopkins University
Applied Physics Laboratory
8621 Georgia Avenue
Silver Spring, Maryland
Attn: Mr. George L. Seielstad

University of Kansas
Electrical Engineering Department
Lawrence, Kansas
Attn: Dr. H. Unz

Lowell Technological Institute
Research Foundation
P. O. Box 709
Lowell, Massachusetts
Attn: Dr. Charles R. Mingins

Massachusetts Institute of Technology
Research Laboratory of Electronics
Building 26, Room 327
Cambridge 39, Massachusetts
Attn: John J. Hewitt

McGill University
Department of Electrical Engineering
Montreal, Canada
Attn: Dr. T. Pavlasek

University of Michigan
Electronic Defense Group
Institute of Science and Technology
Ann Arbor, Michigan
Attn: J. A. Boyd, Supervisor
classified via: Facility Security Officer

University of Michigan
Office of Research Administration
Radiation Laboratory
912 N. Main Street
Ann Arbor, Michigan
Attn: Mr. Ralph E. Hiatt
classified via: Security Officer

University of Michigan
Engineering Research Institute
Willow Run Laboratories
Willow Run Airport
Ypsilanti, Michigan
Attn: Librarian

University of Minnesota
Minneapolis 14, Minnesota
Attn: Mr. Robert H. Stumm, Library

Physical Science Laboratory
New Mexico State University
University Park, New Mexico
Attn: Mr. H. W. Haas

New York University
Institute of Mathematical Sciences
Room 802, 25 Waverly Place
New York 3, New York
Attn: Morris Kline, Dr.

Northwestern University
Microwave Laboratories
Evanston, Illinois
Attn: R. E. Beam

Antenna Laboratory
Department of Electrical Engineering
The Ohio State University
2024 Neil Avenue
Columbus 10, Ohio
Attn: Reports Librarian

The University of Oklahoma
Research Institute
Norman, Oklahoma
Attn: Prof. C. L. Farrar, Chairman
Electrical Engineering

University of Pennsylvania
Institute of Cooperative Research
3400 Walnut Street
Philadelphia, Pennsylvania
Attn: Department of Electrical
Engineering

Polytechnic Institute of Brooklyn
Microwave Research Institute
55 Johnson Street
Brooklyn, New York
Attn: Dr. Arthur A. Oliner

Polytechnic Institute of Brooklyn
Microwave Research Institute
55 Johnson Street
Brooklyn, New York
Attn: Mr. A. E. Laemmel

The Pennsylvania State University
223 Electrical Engineering
University Park, Pennsylvania
Attn: A. H. Waynick, Director
Ionosphere Research Lab.

Purdue University
Department of Electrical
Engineering
Lafayette, Indiana
Attn: Dr. Schultz

Library
W. W. Hansen Laboratory of
Physics
Stanford University
Stanford, California

Syracuse University Research
Institute
Collendale Campus
Syracuse 10, New York
Attn: Dr. C. S. Grove, Jr.
Director of Engineering
Research

Technical University
Oestervoldgade 10 G
Copenhagen, Denmark
Attn: Prof. Hans Lottrup Knudsen

University of Tennessee
Ferris Hall
W. Cumberland Avenue
Knoxville 16, Tennessee

The University of Texas
Electrical Engineering Research
Laboratory
P. O. Box 8026
University Station
Austin 12, Texas
Attn: Mr. John R. Gerhardt
Assistant Director

The University of Texas
Defense Research Laboratory
Austin, Texas
Attn: Claude W. Horton,
Physics Library

University of Toronto
Department of Electrical Engineering
Toronto, Canada
Attn: Prof. G. Sinclair

University of Washington
Department of Electrical Engineering
Seattle 5, Washington
Attn: D. K. Reynolds

University of Wisconsin
Department of Electrical Engineering
Madison, Wisconsin
Attn: Dr. Scheibe

Motorola, Inc.
Phoenix Research Laboratory
3102 N. 56th Street
Phoenix, Arizona
Attn: Dr. A. L. Aden

Massachusetts Institute of Technology
Lincoln Laboratory
P. O. Box 73
Lexington 73, Massachusetts
Attn: Mary A. Granese, Librarian

SR6

Electronics Research Directorate Air Force Cambridge Research Labs. Office of Aerospace Research, USAF, Bedford, Mass. Rpt. No. AFCRL-62-954 SWITCHING PROPERTIES OF FERRITES AND GARNETS Interim Scientific Rpt. No. 6(Series 2) 30 November 1962, 204p., illus., tables, 154 refs. Unclassified Report	1. Microwave applications of ferromagnetic & ferroelectric materials I. AF Project 5633 Task 56332 II. Contract AF19(604)5847 III. Cruft Lab. Harvard University Cambridge, Mass. IV. Rubinstein, H. V. Scientific Rpt. No. 6(Series 2)

This work presents the results of an experimental and theoretical study of the switching properties of ferrimagnetic garnets and spinels. The switching characteristics and the flux switched measurements obtained during the course of this work are given. From these data it would appear that the switching speed is limited by self-imposed processes, since S_w is found to decrease as the microwave resonance relaxation frequency, λ, decreases, until λ reaches a critical value and then to remain constant when λ is further reduced.	VI VII. In ASTIA collection

This work present the results of an experimental and theoretical study of the switching properties of ferrimagnetic garnets and spinels. The switching characteristics and the flux switched measurements obtained during the course of this work are given. From these data it would appear that the switching speed is limited by self-imposed processes, since S_w is found to decrease as the microwave resonance relaxation frequency, λ, decreases, until λ reaches a critical value and then to remain constant when λ is further reduced.

VI. ---------
VII. In ASTIA collection

Electronics Research Directorate
Air Force Cambridge Research Labs.
Office of Aerospace Research, USAF,
Bedford, Mass.
Rpt. No. AFCRL-62-954
SWITCHING PROPERTIES OF FERRITES AND GARNETS
Intermin Scientific Rpt. No6(Series 2)
30 November 1962, 204 p., illus., tables, 154 refs.
Unclassified Report

1. Microwave applications of ferromagnetic & ferroelectric materials
I. AFProject 5633
Task 56332
II. Contract AF19(604)5847
III. Cruft Lab.
Harvard University
IV. Rubinstein, H.
V. Scientific Rpt. No. 6(Series 2)